FACULTY
OF MATHEMATICS
AND PHYSICS
Charles University

DOCTORAL THESIS

Michal Lacko

Studies of reactions of ions with water molecules in the gaseous phase for trace gas analysis

Department of Surface and Plasma Science

Supervisor of the doctoral thesis: Prof. RNDr. Patrik Španěl, Dr. rer. nat.

Study programme: Physics (P1701)
Study branch: Physics of Plasma and Ionized Media

Prague 2022

I declare that I carried out this doctoral thesis independently and only with the cited sources, literature and other professional sources.

I understand that my work relates to the rights and obligations under the Act No. 121/2000 Coll., the Copyright Act, as amended, in particular the fact that Charles University has the right to conclude a license agreement on the use of this work as a school work pursuant to Section 60 paragraph 1 of the Copyright Act.

In Prague date 15.8.2022 Mgr. Michal Lacko, PhD.

“Man, he took his time in the sun

Had a dream to understand

A single grain of sand … “

(Nightwish)

Acknowledgements

First, would like to thank my supervisor Prof. Patrik Španěl for his help and guidance during my studies as well as all members of his group making my work and life in Prague awesome. Dear Ksenia, Anatoli, Krystina, Violet, Pavel, Jan, Niki, thank you. Massive thanks also go to Stephan, who helped me with the language aspect of the thesis. Additionally, I would like to thank all members of the IMPACT project for their unforgivable experiences and great memories. Also, thanks to the members of my faculty for their patience, as the preparation of this work took more time than expected. Finally, the biggest thanks belong to my patient wife and children, for accompanying me during my complicated path to knowledge.

Title: Studies of reactions of ions with water molecules in the gaseous phase for trace gas analysis

Author: Michal Lacko

Department / Institute: Department of Surface and Plasma Science, Faculty of Mathematics and Physics, Charles University in Prague

Department of Chemistry of Ions in Gaseous Phase, J. Heyrovský Institute of Physical Chemistry of the CAS, v. v. i.

Supervisor of the doctoral thesis: Prof. RNDr. Patrik Španěl, Dr. rer. nat., J. Heyrovský Institute of Physical Chemistry of the CAS, v. v. i.

Abstract: Chemical ionization mass spectrometry (CI-MS) is a powerful analytical technique, capable to detect trace levels of organic molecules diluted in air samples in real-time. Processes leading to ionization of organic molecules, necessary for their detection and identification, are however often strongly affected by the presence of water vapours in form of sample humidity. In the present work, I studied the influence of water vapours on ion chemistry and, subsequently, the respective influence on sensitivity and selectivity of CI-MS techniques.

Studies were carried out using several soft chemical ionization mass spectrometry instruments, including Selected Ion Flow Tube Mass Spectrometry (SIFT-MS), Proton Transfer Reaction Mass Spectrometry (PTR-MS) and Selected Ion Flow-Drift Tube Mass Spectrometry (SIFDT-MS). Experimental studies were also supplemented by theoretical simulation of proposed ion chemistry using the Kinetic of Ion-Molecular Interaction simulator (KIMI), developed by the author.

In this thesis, I present a study of formaldehyde, glyoxal and phthalates ion chemistry with H_3O^+, NO^+ and O_2^+ reagent ions, focusing on secondary reactions with water vapours. Additionally, I also studied secondary reactions of protonated hydrated acetic acid with acetone. Finally, I have carried out experiments with fast gas chromatography (CG) coupled with the SIFT-MS instrument, to reduce humidity influence and improve the selectivity of monoterpenes.

Keywords: Soft chemical ionization mass spectrometry, selected ion flow tube mass spectrometry, proton transfer reaction mass spectrometry, selected ion flow drift tube mass spectrometry

Název práce: Studium reakcí iontů s molekulami vody v plynné fázi pro stopovou analýzu

Autor: Michal Lacko

Katedra/Ústav: Katedra fyziky povrchů a plazmatu Matematicko-fyzikální fakulty, Univerzity Karlovy v Praze

Oddělení chemie iontů v plynné fázi, Ústav fyzikální chemie J. Heyrovského AV ČR, v. v. i.

Vedoucí disertační práce: Prof. RNDr. Patrik Španěl, Dr. rer. nat., Ústav fyzikální chemie J. Heyrovského AV ČR, v. v. i.

Abstrakt: Metoda hmotnostní spektrometrie pomocí chemické ionizace je účinná analytická technika, umožňující detekovat v reálném čase stopová množství organických těkavých látek přítomné ve vzduchu. Procesy vedoucí k ionizaci organických molekul, nutné k jejich detekci a následnou identifikaci, jsou bohužel často ovlivněné přítomností vodní páry. V představené práci jsem studoval vliv vodní páry na chemii iontů a její následní vliv na citlivost a selektivitu metod hmotnostní spektrometrie pomocí chemické ionizace.

Pro studium jsme využili několik hmotnostně-spektrometrických přístrojů, mimo jiné techniku hmotnostní spektrometrie v proudové trubici s vybranými ionty (SIFT-MS), techniku hmotnostní spektrometre pomocí reakce přenosu protonu (PTR-MS) a techniku hmotnostní spektrometrie v proudově-driftové trubice s vybranými ionty (SIFDT-MS). Experimentální stude je doplněná teoretickými simulacemi studovaných procesů pomocí autorem vytvořeným simulačním programem KIMI.

V disertační práci prezentuji výsledky zkoumání iontové chemie molekul formaldehydu, glyoxalu a ftalátů pomocí H_3O^+, NO^+ and O_2^+ reakčních iontů, přičemž se zaměřuji na pochopení sekundárních reakci iontových produktů s vodní párou. Následně jsem také studoval sekundární reakce protonovaných a hydratovaných molekul kyseliny mravenčí s acetonem. V práci jsem nakonec zkoumal analýzu monoterpenů kombinací rychlé plynové chromatografie a SIFT-MS, která mimo jiné umožnuje redukovat vliv vodní páry na iontovou chemii.

Klíčová slova: hmotnostní spektrometrie pomocí měkké chemická ionizace, hmotnostní spektrometrie v proudové trubici s vybranými ionty, reakce přenosu protonu

Contents

Preface **3**

1. Introduction to gas phase ion processes for trace gas analysis **5**

1.1. Chemical ionisation of organic molecules 10

1.2. Analytical techniques for trace gas analysis 35

1.3. Areas of application 59

1.4. Limitations of chemical ionization mass spectrometry 65

1.5. Objectives of the thesis 70

2. Construction of fast GC pre-separation for SIFT-MS **73**

3. Complex model of ion chemistry in SCI-MS **76**

4. Results **91**

4.1. Complex study of glyoxal ion chemistry 91

4.2. Ion chemistry of phthalates studied by SIFT-MS 95

4.3 Study of secondary ligand switching reactions of protonated acetic acid hydrates with acetone 98

4.4 Real time detection of Arsene and Selene hydrides by SIFT-MS 100

Conclusion **102**

List of Tables and Figures **107**

List of Abbreviations **110**

List of publications **112**

Bibliography **113**

Attachments **140**

Attachment A.1 143

Attachment A.2 170

Attachment A.3 179

Attachment A.4 222

Attachment A.5 238

Attachment A.6 262

Preface

The dissertation thesis deals with specific problems of chemical ionisation mass spectrometry and its applications for trace gas analysis, mainly focusing on the influence of water molecules on ion chemistry in soft chemical-ionisation mass-spectrometry (SCIMS). The study was carried out as a part of the Interactional Training Network "IMPACT" program, connecting several leading European academic institutions and companies in the area of chemical ionisation, analytical chemistry and instrumental development. The international team, containing 10 PhD students, have been focusing on the identification and solving of specific SCIMS problems as well as the development of new analytical solutions. Present work is an integral part of the IMPACT network, dealing with the fundamental theoretical and experimental research of SCIMS. This thesis reflects on the problems of the SCIMS techniques which were found from interactional and interdisciplinary discussions, which are still ongoing.

The main objective of this thesis is to study the reactions of specific reagent ions H_3O^+, NO^+ and O_2^+ (usually presented in SCIMS), with various molecules in the gas phase and to determine the influence of sample humidity on these reactions. This was achieved by experimental research on individual SCIMS instruments and theoretical simulation of ion molecular interactions.

This thesis consists of four main Chapters. The first part introduces ion chemistry and its application to trace gas analysis, identifying the specific problems connected with SCIMS techniques influencing their sensitivity and selectivity, as well as formulation of objectives dealing with these specific problems.

In the second section, we present the construction of the fast gas chromatography (GC) unit used to pre-separate molecular isomers in a gas sample, along with its coupling with selective ion flow tube mass spectrometry (SIFT-MS). This combination of techniques was used to analyse monoterpenes in several coniferous needle samples.

The following chapter focuses on the development of an interactive numerical model capable of simulating ion chemistry in individual SCIMS analytical techniques which in turn enables us to improve the interpretation of our results. This model was then

successfully applied to several studies, describing and compensating for the effect of sample humidity.

The final chapter presents the main results of the thesis. Firstly, the thesis deals with the ion chemistry surrounding glyoxal molecules in the flow and drift tubes, which were studied using several SCIMS experimental techniques. Later, the ion chemistry of phthalate isomers dimethyl phthalate, dimethyl isophthalate and dimethyl terephthalate together with diethyl phthalate were studied by the SIFT technique. In both studies, we investigated effect of sample humidity on ion chemistry and, using the numerical model, we were capable of identify secondary reactions forming new product ions. Secondary reactions influencing ion chemistry are, however, not exclusively induced by presence of water vapours. In our next study, we studied secondary reactions of protonated acetic acid hydrates induced by presence of acetone vapours. Acetone vapours, similar to water vapours, reacts with primary product ions via association and ligand switching reactions, reducing selectivity and sensitivity of SCIMS analysis. Finally, we demonstrated applicability of SCIMS techniques on inorganic hydrides of arsene and selene, in highly humidified environment of atomizers. This study can help to understand decomposition processes in atomizers and eventually may lead into new analytical applications of SCIMS techniques.

1. Introduction to gas phase ion processes for trace gas analysis

The term ion processes (or ion chemistry) refers to ion-neutral reactions between ionised and neutral molecules (or atoms) in the gas phase. This form of interaction is typical for low-temperature plasmas and ionised gasses which can be found in many technical applications as well as in the environment (planetary ionosphere, interstellar clouds).

The study of ion-molecular reactions started in the middle of the 20th century after the development of quantum chemistry. Development of new materials, improvements in electronics together with new techniques for vacuum generation and mass spectrometry, allowed for the construction of accurate experimental systems capable of carrying out investigations of individual ion-neutral reactions.

The interest in ion-neutral reactions was supported by early astronomical observations, which indicated the presence of the diatomic molecules CH, OH, NH, CN and C_2 in interstellar space. [1, 2] The formation of various diatomic molecules in low-density plasmas under heavy radiation was expected to be carried out by occasional ion-neutral reactions over a long period of time. [3] Nowadays, we know that ion chemistry together with electron-ion recombination are the main processes generating complex molecules in interstellar space, such as dense and diffuse molecular clouds or nebulas. [4-6]

The second area of research where ion chemistry was considered important was the Earth's ionosphere. This topic has become particularly interesting for the development of long-range radio communication; explanation of rare atmospheric phenomena; as well as the future development of space technologies. Initial measurements of ion concentrations in the Earth's ionosphere were carried out on a rocket-borne mass-spectrometer, launched in Canada [7], which observed the presence of NO^+, O_2^+ ions at altitudes above 100 km. Shortly after this initial *in situ* measurement, an intensive experimental study of atmospheric ion chemistry started.

The first pieces of experimental data were obtained using time-resolved stationary afterglow techniques. [8, 9] The mass-spectrometric analysis of ion decay in stationary afterglows provided the first measurements of ion-neutral reaction rate constants at

Maxwellian kinetic energy distributions, defined by gas temperature. These experiments were more useful compared to the direct ion-neutral cross-section estimation carried out by cross beam experiments, as said previous experiments were only able to effectively achieve interaction energies over 1 eV, thus were not reproducing experimental conditions characteristic for either atmospheric or interstellar plasmas. [10] The discharge in stationary afterglow may however ionise not only the gas mixture but also produce a high population of excited neutrals which may interfere with studied ion-neutral processes. [11] Secondly, the presence of electrons in the afterglow allows for the production of an ambipolar diffusion field, preventing the flow of negative ions into the plasma and thus can only be used for the study of cation-neutral reactions.

Significant progress in an experimental study of ion chemistry was achieved by the development of the flowing afterglow (FA) technique by Ferguson and Fehsenfeld [12] at the National Oceanic and Atmospheric Administration (NOAA) in the U.S. The discharge was generated in the stream of carrier gas in a flow tube. Generated ions and radical species were carried by the gas stream from the active discharge region, where they thermalized. A specific gas might be introduced into the fresh afterglow (e.g. a small amount of a specific electronegative gas such as SF_6 to attract remaining free electrons) to adjust the afterglow properties as well as ion formation. The targeted ion chemistry was then studied by injecting molecules of interest into the afterglow. Ions presented in the afterglow interact with the injected sample neutrals, generating product ions which are detected by the mass spectrometer. Reaction times can be reconstructed by changing the positions of the gas injection and detection orifices, as well as the afterglow gas velocity. However, as a limitation, more than one primary ion is often present in such a system and some metastable species (often in Helium) may influence the studied ion chemistry by Penning ionization. Nevertheless, the FA was a popular technique for the determination of reaction rate constants for ion-neutral reactions. [13-17]

Building from the FA, the newly developed flow-drift-tube type (FDT) technique allowed for the study of ion chemistry and estimating ion motilities for both positive and negative ions over a wide range of interaction energies. [18-20] Here, the uniform electric field was applied along the flow tube, accelerating the ion swarm and increasing the relative interaction energy between ions and neutrals. The technique

allowed for the determination of reaction rate constants from thermal energies up to several eV. For higher values of reduced electric field (*E/N*), however, the non-Maxwellian and non-Boltzmann distributions of energy and internal excitation could be achieved. [21]

The possibility to selectively choose specific reagent ions while keeping the ion-neutral reactions at thermal conditions was achieved by the development of the selective ion flow tube (SIFT), developed by Adams and Smith [22]. The SIFT technique uses a mass selective ion injection system providing high ion transmission from a plasma discharge into the flow tube while keeping sufficient resolution of ions (with the mass-to-charge ratios of O_2^+ (*m/z* 32) and NO^+ (*m/z* 30) produced in the discharge being very close in value). The construction was possible due to the unique solution of the flow tube ion injection orifice, providing ion transmission from the low-pressure region of the injection quadrupole mass filter (10^{-5} mbar) into the medium-pressure region of the flow tube (1 mbar). [23] The orifice is made of specifically shaped and orientated injection nozzles placed symmetrically around the ion orifice. Helium gas injected through the nozzles creates a conical gas stream, minimalizing the back flow of gas into the low-pressure injection quadrupole while generating turbulences afterwards, which helps to mix injected ions with carrier gas. The remaining parts of the technique were similar to the FA, including the injection needle for sampled gas at the point where helium flow is laminar and the second quadrupole mass spectrometer for analysis of ion concentrations at the downstream end of the flow tube. The initial concept consisted of a 100 cm long flow tube that required a substantial pumping speed of the main flow tube pump (100 Torr $l.s^{-1}$) to reduce diffusion losses of ions to the flow tube wall. The initial instrument thus achieved a room-size dimension, high operational cost, and despite its popularity, was used rather rarely.

Besides the limitations of FA and SIFT, both techniques were actively used to determine ion products and rate coefficients for many reactions of positive and negative ions [24, 25]. Accumulated data were afterwards compared with theoretical predictions. [13, 26] As a result, SIFT quickly became a standard method for the study of ion-neutral reactions at and near thermal interaction energies. [23]

As stated before, SIFT was initially used to study the ion chemistry of interstellar clouds, planetary atmospheres [27-29] and laboratory plasmas for technical use. [30] The idea of using SIFT for analytical applications became visible after a series of studies related to terrestrial atmospheric chemistry. The concentration of neutral reactants needs to be changed over a wide range to determine the rate constants for studied ion-molecular reactions. Studies showed that when processes occur at the collisional rate, ion products become visible even at low concentrations of neutral reactants. Thus, it should be possible to analyse a gas sample with unknown composition and concentration based on the specific chemical ionization of gas components within the flow tube. Additionally, reagent ions should be chosen on the basis that they do not react with the main components of air, but would react rapidly with trace components of the sample gas (such as organic molecules) and thus allowing for the analysis of their concentration. The idea of using chemical ionization for the detection of trace gas components in air was not new. It was shown previously that organic molecules become protonated after their reaction with specific ions such as CH_5^+. [31] Additionally, Kr^+ and Xe^+ were once used for the analysis of air sample, as their ionization potential lay below the ionization threshold for N_2, thus it was possible to analyze minor air components without interference from the major components. [32] This was beneficial over classical electron ionization mass spectrometry (EI-MS), where only components with partial pressures at the percentage or fraction of percentage levels can be analysed. (i.e. oxygen or carbon dioxide). [33]

The benefit of the SIFT technique was its simple principle. The reaction time is well defined by carrier gas velocity; thus, the concentration of specific neutral components can be directly determined from the abundance of the ion product and known rate constants. Studies of ion chemistry in the Earth's ionosphere provided information about stable ions (H_3O^+, NO^+ and O_2^+) which do not interact with the major components of the Earth's atmosphere. Additionally, data was obtained on their reactions with a series of molecules which could be used for the analysis of trace compounds in it. The possibility to select multiple reagent ions in SIFT has opened new analytical opportunities for SIFT-MS, which was then demonstrated by lab air and breath analysis. [34-36]

Successful introduction of chemical ionization into analytical applications provided benefits over conventional analytical techniques such as gas chromatography-mass

spectrometry (GC-MS). Demonstration of detection limits in the range of 1 ppbv for several volatile organic compounds (VOCs) allows one to analyse complex mixtures without pre-concentration, allowing for the analysis of the gas sample in real-time. [37] As a result of this, chemical ionization techniques are an excellent choice for analysis of breath or samples from environments requiring quick response times (i.e. homeland security).

The potential of chemical ionization for trace gas analysis became even more dominant after the introduction of new analytical techniques. The Proton Transfer Reaction Mass Spectrometry (PTR-MS) technique replaces a flow tube presented in SIFT-MS with a drift tube. [38] The axial electric field presented in the flow tube carries ions instead of drifting carrier gas. The full volume of the drift tube can be filled with a gas sample which increases the sensitivity of the technique down to the pptv region. The next step involved the installation of the axial electric field into the SIFT, creating a flow-drift tube reaction region. So-called Selected Ion Flow-Drift Tube Mass Spectrometry (SIFDT-MS) has the potential to further improve the analytical possibilities of chemical ionization. [39]

In parallel to low-pressure chemical ionization, atmospheric pressure chemical ionization (APCI) was developed, where ion chemistry occurs at atmospheric or near-atmospheric pressure. [40] The absence of powerful vacuum pumps allows APCI to inhabit much smaller instruments. APCI is also often combined with measurements of ion mobility (APCI-IMS) [41] instead of classical mass spectrometry. [42] The latest development is called secondary electrospray ionization (SESI), which ionizes ambient gas by secondary ions formed by the electrospray technique [43]. Although APCI is an important variant of CI, used globally, we will not focus on it in the present work. Instead, we focus on the low-pressure CI occurring in the SIFT, PTR and IMS instruments. The obtained results and surrounding principles, however, may also be applied to APCI.

1.1. Chemical ionisation of organic molecules

Chemical ionisation is a process achieved through the chemical reaction between ions and molecules. Compared to other ionisation techniques (such as electron ionisation or photoionization), the chemical ionisation here cannot be described by Franck-Condon's vertical electronic transition. Rather, the slower adiabatic approximation has to be considered, assuming adjustment of electronic states and atomic position during the interaction. [44] The amount of energy required to overcome an ionisation threshold is contained in the potential of electronic states of one of the reactants and not necessarily in the kinetic energy of particles. Chemical ionisation can thus be efficient even at low temperatures, characteristic, for example, for interstellar space.

Chemical ionization requires at least two reacting species, A and B, with one of the species carrying a positive or negative charge:

$$A^{+/-} + B \rightarrow products. \quad (1)$$

Such interaction may result in several reaction channels based on the individual properties of both reactants. Apart from elastic collisions and trivial non-elastic collisions, where reactants thermalize by adjustment of their vibrational and rotational excitation states, we are interested in reactions where reactants change their electronic states. This can lead to rearrangement of electron positions, leading to transfer of charge on the second particle, or eventually initiate atomic rearrangement leading to the formation of new products.

The formation of such products is described by the reaction rate coefficient, individual for each reaction path:

$$k_{\mathrm{exp}}(T) \sim k_{\mathrm{col}}(T)\omega(T), \quad (2)$$

where $k_{\mathrm{col}}(T)$ is the collisional rate of both reactants and $\omega(T)$ is the thermal reaction probability. While the collisional rate is a property shared between all possible reaction channels, depending on the collision cross-section between reactants, the thermal reaction probability is unique for each reaction channel, determined by its reaction potential. Therefore, both reaction kinetics and thermodynamics have to be considered.

Collision rate of ion – molecular reactions

The initial theory describing the interaction between ions and molecules was created by Langevin. [45] A moving charged particle generates an electric field, creating a long-range interaction via the formation of an induced dipole moment on a neutral molecule. The interaction potential between a point ion and spherical molecule at distance *r* takes the form:

$$V(r) = -\frac{1}{4\pi\varepsilon_0}\frac{\alpha q^2}{2r^4}, \tag{3}$$

where *q* represents the charge of the ion, α is the polarizability of the neutral molecule and ε_0 is the permittivity of the vacuum. The ion-molecular interaction potential decreases with distance (due to the r^{-4} term) much slower than classical Lennard-Jones' potential for neutral-neutral collision [46], influenced by Van der Vaal interaction (which decreases as r^{-6}). The crucial parameter is the polarizability (α), which will force the neutral to move towards the ion. Higher polarizability will directly lead to a stronger interaction between particles. The reaction cross-section of such interactions can be determined by a simple collision model as a function of relative ion velocity *v* [47], also referred to as the capture cross-section,

$$\sigma(v) = \frac{\pi}{v}\left(\frac{4\alpha q^2}{\mu}\right)^{1/2}, \tag{4}$$

where $\mu = m_1 m_2/(m_1 + m_2)$ represents the reduced mass of colliding particles, where m_1 stands for the ion mass and m_2 for the mass of the neutral molecule. This cross-section represents the associated area around the molecule on which a reaction will occur in the event of a collision. For Maxwellian distribution of particle velocities, the cross-section leads to the temperature-independent Langevin reaction rate coefficient:

$$k_L = \sqrt{\frac{\pi\alpha q^2}{\mu\varepsilon_0}}. \tag{5}$$

This reaction model may however only predict the ion-molecular interaction accurately for atomic ions reacting with small non-polar molecules.

For polar molecules containing permanent dipole moments, the shape of the interaction potential differs from Eq. 1. Charge-dipole potential depends on the angle, Θ, between

the vector of the permanent dipole moment relative to the mutual orientation of both interacting particles as:

$$V(r,\Theta) = -\frac{1}{4\pi\varepsilon_0}\frac{\alpha\mu_D}{2r^2}\cos\Theta, \tag{6}$$

where μ_D represents the value of the permanent dipole moment of the neutral molecule. The range of the potential is much greater as now it falls as a function of r^{-2}. For most ion-molecular interactions, both permeability and permanent dipole moment will be non-zero values. Thus, dipole forces cannot be ignored, and both potentials have to be considered. [48] The issue which surrounds modelling is that the mean value of the relative dipole orientation, Θ, depends on the specific molecular system and differs between molecules in a non-trivial way. Two main approaches have been developed to describe the effect of permanent dipole moments; the average dipole orientation (ADO) theory and the parametrised trajectory calculation.

The ADO theory uses a specific locking constant, *C*, to reflect the effect of the permanent dipole moment. Modelling of such systems shows that for Maxwell-Boltzmann distribution of relative velocities, the locking constant can be parametrised as a function of $\mu_D/\alpha^{1/2}$ for a temperature range 150 – 500 K. [49-51] Using this approach, the collision rate constant for the specific thermal energy is

$$k_{\mathrm{ADO}}(\mathrm{therm}) = \sqrt{\frac{\pi\alpha q^2}{\mu\varepsilon_0}} + \frac{C\mu_D q}{\varepsilon_0}\sqrt{\frac{1}{2\pi\mu k_B T}}. \tag{7}$$

Even for large values of dipole moment, the locking constant *C* does not exceed the value of 0.3. However, in such a situation, it may still enhance the rate constant by a factor of 2 to 4 compared to the Langevin reaction rate coefficient. Numerous experimental studies showed that even ADO theory tends to underestimate reaction rates by 10 – 25%. [52].

The parametrised trajectory calculation model's ion-molecular interactions via a series of classical trajectory calculations rather than looking for an exact interpretation of dipole interaction. The extensive modelling provided by Chesnavich, Su and Bowers show a good estimation of an upper bound for the true capture rate coefficients. [53] Assuming that the actual reaction rate is always lower or equal to the collisional or capture rate, the theory provides a good estimation of the upper reaction rate limit. The

capture rate coefficient was then parametrised by the quantity $K_{cap}(T_R, I^*)$, depending on the polarizability, α, and dipole moment, μ_D, of the neutral molecule

$$k_{\mathrm{cap}}(T) = k_L \times K_{cap}(T_{\mathrm{R}}, I^*),$$
$$T_{\mathrm{R}} = 4\pi\varepsilon_0 \frac{2\alpha k_{\mathrm{B}} T}{\mu_{\mathrm{D}}^2}, \quad (8)$$
$$I^* = \frac{\mu_D I}{\alpha q \mu},$$

where k_L is the Langevin reaction rate coefficient and I is the moment of inertia of the neutral molecule. [54]

Both theories can be applied to determine collisional rate coefficients, as they only require the available values of polarizability and permanent dipole moment. Nowadays, such values can be easily obtained by using density functional theory (DFT) calculations and thus the collisional rates can be estimated for a large number of molecules. [55]

Thermodynamics of ion-molecular reactions

Based on the thermodynamic properties of reagents, several reaction channels can be observed, as summarized in Table 1. At the low pressures (below 10 mbar), the most important are bimolecular reactions, as they are usually very fast and occur at rates comparable to the collisional rate. This is true if the chemical energy of the reaction sufficiently exceeds the specific reaction barrier. Such reactions are very important for chemical ionization as they occur in almost every single collision. Some reactions, however, may require a specific mutual orientation of reactants described by a steric factor, which is often much less than 1.

The reactions of positive ions can be divided into five main reaction channels (Table 1, a-e). Most of them can be supplemented by additional dissociation if the chemical potential is high enough to excite the molecule after ionization (into a repulsive state) and thus overcome the bounding energy which leads to dissociation.

Table 1 List of ion-molecular reactions used for CI.

	Reactants		Products	Condition
Positive CI				
a,	$A^{+\cdot} + B$	→	$B^{+\cdot} + A$	$IE(A) > IE(B)$
b,	$AH^+ + B$	→	$BH^+ + A$	$PA(B) > PA(A)$
c,	$A^{+\cdot} + BH$	→	$B^{+\cdot} + AH$	if exothermic
	$A^{+\cdot} + BR$	→	$B^+ + AR$	if exothermic
d,	$A^+ + B + C$	→	$AB^+ + C$	if exergonic
e,	$AL^+ + B$	→	$BL^+ + A$	if exergonic
Negative CI				
f,	$A^- + B$	→	$B^- + A$	EA(B) > EA(A)
g,	$A^- + BH$	→	$B^- + AH$	$PA(A^-) > PA(B^-)$
h,	$A^- + BL$	→	$B^- + AL$	if exergonic
i,	$A^- + B + C$	→	$AB^- + C$	if exergonic

The first typical process is a charge transfer (Table 1, a), where a cation radical $A^{+\cdot}$ takes an electron from a neutral molecule B, leaving molecule B ionised. The process is exothermic if the ionization energy of neutral B is lower than the recombination energy of the reactant ion, $A^{+\cdot}$. As reactions often occur at thermal conditions, only a negative difference in respective adiabatic ionization energies, IE(A) > IE(B) is required. In practical applications, the reaction is triggered by using ions of noble gases, as their IE exceeds most of the IE of other atoms and molecules. [56] $O_2^{+\cdot}$ ions are often used as they can be easily produced by a discharge in air, for which the IE(O_2) = 12.07 eV exceeds the IE of most organic molecules. [57] As the difference in ionization energies for both A and B often exceed 2 eV, reactions are frequently accompanied by the dissociation of the B^+ molecular ion. The dissociation pattern is very similar to electron ionization, as both reactions form an odd-electron molecular ion by removing the electron from the highest occupied molecular orbital (HOMO). The fragmentation rates will however differ as the energy distribution for charge transfer is strictly limited by the exothermicity of the process (usually 2-3 eV for the charge transfer which compares to 70 eV for electron ionization). The reaction rates for charge transfer are very dependent on the electronic and vibrational state of the

reactants, as the charge transfer (similar to electron ionization) abides by the Franck-Condon principle. If the electronic states of the reactant neutrals are accessible, the reaction will occur as a fast reaction with reaction rates close to the collisional rate. If not (i.e. HOMO is not accessible), the reaction will either form a long-lived intermediate complex where the reaction may be triggered after isotropic redistribution of energies or as more frequently seen, the reaction would result in elastic or non-elastic scattering (even though the reaction is exothermic). We will discuss this scenario later. In summary, in such a situation, the reaction rate is much slower than the collisional rate.

An additional process which is very characteristic for CI, is proton transfer (Table 1, b) from a conjugated base (AH^+) to a neutral base (B). The ability of a molecule to bind a proton is represented by its basicity, defined as the negative change of the Gibbs free energy (ΔG) when a neutral molecule accepts a proton. During the reaction, a proton is more likely to be attached to a base with higher associated basicity, while the reaction equilibrium rises with a larger basicity difference. However, as the transfer of a single proton from one base to another does not significantly change the entropy ($T\Delta S$), only the enthalpy change (ΔH) is usually important. The condition for successful proton transfer is for the proton affinity of the neutral molecule (B) to exceed the proton affinity of the neutral (A) currently binding the proton; PA(B) > PA(A). As the proton transfer does not face a potential barrier, the process will be spontaneous after the condition is fulfilled. A series of experiments showed that proton transfer is extremely efficient as the reaction rate almost equals the collisional rate, meaning that a reaction occurs on almost every single collision if the reaction is exothermic by at least 20 kJ/mol. [58] This makes proton transfer the most used CI process for analytical applications. A variety of reagent ions can be used, although should be chosen based on their PA and how easily they may be generated in a discharge. Initially, CH_5^+ together with $C_2H_5^+$ was used as reagent ions as they were easily generated by electron bombardment of methane gas in a discharge yielding approximately a 1:1 ratio. [44] The proton affinity of methane PA(CH_4) = 543.5 kJ/mol and ethylene PA(C_2H_4) = 680.5 kJ/mol were sufficient for proton transfer to almost all organic molecules. [57] However, the low PA of methane represents a significant chemical potential for most reactions as the PA of organic molecules is around 800 kJ/mol. [57] The energy difference of around 250 kJ/mol

(~2.6 eV) triggers the repulsive behaviour and molecules tend to dissociate. More consistent formation of protonated products can be achieved by hydronium (H_3O^+), easily generated in by discharge in pure water vapours. As PA(H_2O) = 691 kJ/mol [57], hydronium can protonate most organic molecules (except for light alkanes from methane to propane, and a few others), and the dissociation probability is significantly reduced. The last considered ion is NH_4^+, produced by discharge in pure ammonia gas. The use of NH_4^+ is however limited as the PA(NH_3) = 853.6 kJ/mol is above the PA of most organic molecules. It was shown that NH_4^+ can be used for the specific identification of some molecules, demonstrated when distinguishing between pinenes and 2-ethyl-3,5-dimethylpyrazine. [59] However, except for specific applications, the use of NH_4^+ as a proton donor is limited, as for most organic molecules it forms ion adducts via an association reaction. [60, 61]

The next process (Table 1, c**)** indicates a series of different ratio channels, where the reagent ion $A^{+\cdot}$ removes hydrogen or a radical R from the neutral molecule B. The molecule B then remains charged (although with a lighter mass due to the transferred radical, R, or the proton, H). The initial reagent ion becomes neutral as it reacts with the removed fragments. An example of such hydride ion abstractions is found in the reactions of unsaturated hydrocarbon ions with other hydrocarbons, such as $C_3H_5^+$ + neo-$C_5H_{12} \rightarrow C_5H_{11}^+ + C_3H_6$ [62]. However, hydrocarbon ions are not frequently used for analytical applications due to their rapid proton transfer to H_2O molecules, and therefore the reaction between hydrocarbons and NO^+ is of greater use. NO^+ may also induce hydrogen transfer on reaction with sample molecules by forming NOH when reacting with ethers [63], aldehydes [64], amines [65] and alcohols [66]. The hydrogen transfer reaction is determined by the difference in hydrogen affinity between the reagent ions and B (where BH is the neutral reactant molecule, as shown in Table 1). Again, if the reagent ion has a higher hydrogen affinity, the reaction is exothermic and can proceed.

In addition to hydride ion abstraction, more complex radicals from the neutral may be transferred onto the reagent ion. A typical example of this is found in the transfer of OH^- hydroxide ions which has been observed for alcohols [66] and diols [67]; or carboxylic acids [68] observed for hydronium (H_3O^+) and NO^+ reagent ions, respectively. For alcohols reacting with hydronium, the reaction results in the elimination of an additional H_2O neutral from the molecule, producing a dehydrated

ion (typical for heavier alcohols). For the NO^+ reagent ion, the reaction produces HNO_2 as a neutral product alongside the dehydrated molecular ion. This reaction is very important for the use of chemical ionisation in an analytical setting. This is because if this process is exothermic, then this reaction would most likely be dominant over other processes.

Last but not least, the association (or adduct formation) reaction (Table 1, d), where the colliding particles A^+ and B form a short-lived ion-neutral complex AB^{+*}, is discussed. The complex exists due to the presence of a resonance structure formed by a centrifugal barrier, as the charge can be partially located on both molecules. The complex can spontaneously dissociate back to its original form or be stabilized by the emission of a photon, or more likely in CI, by a collision with a third particle, C. The third particle removes part of the potential energy from the excited transition complex and acquires this energy itself, in the form of kinetic energy. The reaction complex may thus become bounded inside the barrier. The efficiency of the energy transfer during the collision depends on the reduced mass of the complex, as well as on the mass and the number of degrees of freedom of the C particle. The bound energy can be small or significantly high, depending on the type of the reactants defining the enthalpy and the entropy change between the free and bounded states. For hydronium, the enthalpy difference changes from 33 kJ/mol to 60 kJ/mol for the association reaction with non-polar CH_4 and CO_2, respectively. These differences reach up to 92 kJ/mol and 136 kJ/mol for the association reactions between hydronium with polar SO_2 and H_2O, respectively. [57] Polar molecules tend to form even larger structures, as the reaction complex after stabilisation may react with more neutrals, thus forming bigger clusters. However, the bound energy between elements of such a cluster decreases with each new neutral added to the cluster. The size of the cluster is based on the temperature and pressure of the gas, as larger clusters will spontaneously dissociate under thermal collisions with other molecules. The association rate drops rapidly for higher temperatures, as T^{-n}, where n ranges from 3-5. [69]

Association is a third-order reaction with the unit $cm^{-6}s^{-1}$. As the reaction often occurs in a drift or a flow tube at constant pressure and temperature, it is practical to consider this as an effective second-order reaction. As an example, for a carrier gas at 1.3 mbar and 300 K, the number density is $3.22x10^{16}$ cm^{-3}. A third-order association rate

constant of $1x10^{-25}$ cm^6s^{-1} corresponds to an effective second-order rate of $3.22x10^{-9}$ $cm^{-3}s^{-1}$.

Ligand switching (Table 1, e**)** is often not considered as a primary reaction channel, as it cannot proceed from the injected reagent ions. However, the reaction is important for its presence as a secondary process occurring in the ion–molecular system. The reaction often involves neutral or ionised clusters, from which one or more cluster ligands can be transferred to the other reactant. An example of this is when hydronium water clusters [70] react with organic molecules in the system:

$$H_3O^+ + H_2O + He \rightarrow H_3O^+.H_2O + He, \quad (9a)$$

$$H_3O^+H_2O + M \leftrightarrow M.H_3O^+ + H_2O. \quad (9b)$$

The thermochemistry of the process (9b) depends primarily on the different affinity of the transferred ligand (H_3O^+ affinity in the present example). However, as the reaction system contains many molecules, the change in entropy becomes significant. Therefore, describing the reaction only as the difference in particular affinities (otherwise sufficient for proton transfer reactions) is not possible and the total Gibbs free energy must be considered. Additionally, in practical applications, the fact that the reaction is exergonic or endergonic does not necessarily define the reaction equilibrium. That is mainly established by the difference in the number densities of particular neutrals. In typical analytical applications, the number density of the H_2O is six orders of magnitude higher than the number density of the organic molecule, M. Therefore, the reaction will run heavily in favour of hydronium cluster production even if the process is endergonic, as seen in the case of the reaction between formaldehyde and hydronium clusters. [71, 72]

Finally, it is necessary to mention reactions which involve negative ions. However, as we have not used negative ions in the present work, we will only briefly summarize some important reactions. In the environment, negative ions may naturally occur in the upper level of atmosphere as free electrons (generated by solar radiation) are captured by surrounding molecules. [73] Therefore, the study of molecular reactions with negative ions is highly relevant to the ion chemistry of planetary atmospheres in our solar system. [74-76] For analytical applications, using negative ions as reagents are not as popular as positive ions. This is because reactions involving negative ions are more selective and thus are not universal for all applications. However, they can serve

as a beneficial supplement to the analysis with positive ions as well as be used for the analysis of specific molecules (especially halogenated molecules).

A set of four of the most important reactions is listed in Table 1, f-i. Electron transfer (or charge exchange) (f) is the reaction equivalent to the charge transfer reaction observed for positive ions. The exothermicity of the process is defined by the difference between the electron affinity (EA) of the reacting molecules. If the EA of the neutral molecule (B) is greater than the EA of the reacting molecular ion in the neutral state (A), the process is exothermic and may proceed. In the stable negative ion, the electron is captured in the Feshbach resonance state and occupies the lowest unoccupied molecular orbital (LUMO) of the neutral molecule. This electron state is usually easily accessible and the reaction may proceed at the reaction rate close to the collisional rate. However, if the difference between the geometries of the neutral molecule and the negative ion is too great, the reaction rate may be reduced. This is due to the formation of a potential barrier as the neutral reagent becomes ionised. [77]

All remaining reactions share many similarities with the reactions of positive ions. For proton transfer reaction (Table 1, g), exothermicity depends on the difference between the respective PAs of the negative ions, A^- and B^-. If the PA of A^- is greater than the PA of B^-, the proton will be transferred from BH on A^-, leaving the B^- ion. The reaction rate behaves similar to positive proton transfer. If the PA difference is above 10 $kcal.mol^{-1}$, the reaction rate becomes almost identical to the collisional rate. [69] This, however, may not be true for the anions where electrons are delocalized. [78] The ligand switching (or the displacement reaction) (Table 1, h) will proceed in the absence of the effective proton transfer reaction if the displacement process is exothermic. An interesting example is the reaction of OH^- with CH_3CN, where a displacement of CN^- is suppressed by proton transfer. [79] Finally, association (Table 1, i), as a third-order reaction, is also common for negative ions, especially in the presence of polar molecules. The mechanism and reaction rate are comparable with the equivalent association for positive ions.

In conclusion, molecular ions react with neutral molecules in various ways, based on the thermodynamic and physical properties of the reaction system. The effect of the physical parameters (i.e. gas temperature) was not discussed carefully in this chapter, as we will focus on it later in the work. However, it may be seen that ion products of

the reactions carry information about the neutral reactant (M) on the formation of ions such as M^+, $(M+H)^+$, $(M-H)^+$, that can be detected using mass spectrometry. The presence of such ions can be thus used to retrospectively determine the presence of the neutral reactant M in the system. This fact led to the development of chemical ionization mass spectrometry (CI-MS). Unlike electron ionization mass spectrometry (EI-MS) often used for analytical applications, CI-MS cannot provide useful information about molecular structure due to a lack of fragmentation of molecules. However, a small amount of reaction products that are closely related to the neutral reactants can be effectively used to analyse complex molecular systems containing several molecules.

The effect of an external electric field

So far, we have described various types of ion molecular reactions and collisional reaction rates for thermalized systems. The energy distribution of the internal energy states, as well as the kinetic energy of all involved particles, is defined by the gas temperature. Most laboratory applications occur at temperatures around 300 K and below, thus we may assume all involved particles are presented in their ground energetic states. In such a situation it is easy to determine or predict the reactions, as we can simply compare important thermodynamic parameters of reactants and products and assume the thermodynamic availability of the selected process (for example difference in proton affinity of ionization energy) and also determine the collisional rate, representing the upper limit for the reaction rate.

The Boltzmann distribution may however be disrupted by external factors. One practical example is the injection of ions from an ion source into the reactor. Ions are often generated in a discharge – an energy-dense environment – from where they can preserve a range of electronically excited states. The high internal energy of such excited ions has to be first dissipated into the gas via (in the best scenario) inelastic collisions for the ion to be thermalized. Until that point, excited ions carry much more chemical energy and classical determination of the collisional rate nor the determination of the thermodynamic availability may be applied. In most applications, this effect is not significant as instrumental design tends to avoid or minimize such situations by letting ions “relax” and thermalize before reacting with molecules of interest.

The external electric field is an additional source of potential disruption. In the presence of an electric field, ions in the gas phase accelerate along the vector of the electric field, E. Collisions with gas molecules cause ions to maintain a mean ion drift velocity, v_d, characterized by ion mobility, μ, as:

$$v_d = \mu E. \tag{10}$$

For low electric fields (comparable to or below the thermal velocity), the ion mobility is constant. However, for higher electric fields it acquires a non-linear form:

$$\mu(E) = \mu(0)[1 + \alpha_1(E/N)^2 + \alpha_2(E/N)^4 + \cdots] \tag{11}$$

The ion mobility depends on a collisional cross-section between ions and a buffer gas but is also highly sensitive on gas pressure and temperature. Determination of ion drift velocity, as well as ion mobility, is important for the calculation of ion transit time through the drift tube. Both parameters can be obtained by their direct measurement in the drift tube if the apparatus is capable of generating short pulses of ions entering the drift tube. Alternatively, ion mobility can be found in the literature [80-82] for the most common ions, from which the drift velocity may be calculated.

Increased ion velocity has a direct effect on the kinetic energy of the ion and thus on the reaction cross-section. Collisions of ions with neutrals thus do not occur at thermal energies. To describe this effect, we defined the mean collisional energy (KE_{CM}) as the relative kinetic energy available for the reaction process at the centre-of-mass, which is related to the two interacting particles through:

$$KE_{CM} = \frac{1}{2}\left(\frac{m_n m_{ion}}{m_n + m_{ion}}\right)(v_{ion}^2 + v_n^2), \tag{12}$$

where m_{ion} and m_n refer to the mass of the colliding ion and neutral. The v_{ion} and v_n represent the mean velocities of the colliding ion and neutral at the centre-of-mass, respectively defined as:

$$\frac{1}{2}m_i v_{ion}^2 = KE_{ion}, \tag{13}$$

$$\frac{1}{2}m_n v_n^2 = \frac{3}{2}k_B T. \tag{14}$$

Eq. 12 is then often expressed in a more convenient form

$$KE_{CM} = \frac{m_n}{m_n + m_{ion}}\left(KE_{ion} - \frac{3}{2}k_B T\right) + \frac{3}{2}k_B T. \tag{15}$$

The ion reactions often take place in a system where the analyte molecule is diluted in a buffer (or carrier) gas. The reagent ions thus mainly collide with the buffer gas molecules, while the main interest is to describe the reaction with the analyte. The kinetic energy of the reagent ion is thus characterised by the mass of the buffer gas, m_b, and can be calculated from its drift velocity using the Wannier formula [83]:

$$KE_{ion} = \frac{3}{2}k_B T + \frac{1}{2}m_{ion}v_d^2 + \frac{1}{2}m_b v_d^2. \quad (16)$$

The KE_{CM} can be thus defined for collisions with both buffer gas, $KE_{CM,b}$, and the analyte (neutral reactant), $KE_{CM,r}$:

$$KE_{CM,b} = \frac{m_b}{m_b + m_{ion}}\left(KE_{ion} - \frac{3}{2}k_B T\right) + \frac{3}{2}k_B T, \quad (17)$$

$$KE_{CM,r} = \frac{m_r}{m_r + m_{ion}}\left(KE_{ion} - \frac{3}{2}k_B T\right) + \frac{3}{2}k_B T, \quad (18)$$

where m_r represents the mass of the neutral reactant molecule. The $KM_{CM,b}$ is related to the internal excitation of the reagent ions. An increase of the $KM_{CM,b}$ over the thermal energy causes a redistribution of the rotational and vibrational equilibrium into energetically higher states, resulting in a change in ion reactivity. The $KM_{CM,r}$ then represents the translational collision energy of the reagent ion with the analyte.

The energy transfer at the centre-of-mass depends on the mass of the neutral particle and is less effective for lighter neutral reactants (see Figure 1). For the reaction of hydronium (*m/z* 19) with helium (4 amu) and argon (40 amu), the mass coefficient is 0.17 and 0.68, respectively. This rapid increase in the effectivity of energy transfer, however, is not that significant, due to ion mobility and thus an ion mean drift velocity decrease for a heavier buffer gas. At this point, it would be convenient to recap on the situation introduced previously, where ions were injected from the ion source into the buffer gas. In such a situation, the mean velocity of the particle is defined by the potential difference between the ion source and the reaction region (and may achieve several eV). Reagent ions in the injection region, before deceleration, collide with the buffer gas regardless of ion mobility. The mass of the buffer gas molecules thus significantly influences the collisional energy.

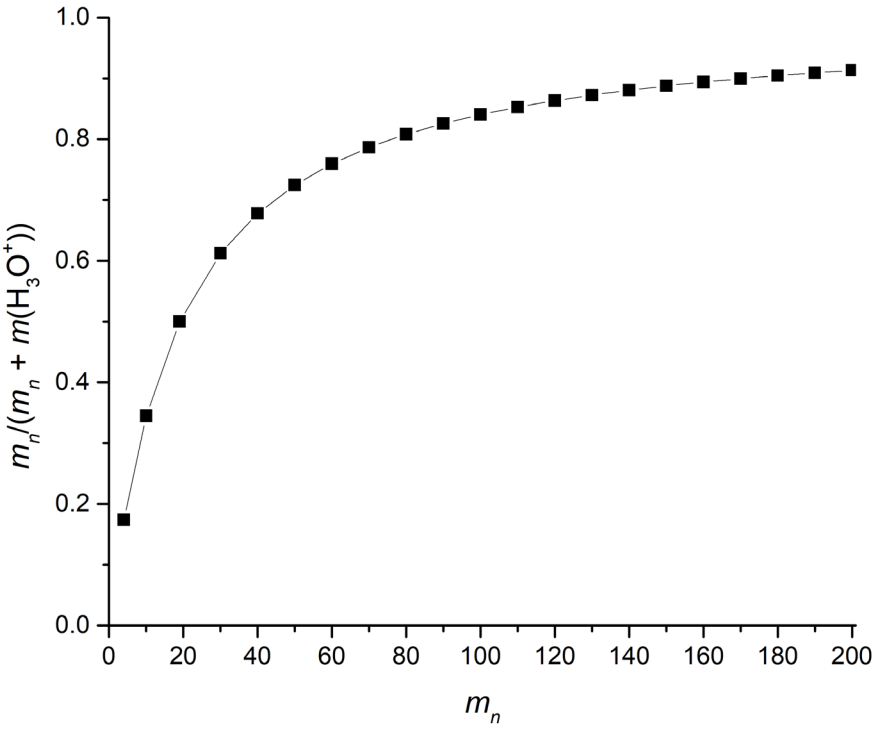

Figure 1 The mass coefficient for conversion of the laboratory ion kinetic energy into the centre-of-mass collisional energy (see Eq. 15). The profile represents the energy conversion for the hydronium ion colliding with neutrals from 4 up to 200 amu.

The $KM_{CM,r}$ is a crucial parameter for ion-molecular reactions and describes the amount of translational energy in addition to the internal chemical energy which is available for that particular reaction. This significantly affects the thermodynamics of the reaction as well as the reaction cross-sections. To visualize this effect, we may consider the typical drift velocity of hydronium in PTR-MS (see Section 1.2), of 995 ms^{-1}. The translational collisional energy with neutral particles of molar mass 30 g/mol, 60 g/mol and 100 g/mol is 0.19 eV, 0.35 eV and 0.55 eV, respectively. At the temperature T = 300 K, the mean thermal energy is 0.039 eV. The collisional energy may exceed the average thermal energy and thus significantly affect ion-molecular reactions. The increase in the reaction energy affects both the collisional cross-section as well as the thermodynamics of individual reactions and thus the reaction cross-section.

The influence of an electric field (and therefore KM_{CM}) on the collisional rate was in most cases determined indirectly. Assuming Maxwellian ion velocity distribution, we can define an effective temperature of the system, T_{eff}, as:

$$\frac{3}{2}k_B T_{eff} = KE_{ion} = \frac{3}{2}k_B T + \frac{1}{2}m_{ion}v_d^2 + \frac{1}{2}m_b v_d^2. \tag{19}$$

Thus, T_{eff} is the kinetic temperature corresponding to three degrees of freedom in the centre-of-mass system of the ion and reactant molecule, where the first term represents the thermal energy; the second term represents the energy absorbed from the field which is converted into the ion drift motion; and the last term represents the energy of random motion from collisions with gas molecules. [21, 84] This assumption allows us to simplify the reaction rate function from $k(T, E, p)$ to $k(T_{\text{eff}})$. It should however be stressed that Eq. 19 represents only the first-order approximation, derived by Wannier. [83] The higher orders of Eq. 19 are usually ignored, as their effect on the calculated value is below 15%. [84] The conclusions also apply only to an atomic ion drifting in an atomic buffer gas, where internal excitations do not affect reactions.

Looking back at the Langevin reaction rate coefficient, k_L, (Eq. 5), we see that it is temperature independent. Thus, the collisional rate of non-polar molecules is not affected by elevated collisional energy. For polar molecules, the ADO theory, Eq. 7, predicts the temperature dependence as $T^{-1/2}$. Su [85] also developed a parametric representation of the ion-polar molecular collision rate for kinetic energy dependence, where:

$$\begin{aligned} k_{\text{cap}} &= k_L \times K_c(\tau, \varepsilon), \\ \tau &= \frac{\mu_D}{\sqrt{\alpha T}}, \\ \epsilon &= \frac{\mu_D}{\sqrt{\alpha KE_{cm}}}. \end{aligned} \tag{20}$$

The parametric representation of Su was tested for the rotational temperature T up to 1000 K and KE_{cm} up to several eV, achieving good agreement with available experimental data. Additionally, Su concluded that the parametric representation is sufficient without introducing the dipole–induced dipole potential. [86] A trajectory calculation approach may also be used, but good agreement with experimental data has only been reported at low temperatures and low relative kinetic energies. [87] In conclusion, all theories predict the reduction of the collisional reaction rate for polar

molecules, as KE_{cm} increases as a function of $T_{eff}^{-1/2}$, or eventually with a slightly faster reduction when also considering higher orders of Eq. 19.

The reaction rate however differs from the collisional rate and the dependence on KE_{cm} and T_{eff} changes with the type of reaction. Multiple studies can be found investigating ion molecular reaction rates under variable electric fields, or more frequently, under variable gas temperatures. Also, reactions shall be divided into several sub-categories, reflecting the different natures of ion-molecular reactions which include whether the reaction is exothermic or endothermic; slow or fast (compare to collisional rate); unimolecular or bimolecular; and if ions react with non-polar or polar neutrals.

The most common are bimolecular reactions:

$$A^+ + B \leftrightarrow AB^{*+} \rightarrow \text{products.} \quad (21)$$

Fast bimolecular reactions are exothermic, proceeding at reaction rates close to the collisional rate. The distribution and stabilisation of atoms and charge in the formed AB^{*+} nascent complex have to occur rapidly. A good example is a charge or proton transfer, that is very rapid and can effectively proceed even as the interaction time (the time interval for when both reactants are in close proximity to each other and a reaction can occur) decreases due to increased relative ion velocity. These reactions follow the profile of the collisional reaction rate, thus there is no thermal dependence for non-polar neutral reactants and small negative temperature dependence for polar molecules, as predicted by theory. [73] As an example, we may choose a dissociative charge transfer reaction $He^+ + N_2 \rightarrow N^+ + N + He$ with a reaction rate 1.5 x 10^{-9} cm^3s^{-1} and with no thermal dependence [88-90]. Also, the proton transfer reaction $N_2H^+ + CH_4$ with a reaction 1.3 x 10^{-9} cm^3s^{-1} shows no thermal dependence. [91] For polar reactants, the exothermic proton transfer reaction $N_2H^+ + CH_3CHOH$ follows the negative thermal dependence as predicted by ADO theory. [91]

Slow bimolecular reactions have reaction rates significantly lower than the collisional rate, even at normal laboratory temperatures. This may occur when a reaction is endothermic (or endogenic) and thus an energetic barrier is present. The thermal dependence of a reaction rate consists of a combination of collisional rate thermal dependence and the Arrhenius function, describing the increase of reactivity when temperatures or collisional energies close the difference in the activation energy:

$$k_r = k_{cap} \times exp\left(-\frac{E_a}{k_B T_{eff}}\right). \quad (22)$$

The reaction rate of such a reaction may have negative thermal dependence (at the beginning); however, it will change into positive thermal dependence when the reaction channel starts to open up as the translational or internal energy of the reactant can overcome the reaction barrier. After the reaction channel opens, the reaction becomes fast. An example is the charge transfer reaction $CO_2^+ + O_2$ which has a negative thermal dependence on reaction rate up to 740K, where it changes into a positive thermal dependence. [92]

Some reactions are however slow naturally. A reaction may become less effective when a reagent ion is excited from its ground vibrational state (due to collisions with buffer gas, Eq. 17) or when the reverse reaction channel occurs faster than the forward reaction, transferring the products back into the reactants. This may happen for reactions of small molecules with high exothermicity, while the nascent reaction intermediate AB^{*+} does not have an accessibly fast reaction potential towards new products. In other words, the nascent intermediate requires a longer period of time to rearrange the electronic or atomic distribution. The lifetime of the nascent intermediate must be long enough to allow for the statistical redistribution of energy into all degrees of freedom and thus favour the most exothermic channel. However, the lifetime of the nascent intermediate decreases with the total energy. Thus, an increase in the translational energy results in a higher probability of elastic scattering

$$A^+ + B \rightarrow AB^{*+} \rightarrow A^+ + B. \quad (23)$$

An example of this is the charge transfer reaction $O^+ + O_2$, where the reaction rate was estimated to be $3.4 \times 10^{-15} \times T^{-0.48}$. [93, 94]

The thermal dependence for slow reaction, however, does not necessarily follow the $T^{-1/2}$ profile. Often, the exponent is much larger than 0.5. This can happen if, for example, during processes involving the exchange or relocation of massive particles. The proton transfer reaction of $t\text{-}C_4H_9^+$ conversion to benzyl acetate follows a temperature dependence from T^{-6} to T^{-10}. [95] Also, for the proton transfer from CH_4D^+ to CH_4, the data suggest a thermal dependence of T^{-8}. [96, 97] Similar thermal profiles can be found also for association reactions, where in the first reaction step a nascent intermediate is also formed, followed by its stabilisation via collision with a third particle. [73]

$$A^+ + B \rightarrow AB^{*+},$$
$$AB^{*+} + M \rightarrow AB^+ + M. \quad (24)$$

As an example, the association reaction $N_2^+ + 2N_2$ forming $N_4^+ + N_2$ proceeds with a third-order rate constant of 8 x 10^{-29} cm^6s^{-1} at 300 K, (while following a thermal dependence of T^{-4}). [98]

H^- transfer reactions are unique to certain processes, an example being *s*-$C_3H_7^+$ + *i*-$C_4H_{10} \rightarrow C_3H_8 + C_4H_9^+$, which requires little or no activation energy. These reactions occur rapidly at low temperatures, but after a critical temperature, a strong negative thermal dependence ranging from $T^{-1.5}$ to $T^{-6.8}$ appears. [91, 99] The exponent is smaller for the increasing exothermicity of the reaction.

The strong thermal dependence originates in the presence of the nascent intermediate AB^{*+} and a long reaction time. These reactions thus need to be thought of as unimolecular decompositions of the ions. For H^- transfer reactions, the authors used transition state theory (TST) to explain the negative thermal profile. [91, 100] The TST is however used to describe the neutral chemical reactions in the presence of activation energy. In the general TST, the forward reaction rate constant takes the Eyring form:

$$k_f = \kappa \frac{kT}{h} \frac{Q_{tr}^{\ddagger} Q_{rot}^{\ddagger} Q_{vib}^{\ddagger} Q_{elec}^{\ddagger}}{\prod_{i=1}^{n} (Q_i)_{tr} (Q_i)_{rot} (Q_i)_{vib} (Q_i)_{elec}} exp\left(\frac{-E_a}{kT}\right), \quad (25)$$

where κ is the transmission coefficient, $Q^{\ddagger}$ and Q_i are the respective partition functions for the transition complex AB^{*+} and the reactants, respectively. Assuming the activation energy is negligible, the exponential factor is unity. The influence of electronic and vibrational terms may be neglected at moderate temperatures. Thus, the forward rate constant may be expressed as:

$$k_f = CT \frac{\left(T_{trans}^{\ddagger}\right)^{3/2} \left(T_{rot}^{\ddagger}\right)^{3/2}}{\prod (T_{trans})^{3/2} (T_{rot})^{3/2}} T_{int.rot}^{-r/2} = CT^{-\left(2+\frac{r}{2}\right)}, \quad (26)$$

where *r* represents the change in the number of internal rotations upon the formation of the transient complex and *C* is a constant. Note that the exponent of 3/2 in the rotational temperature terms is for nonlinear molecules, whereas for linear molecules a 2/2 exponent is used. The *r* term may be positive or negative if more or less internal rotors are hindered upon the formation of the complex compared to new internal rotors formed in the process. The TST represents a simple explanation, that follows the observed T^{-n} profile of thermal dependence and explains the changes in reaction rates

for changing complexity of the reactions. However, the TST does not account for changes in the exothermicity or the kinetic parameters. [73]

The more universal approach to this problem is the application of RRK [101] or RRKM [102] theory. Their theories represent a semi-classical approach to unimolecular decomposition of transient ion species, first described by Rice-Ramsperger-Kassel and later reformulated by Marcus-Rice. Both theories assume that the molecule behaves as a harmonic oscillator with Boltzmann energy distribution. The molecule may undergo unimolecular decomposition when the critical energy, ε_0, is achieved, allowing the molecule to isomerize into a transition complex, $X^{\ddagger}$, of which decomposition is inevitable: $X^{*} \leftrightarrow X^{\ddagger} \rightarrow$ *products*. Also, the distribution of energy between oscillators is much faster than the reaction itself.

Kassel (RRK theory, [101]) assumes a system of s classical harmonic oscillators (s = $3n$-6 for non-linear molecules, where n represents the number of atoms). The distribution function in such discrete systems at a given energy, ε, takes the form:

$$P(\varepsilon) = \frac{\varepsilon^{s-1}}{(kT)^{s}} \frac{exp(-\varepsilon/kT)}{(s-1)!}. \tag{27}$$

The energy-dependent microscopic rate constant for decomposition is

$$k(\varepsilon) = A\left(\frac{\varepsilon - \varepsilon_0}{\varepsilon}\right)^{s-1}, \tag{28}$$

where ε_0 is the zero-point energy difference between $X^{\ddagger}$ and X^{*}, $\varepsilon_0 = \varepsilon_{ZPE}(X^{\ddagger}) - \varepsilon_{ZPE}(X^{*})$, ε is the excitation energy of X^{*} and A is a constant factor representing the lifetime of the transition complex, in the order of magnitude of the vibrational frequency. [103]

Marcus (RRKM theory, [102]) assumes that the density of energy states in the excited complex X^{*} is high, so the distribution function is continuous. In addition, only a few vibrational states of the transient complex $X^{\ddagger}$ (located above the threshold) need to be considered. Also, the initial energy ε of the excited complex X^{*} is distributed between the vibrational energy $\varepsilon^{\ddagger}_{v}$ and the reaction coordinate translational energy $\varepsilon^{\ddagger}_{t}$ of the transient complex $X^{\ddagger}$: $\varepsilon - \varepsilon_0 = \varepsilon^{\ddagger} = \varepsilon^{\ddagger}_{v} + \varepsilon^{\ddagger}_{t}$. The reaction thus proceeds as $X^{*}(\varepsilon) \leftrightarrow X^{\ddagger}(\varepsilon^{\ddagger}_{v}) \rightarrow$ *products*, where the microscopic rate constant k is a function of $f(\varepsilon, \varepsilon^{\ddagger}_{v})$. In such systems, the distribution function takes the form:

$$P(\varepsilon) = \frac{\Omega(\varepsilon)}{Q} exp(-\varepsilon/kT), \tag{29}$$

and the energy-dependent microscopic rate constant for decomposition is:

$$k(\varepsilon) = \sum_{0 \le \varepsilon_v^{\ddagger} \le \varepsilon^{\ddagger}} \frac{1}{h\Omega(\varepsilon)} = \frac{1}{h} \frac{W(\varepsilon_v^{\ddagger})}{\Omega(\varepsilon)}, \tag{30}$$

where Q represents the corresponding partition function, $\Omega(\varepsilon)$ is the density of the considered active vibrational (or rotational) states per unit of energy at energy ε; and $W(\varepsilon^{\ddagger}_v)$ is the total number of active states in the transient complex in the energy range ε - ε_0. [103]

It is important to point out that the RRKM approach is better, mainly in the near-threshold region. [103] Furthermore, in the RRK theory, the s parameter is often not consistent. [104] Moreover, both previous forms of the microscopic rate constant (Eyring and Kassel forms, Eq. 25 and Eq. 28) can be reduced from the Marcus representation. The reader may thus ask why we have also discussed these previous theories? Both Eyring and Kassel forms are good first-order approximations. Both clearly indicate a trend with increasing temperature, which is not obvious in the Marcus representation.

Considering an association reaction

$$\mathrm{A^+ + B} \underset{k_{-1}}{\overset{k_1}{\longleftrightarrow}} \mathrm{AB^{+*}}, \quad \mathrm{AB^{+*} + M} \overset{k_2}{\rightarrow} \mathrm{AB^+ + M}, \tag{31}$$

the forward reaction rate takes the form

$$k_f = \frac{k_1 k_2 [\mathrm{M}]}{k_{-1} + k_2 [\mathrm{M}]}, \tag{32}$$

which at low pressures ($k_{-1} >> k_s[\mathrm{M}]$) reduces to:

$$k_f = \frac{k_1 k_2}{k_{-1}} [M]. \tag{33}$$

Considering the substitution $\varepsilon - \varepsilon_0 = \varepsilon^{\ddagger} = rkT$ for r squared terms contributing to the internal energy of the transient complex $\mathrm{AB^{+*}}$; and $\varepsilon_0 = D_e$ to represent the dissociation energy of $\mathrm{AB^{+*}}$, Eq. 28 may be integrated into Eq. 33 as:

$$k_f = k_1 k_2 [M] \left(\frac{rkT}{D_e + rkT} \right)^{-(s-1)}, \tag{34}$$

for which the approximation $D_e >> rkT$, may be applied, assuming the reaction rates k_1 and k_2 do not significantly depend on T:

$$k_f = k_1 k_2 [M] \left(\frac{rkT}{D_e}\right)^{-(s-1)} \sim CT^{-n}. \quad (35)$$

Clearly, this interpretation uses several assumptions. Also, contributions from the rotational excitations may be significant. However, processes lacking a fast reaction channel will undergo a unimolecular decomposition back to the reactants with a temperature dependence T^{-n}, where n depends on the degrees of freedom in the produced transient complex.

In this extensive discussion, we should finally compare how the predicted profiles of temperature-dependent rate coefficients apply to ion molecular reactions under the presence of an electric field. In the typical application, the ion translational energy is between 0.04 eV up to (1-2) eV.

For fast ion-molecular reactions characterised by the lack of the internal energy barrier, there is no significant dependence of the reaction rate on EK_{CM}. [105, 106] This includes fast charge transfer reactions as well as fast proton transfer reactions with the exothermicity above 10 kJ/mol. Reactions thus follow the expected profiles of the collision rate. As an example, we can present the study of Lindinger et al. [107], studying the reactions of metastable $O_2^+(a\ ^4\Pi_u)$ with N_2, Ar, H_2, O_2. All reaction rates are close to Langevin collisional rate. The proton transfer reaction $H_3O^+ + CH_2O$ studied by Hansel et al. follows a steady decay expected for the interaction of polar molecules. [108] Some reactions have, however, even positive trends where the reaction rate overcomes the Langevin limit. [105] This interesting behaviour was discussed by Smith et al. [109], showing that at sufficiently high energies the shape of the interaction potential described by Langevin (Eq. 5) changes into a hard-spherical potential, leading to a $k_c \sim T^{1/2}$ profile of collision rate.

In practical applications for trace gas analysis, proton transfer reactions that are exothermic at zero-field conditions are affected only minimally, as the higher relative kinetic energy results in a minor decrease of the collisional cross-section. However, added collisional energy may open new reaction channels that were not previously possible due to lower PA. For example, propane or i-butane both have PA values lower than that of water (PA(propane) = 6.49 eV, PA(i-butane) = 7.03 eV, PA(water) =

7.16 eV, from [57]) and in flow tube experiments do not react with hydronium. In the presence of an electric field, however, the reaction is possible. Furthermore, the increased collisional energy opens new and changes existing dissociation channels, mainly for more complex molecules. For example, hydronium reacting with 3-pentanone at zero-field conditions in SIFT-MS produces only a protonated 3-pentanone ($C_5H_{11}O^+$) molecule [64], while in PTR-MS at 140 Td, 20 % of the protonated 3-pentanone dissociates into $C_2H_5O^+$ [110]. A similar conclusion applies to charge transfer reactions. Fast charge transfer reactions between reagent ions and neural analyte molecules remain stable. The increased collisional energy, however, may also open new dissociative channels. The profile of dissociative channels will then follow the Arrhenius form.

For slow ion-molecular reactions, the negative energy dependence was of course also observed, following the previous assumption of transient complex formation. However, some differences need to be discussed. Typically, the reaction rate profile for ion-molecular processes follows a "U" shape. Initially decreasing, following the power-law profile of $EK_{CM}{}^{-n}$ and after reaching the reaction rate minimum, the reactivity increases. This character was observed for many reactions, where the formation of an intermediate complex is expected. [105] For very low temperatures, reaction rates reach the collisional rate. However, an increase in temperature results in negative energy dependence. The negative energy dependence is present until the lifetime of the transient complex is above the typical vibrational time constant. If the lifetime of the transient complex is shorter, then there is no sufficient statistical randomisation of the energy between vibrational modes. This induces a change in the energy from an isotropic to an anisotropic distribution and in turn causes a change in the reaction mechanism, resulting in the opening of a new ("direct") reaction channel. [19] In other words, the generated reaction potential has a double-minima shape, where one minimum generates a "loose" complex and the second minimum a "tight" complex. For low energy interaction, the long-lived "loose" complex is formed and is sensitive to unimolecular decomposition. However, after reaction energy exceeds the central barrier between the two states and a "tight" complex is formed, this results in the opening of a new reaction channel. [106] This behaviour can be practically demonstrated by the work of Glosik et al. [111], who studied the reactions of several ions with an HCl molecule as a function of the centre-of-mass energy. Reactions

forming intermediate complexes, showing transitions from the "loose" to the "tight" arrangement in the studied energy range, were described as a combination of two independent reaction channels, I and II, where the total reaction rate may be described as:

$$k(KE_{CM}) = k_I + k_{II} = k_1 \frac{1}{1 + \left(\frac{KE_{CM}}{KE_{CM,1}}\right)^m} + k_{II,0} \exp\left[\frac{-\Delta E_a}{(2/3\, KE_{CM})}\right]. \quad (36)$$

In this interpretation, k_I represents the low energy reaction rate for the indirect process forming the "loose" complex and $k_{II,0}$ represents the total reaction rate for the direct process proceeding via the formation of the "tight" complex. The power dependence of k_I originates from the assumption [105]:

$$\frac{k_1}{k_{-1}} = \left(\frac{KE_{CM}}{KE_{CM,1}}\right)^m, \quad (37)$$

where m is a constant exponent describing the unimolecular decomposition and $KE_{CM,1}$ is the value of energy where $k_1 = k_{-1}$. This concept was afterwards also implemented in several of the following studies. [112, 113]

The parameter, m, can be found by interpolating experimental data using a $\log(k_{-1}/k_f - 1)$ versus $\log(KE_{CM})$ plot. To obtain a predicted value of m, the Eyring form (Eq. 26) is frequently used [114] and considers the total forward reaction rate:

$$k_f = f k_c \frac{Q^{\ddagger}(\mathrm{AB}^{+*})}{Q_{rel} Q_{rot}(\mathrm{A}^{+}) Q_{rot}(\mathrm{B})} \sim \frac{T_c^{r_c/2}}{T_t^{3/2} T_i^{r_i/2} T_n^{r_n/2}}, \quad (38)$$

where $Q^{\ddagger}$ and Q represent partition functions of the intermediate complex and the reactants, respectively. In the final notation, the translational temperature is T_t; the temperature of the reaction complex is T_c; the reaction ion temperature is T_i; the reaction neutral temperature is T_n. Also, r_c, r_i and r_n refer to the respective number of rotational degrees of freedom. We discuss before that the Eyring interpretation is not a correct approach to unimolecular dissociation, however, some important conclusions about ion-molecular interactions should be pointed out. For thermalized systems (under isotropic energy distribution) the reaction rate should decay as a function of $T^{-r/2}$, considering only rotational excitation (and as $T^{-(r/2+2)}$ considering also vibrational modes, Eq. 26). Under the presence of an electric field, the translational temperature

is mainly determined by $EK_{CM,r}$ (Eq. 18), $3/2kT_t = EK_{CM,r}$. The temperature of reaction neutrals, T_n, is represented by the true temperature of the gas, T, and the temperature of reaction ions is determined by the centre-of-mass energy between ions and the buffer gas $EK_{CM,b}$ (Eq. 17), $3/2kT_i = EK_{CM,b}$. [114] The temperature of the transient complex, T_c, can originate in all related forms of energy, thus we have to consider the major contributor. In the drift field, T_t and T_i will be larger than T_n. Thus, the reaction will be mainly driven by direct collision via the translational energy, $EK_{CM,r}$, or via the internal excitation of the reagent ion, $EK_{CM,b}$. Both parameters depend on the type of reaction neutral as well as the buffer gas. For example, the reaction of CH_3^+ with N_2 in He buffer gas results in $EK_{CM,r} > EK_{CM,b}$ (as mass $m(N_2) > m(He)$) and T_c is mainly determined by T_t. However, for the same reaction with H_2 instead of N_2, $EK_{CM,r} < EK_{CM,b}$ and T_c are mainly determined by T_i. This leads to the cancellation of the temperature component in Eq. 38. Therefore (considering the three rotational degrees of freedom for CH_3^+) $k_f \sim EK_{CM,b}^{-3/2}$ is associated with this particular reaction for N_2; and $k_f \sim EK_{CM,r}^{-3/2}$ is associated with this reaction with H_2. The change in the characteristics of this reaction was also observed experimentally. [114] Similar results were shown by Glosik et al. who studied the reaction of CH_3^+ with HCl in He and Ar buffer gas. [115] In He buffer gas $EK_{CM,r} > EK_{CM,b}$, whereas in the Ar buffer gas $EK_{CM,r} \approx EK_{CM,b}$. The study showed that the reaction in He buffer gas followed the power law of $k_f \sim EK_{CM,b}^{-1.7}$, whereas the field-free variable temperature found in the SIFT study depended on the "true" temperature, T, as a result of $k_f \sim T^{-2.1}$. The predicted value of the exponent (Eq. 38, not considering vibrational excitation) m = -2.5, close to the thermal studies. Comparing the effect of He and Ar buffer gases, the authors showed that for the same value of $EK_{CM,r}$ (and thus T_t), the reaction rate for the Ar buffer gas is larger than for the He buffer gas. This is a significant observation as the total reaction energy (sum of the internal and translation energy) in the Ar buffer gas is higher than in He. In our theoretical discussion above, we assumed isotropic energy distribution among all energy states of the formed transient complex. This clearly does not correspond with the observation of Glosik et al. [115], where the translational energy reduces the reaction rate (where the internal ion energy has a positive effect on the reaction rate). The positive effect of internal excitation was also observed and discussed by Ferguson et al. [105], McFarland et al. [19] and Viggiano et al. [106]. According to these authors, both vibrational and rotational excitation may influence the formation of transient ions. This is often present in charge transfer reactions, where

the Franck-Condon principle and energy resonance have a direct effect. In many situations, internal excitation has no or little effect on reactivity. However, if one of the reactants has a large rotational constant or if the reaction is endothermic but the reaction threshold is energetically similar, the effect is recognizable. Moreover, if the vibrational mode is located on the anticipated reaction coordinate, the effect is dramatic. [116]

We should note that slow charge transfer reactions are not highly significant for trace gas analysis. However, some slow reactions like association reactions or ligand switching reactions can be abundant and important. Association reactions are mentioned separately, as the formation and decomposition of the ion adducts is a characteristic feature of analytical applications of chemical ionisation, in the presence of an electric field. As we already understand, the reaction rates for the formation of ion adducts (Eq. 31 – 33) are known to be at low pressures for third-order reactions, where the forward reaction rate depends on the energy, as $k_f \sim KE_{CM}^{-n}$.

We can make an interesting comparison between the power-law exponent of the reaction rate obtained in the presence of an electric field (as a function of KE_{CM}), in variable temperature experiments (as a function of true temperature, T) and with the exponent predicted by theory. The study of Adams and Smith [114] predicted non-linear reagent molecules in drift field $k_f \sim EK_{CM}^{-3/2}$ (not considering vibrational excitation) and $k_f \sim T^{-5/2}$ in the thermalized environment. Experimental data for CH_3^+ association with N_2, CO and H_2 in He buffer gas agrees with the prediction. However, different experiments do not agree with the prediction well. H_3O^+ association with H_2O in He follows the $EK_{CM,b}^{-1}$ profile, whereas in the thermalized system T^{-3} decay is expected. [39] In a study of $H_3O^+(H_2O)_n$ (n = 2,3,4) association with deuterated ammonia in He, the reaction rates' fall-offs were estimated as $EK_{CM,r}^{-0.7}$ for n = 2, $EK_{CM,r}^{-1.1}$ for n = 3 and $EK_{CM,r}^{-1.2}$ for n = 4. [117] Finally, NO^+ association with ketones in He should follow an $EK_{CM,b}^{-1}$ profile, as r = 2 for the linear NO^+ molecule. However, much faster decay was observed in the experiments: $EK_{CM,b}^{-2.5}$ for acetone; $EK_{CM,b}^{-2.3}$ for 2-butanone and 3-pentanone. [118]

To summarize, the presence of a drift electric field influences ion chemistry. The reactions are affected not only by elevated translation energy of reacting ions but also via the internal rotational and vibrational excitations resulting from their frequent

collisions with the neutral buffer gas. The significance of such excitations and the translational energy for ion molecular interactions has to be evaluated individually for every reaction, as it differs depending on the reactants and buffer gasses. In the context of chemical ionization for trace gas analysis, the application of an electric field has the following consequences:

1, The reaction rates for the main ionization processes (charge transfer and proton transfer) are affected only slightly. However, for increased collisional energies a new dissociation channel may open, producing ion fragments.

2, Slow ion molecular reactions will have their reaction rates reduced following the power-law decay. However, for higher collisional energies the internal excitation of the reagent ion may change the character of the reaction resulting in the reaction becoming fast and thus significant.

3, Ligand switching reactions (when slow) also undergo a negative energy dependence.

4, The reaction rate for association reactions also follows the power-law decay. Additionally, the formed ion complex is usually weakly bounded. Therefore, a reversed collisional-induced dissociation reaction reduces the abundance of the associated complexes, even more. Thus, for collisional energies above the cluster bound energy, the abundance of ion clusters decays much faster.

5, The energy dependence of reaction rate for slow ion molecular reactions cannot be directly compared with the thermal dependence obtained in thermalized experiments.

6, For collisional energies at around 1 eV and above, slow reactions are no more visible as collisional-induced dissociation. Dissociative charge transfer and dissociative proton transfer reactions dominate over other reaction channels.

1.2. Analytical techniques for trace gas analysis

Chemical ionisation (CI) (described in the previous chapter) can be effectively used for the analysis of various molecules in the gas phase by producing molecular ions, that may be detected by several techniques. With a careful selection of reagent ions, reaction pathways are open for the analysis of targeted molecules. This is crucial as most gas samples are diluted in the air. With the proper selection of reagent ions, any

reaction with the main components of air (N_2, O_2, CO_2) will be negligible. In addition, the reagent ions will react rapidly with any remaining molecules diluted in the sample. If the analysis requires the observation of all species within the sample mixture, more aggressive reagent ions (like He^+ or Xe^+) may be needed. The selection of reagent ions depends on individual applications. The most common application is for the analysis of volatile organic molecules (VOCs) presented at trace levels in the air. Therefore, H_3O^+, O_2^+ or NO^+ are often used as the reagent ion of choice as they do not react rapidly with the main components within the air. Additionally, they provide the effective chemical ionisation of most VOCs, as well as other volatile compounds. [37, 52]

Before we start with the description of the chemical ionisation analytical techniques, it is necessary to mention a referential technique. The golden standard for the quantitative analysis of VOCs in the air has always been gas chromatography coupled with electron ionisation mass spectrometry (GC-MS). [119] This approach provides the determination of molecules based on the retention time of a particular species within the column, as well as by the characteristic dissociation pattern in the mass spectrum provided by electron ionisation. Conducting an appropriate preconcentration step, this technique may quantitatively determine the concentration of molecules at the pptv level. [120, 121] However, the downside of this technique is the extensive length of time required for sample analysis (usually several minutes). This technique is also associated with a difficult calibration procedure before any measurement due to the many different influential factors from the instrument. Analytical techniques based on CI are alternative to the classical GC-MS, as will be shown later because they do not require chromatographic separation. However, CI is successfully used with GC as an alternative to EI. This application uses EI to generate reagent ions which go on to react in the ionisation tube, with the gas leaving the GC. This is however not very popular, as the combination of GC with EI is usually enough to analyse most compounds. Nonetheless, it is still useful for compounds with similar MS patterns, such as phthalates [122].

A typical technical solution for chemical ionisation analysis contains three general stages. Firstly, reagent ions are generated by a discharge or another ionization method (e.g. photoionization or radiation). Secondly, reagent ions react with sampled volatiles under specific conditions (pressure, temperature, reaction time, etc.) while producing

reaction products characteristic of the studied VOCs. Finally, all ion products are analysed using analytical techniques capable of detecting ions. Until now, various analytical techniques were developed. These techniques are mainly identified by the characteristic pressure in the reaction region. Atmospheric pressure chemical ionisation (APCI) operates near atmospheric pressure, whereas classical CI operates in the order of mbar pressure.

The use of APCI has several benefits. This approach does not require powerful vacuum pumps to generate low pressures and thus such instruments are much easier to construct. Additionally, at atmospheric pressure ions undergo more frequent collisions within the sampled gas, which increases the likelihood of a successful reaction occurring. Moreover, all ions are quickly thermalized and the Boltzmann distribution is established. A typical APCI technique is known as ion mobility spectrometry (IMS). This technique commonly uses radioactive radiation or a corona discharge to produce reagent ions at atmospheric pressure. The reagent ions react with VOCs; products are analysed using the different mobilities of individual ions in a homogenous electric field. As the number of produced ions is high, this technique does not require a sensitive ion multiplier as a detector; instead, a classical Faraday cap with an associated preamplifier is sufficient. This technique is very popular as a result of its compactness and high sensitivity. It is often used in a military and security setting, to detect traces of drugs and explosives. [123, 124] Field Asymmetric Ion Mobility Spectrometry (FAIMS) is a modification worth mentioning. [125, 126] Here, an asymmetric RF field is applied radially to the drift tube alongside the axial field, forcing ions to move towards the wall of the drift tube. Only ions with the correct mobility can penetrate through the modular RF and thus be detected. This unique solution allows for the device to be produced on a chip. [127] The last two techniques necessary to mention (also highly used for analytical applications) include electrospray ionization [128] and secondary electrospray ionization (SESI) [43]. The techniques use a high voltage which is applied on a capillary to disperse the solvent into a fine aerosol. The droplets carry an initial charge (acquired from a high voltage electrode) which continuously evaporates until the droplets meet the Rayleigh limit [129]. The Rayleigh limit is where the Coulomb forces disassemble the droplet to even smaller sizes. In electrospray ionization, the solvent contains a diluted analyte and the combination of evaporation with Coulomb explosion generates the molecular ions

(and their associated clusters) which are detected by MS. Therefore, electrospray-MS is often combined with liquid chromatography (LC) to produce a powerful analytical approach for the analysis of various biological molecules. SESI uses electrospray indirectly, first generating droplets of pure solvent. Generated ions and ionized clusters of initial solvents may then react with molecules presented in the surrounding atmosphere, in a secondary reaction. Formed ionised products are then analysed using MS.

Instruments operating at low pressures have already been mentioned. SIFT-MS was developed to study chemical ionisation processes [22], however, it was quickly applied to gas-phase analysis [34, 130]. This technique generates ions in a microwave discharge, for which the reagent ions are selected using a quadrupole mass filter. Reactions with the analyte gas are carried out in helium after which the generated ions are analysed in a mass spectrometer. Following this PTR-MS was developed, optimising previous designs for more sensitive analysis. [59] PTR-MS uses a glow discharge to produce hydronium ions almost exclusively. The H_3O^+ ions are then injected into the reaction region via ion optics. The lack of a mass filter allows for a high ion throughput from the discharge and this, in turn, enhances the probability of a successful reaction occurring. In the reaction region, a drift tube occupied an axial electric field with an intensity of around 130 Td is used instead of a carrier gas to carry ions through into the reaction region. The sampled gas is not diluted within the carrier gas and therefore the full volume of the drift tube may be filled with the gaseous sample. Parasitic association reactions are depressed by the presence of a high drift field increasing the mean reaction temperature above an association threshold. The ions produced are subsequently detected by mass spectrometry. Finally, SIFDT-MS combines both SIFT and PTR [39]. The technique consists of a selected ion source composed of a glow discharge and a quadrupole mass filter, similar to SIFT. However, the flow tube is replaced by a drift tube similar to PTR. This combination allows for the injection of various reagent ions and therefore allows us to determine the sample composition through different reaction channels. Furthermore, the addition of a drift tube allows for the variation of reaction temperature (due to the presence of a homogenous electric field). Higher reaction temperatures are useful for the determination between various isomers. In SIFT, isomers often produce similar

molecular ions, however at higher reaction temperatures the product branching ratios for various isomers change, allowing isomers to be distinguished and measured.

Note that we have briefly mentioned only the most important techniques in their most basic form. These techniques may be modified and combined with others, producing unique analytical systems. For example, electrospray and SESI may be combined with tandem mass spectrometry [131, 132]; IMS may be combined with MS, producing 2D IMS-MS spectra [42]. The recent development of IMS has resulted in the production of high kinetic energy IMS (HIKE-IMS), operating within the mbar pressure range, containing a reaction region previously characteristic of PTR-MS or SIFDT-MS. [133] It is beyond the scope of this thesis to fully cover all variations. Thus, we focus only on the relevant ones:

In the present work, we have studied how water vapour affects ion chemistry in the mentioned CI-MS techniques. In this study, we have only used instruments which may provide a direct and detailed study of ion chemistry, such as SIFT-MS, PTR-MS and SIFDT-MS. These instruments operate at ~1 mbar pressure, in which primary reactions dominate over secondary reactions with water, under normal operational conditions. This is important as ion distribution is not in an ideal equilibrium and ions may dynamically respond to a change in the concentration of the neutrals. This therefore allowed for the study of the full set of ion-neutral reactions. Additionally, each technique has a unique construction, allowing one to focus on the different reaction parameters. APCI experiments were not included as they operate near atmospheric pressure where the reaction equilibrium between primary and secondary processes is quickly established due to the high frequency of collisions. Water vapours also affect the ion chemistry in APCI, although they are not ideal for the study of complex reactions. Thus, we will now introduce SIFT-MS, PTR-MS and SIFDT-MS in greater detail.

Selected ion flow tube mass spectrometry (SIFT-MS)

The SIFT technique was developed in 1976 by Adams and Smith [22] and quickly became the standard in the study of ion-neutral reactions, near to thermal interaction energies [23]. For analytical applications, the SIFT technique was implemented into the SIFT-MS instrument. The instrument consists of four main parts: a discharge generating reagent ions; a mass filter selecting one specific ion; a flow tube where selected ions react with gasses in the presence of a carrier gas; and finally, a mass spectrometer at the end of the flow tube.

The setup is characterised by several regions operating at different pressures; ~1 mbar for the discharge and the flow tube; and ~10^{-5} mbar for both the filter and the mass spectrometer. Differential pumping of the system requires a series of orifices, providing the ion transfer between different pressurized regions. The orifices inserted into the SIFT-MS are designed to reduce the back-flow of gases from the flow tube back into the two low-pressure regions. [23] The series of orifices as well as the presence of the mass filter, however, limit the total ion current and number of reagent ions provided by this setup. In the present work, we used a SIFT-MS Profile 3 instrument (see Figure 2) developed by Instrument Science, Crewe, UK, providing ~10^6 ions per cm^3 in the flow tube. The ion current at the injection venturi-type orifice (1mm diameter) leads into the flow tube (tens of nanoamps) and the ion current is reduced by the time it reaches the end of the flow tube (by a factor of 1000). This current drop, partially caused by diffusion to the walls of the flow tube (but mainly occurring during ion transfer through the orifice) represents the main limitation of the instrument.

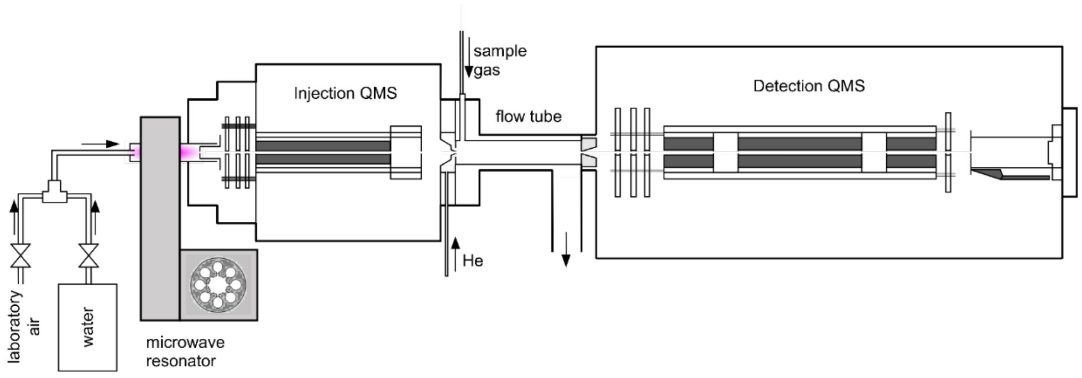

Figure 2 The schema of SIFT-MS experiment. *QMS* - quadrupole mass filter

The SIFT-MS uses a microwave discharge usually within a mixture of water vapour and air. The combination of both gasses allows for the formation of several stable ions, mainly H_3O^+, NO^+ and O_2^+ which may be used in analytical applications. The relevant reaction channels occurring in the RF plasma are listed in Figure 3. In the presence of pure water vapour, the H_3O^+ ions are produced from a series of primary and secondary reactions, mainly by binary reactions of H_2O^+ and OH^+ ions with H_2O (highlighted in blue). By introduction of air into the discharge, the ion reactions also generate O_2^+ and NO^+ ions. The ion composition in the discharge depends strongly on the pressure ratio between individual gaseous components (water vapour and air). Therefore, the ion composition may be optimized to preferentially sift through one of the selected ions, or allow all of the reagent ions through (in comparable concentrations).

Primary ionization reactions

$$H_2O + e^- \rightarrow H_2O^+ + 2e^-$$
$$\rightarrow OH^+ + H + 2e^-$$
$$\rightarrow O^+ + H_2 + 2e^-$$

$$O_2 + e^- \rightarrow \mathbf{O_2^+} + 2e^-$$
$$\rightarrow O^+ + O + 2e^-$$

$$N_2 + e^- \rightarrow N_2^+ + 2e^-$$
$$\rightarrow N^+ + N + 2e^-$$

Secondary ion reactions

$$H_2O^+ + H_2O \rightarrow \mathbf{H_3O^+} + OH$$
$$H_2O^+ + OH \rightarrow \mathbf{H_3O^+} + O$$
$$H_2O^+ + O_2 \rightarrow \mathbf{O_2^+} + H_2O$$

$$OH^+ + H_2O \rightarrow \mathbf{H_3O^+} + O$$
$$\rightarrow H_2O^+ + OH$$
$$OH^+ + OH \rightarrow H_2O^+ + O$$
$$OH^+ + O_2 \rightarrow \mathbf{O_2^+} + OH$$
$$OH^+ + N_2 \rightarrow N_2H^+ + O$$

$$O^+ + H_2O \rightarrow H_2O^+ + O$$
$$O^+ + O_2 \rightarrow \mathbf{O_2^+} + O$$
$$O^+ + N_2 \rightarrow \mathbf{NO^+} + N$$

$$N_2^+ + H_2O \rightarrow N_2H^+ + OH$$
$$N_2^+ + O \rightarrow \mathbf{NO^+} + N$$
$$N_2^+ + O_2 \rightarrow \mathbf{O_2^+} + N_2$$
$$N_2^+ + OH \rightarrow OH^+ + N_2$$
$$N_2^+ + N \rightarrow N^+ + N_2$$

$$O_2^+ + N \rightarrow \mathbf{NO^+} + O$$

$$N^+ + H_2O \rightarrow H_2O^+ + N$$
$$N^+ + O_2 \rightarrow \mathbf{NO^+} + O$$
$$\rightarrow O^+ + NO$$

$$N_2H^+ + H_2O \rightarrow \mathbf{H_3O^+} + N_2$$

Figure 3 List of relevant ion-molecular reactions occurring in the RF plasma ion source in the mixture of air and water vapours. [134] Reactions in blue represent those active in pure water vapour discharges. The remaining reactions are active in water vapour/air mixtures. The ions in bold (H_3O^+, NO^+ and O_2^+) are the main reagent ions produced in the discharge at high concentrations.

From the discharge, ions are selected according to their *m/z*, first by a quadrupole mass filter; subsequently by a series of electrostatic lenses focused into the centre of a Venturi-type orifice; and injected into the flow tube. The injection energy, determined by the potential of a quadrupole mass filter, may be several eV. The relatively high energy is necessary for ions to efficiently penetrate into the drift tube. This kinetic energy is then removed from the reagent ions by collisions with a carrier gas, usually helium. Other gasses may be used instead of helium, however, the injection energy must be adjusted to prevent any potential ion-carrier gas reactions within this region.

In the flow tube, reagent ions are mixed with helium and are carried along by the carrier gas stream through the flow tube. At typical conditions (300 K, 1 mbar), the laminar flow distribution is established, while ions are mostly concentrated in the centre of the stream. To minimize diffusion losses, the helium carrier gas flows at a speed of ~10,000 cm/s which requires a powerful vacuum pump. A 5 cm long flow tube used in the present instrument requires a pumping speed of 20 - 30 m^3/h to achieve the required conditions.

The sample inlet is positioned in the flow tube 1 cm downstream from the injection orifice. This distance is sufficient for helium gas to remove any additional energy found in the reagent ions. Therefore, the ion-molecule interaction (with the sample species) will occur at thermal energies. A gaseous sample is introduced through the inlet into the centre of the helium gas stream, where they are mixed with the carrier gas and reagent ions. From this point, the mixture of all components travels to the end of the flow tube, (4 cm from the sample inlet). During this transport, the reagent ions react with the neutral molecules at a defined pressure and temperature, typically 1 mbar and 300 K. The flow tube design does however also allow for ion-molecular experiments to be carried out at varying temperatures, as to determine the temperature dependence on reaction kinetics. [76, 135] At the end of the flow tube, ions are sampled through the exit orifice into the quadrupole mass spectrometer and are detected by a Channeltron detector.

The defined position of the sample inlet and exit orifice, together with the defined ion speed within the helium carrier gas allows a simple calculation of the reaction time t_r, to be conducted (usually 300 µs), schematically illustrated in Figure 4. The known

time constant is then used to determine the concentration of neutral molecules if the reaction rate constants are known.

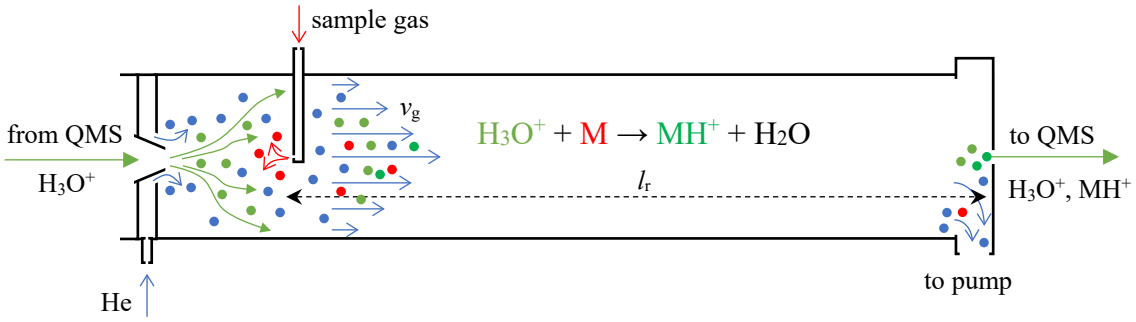

Figure 4 The schematic interpretation of physical and chemical processes in the flow tube. The reagent ions (orange) are injected into the flow tube and mixed with the helium carrier gas. Sample gas (red) is introduced into the mixture as well. The laminar flow of the helium carrier gas transports the reagent ions and sample gas along the defined reaction length l_r, from the injection point up until the end of the flow tube, where neutrals are separated from the ions. Ion-neutral reactions take place along the reaction length (in the flow tube).

For a typical bimolecular exothermic proton transfer reaction between hydronium and an organic molecule M, $H_3O^+ + M \rightarrow MH^+ + H_2O$, the number density of the primary reagent ion $[H_3O^+]$ and protonated product $[MH^+]$ is described by a simple kinetic equation:

$$\frac{d[H_3O^+]}{dt} = -k[M][H_3O^+] - [H_3O^+]\frac{D_{H_3O^+}}{\Lambda^2}, \quad (39)$$

$$\frac{d[MH^+]}{dt} = k[M][H_3O^+] - [MH^+]\frac{D_{MH^+}}{\Lambda^2}, \quad (40)$$

where k represents the reaction rate constant; D_{MH^+} and $D_{H_3O^+}$ stand for the respective MH^+ and H_3O^+ ion diffusion coefficients; and Λ represents the characteristic diffusion length, characterized by the diameter of the flow tube. Integration of Eq. 39 over the reaction time $t_r = l_r/v_d$ leads to an exponential solution showing the concentration of the reagent ion at the end of the flow tube:

$$[H_3O^+] = [H_3O^+]_0 exp(-k[M]t_r), \quad (41)$$

where the reaction rate constant may be determined from a semilogarithmic plot of $\log[H_3O^+]$ vs [M]. This same approach may be used for other reagent ions as well. The uncertainty of this method is however augmented by knowing only a rough estimate of the ion reaction time. Thus, the reaction rate constants are determined via a different approach. It was shown that parametrised trajectory calculations give very good results of collisional rate constants [54], which are almost identical to reaction rate constants for proton transfer reactions if the reactions are sufficiently exothermic [69]. Using this fact, we can take the theoretical reaction rate constant as a reference for the rate constants determined by SIFT-MS. In the experiment, we allow all reagent ions to travel into the drift tube simultaneously, which allows for all the investigated primary reactions to happen at the same time. This allows us to determine the slope of the logarithmic curve for the relationship between the reagent ions signal vs the neutral molecule concentration. It also allows us to estimate the relative ratio between the individual primary reaction rate constants. Normalizing the proton transfer reaction rate data to the theoretical values obtained by parametrised trajectory calculations can give an accurate result for reaction rate constant estimates with other reagent ions. This is necessary as one cannot expect the reactions of the neutral molecule with NO^+ or O_2^+ to proceed at the collisional rate. This approach has been used previously on several organic molecules, allowing for the acquisition of calculated reaction rate constants for the reactions of the neutral molecule with NO^+ and O_2^+ ions, as well. [64, 66]

Determination of the analyte concentration in the flow tube may also be achieved by monitoring the decrease in the reagent ions' signal if the reaction rate constant is known. However, if the sample contains several different molecules, they will all react with the reagent ions present and analysis cannot be achieved. Alternatively, we need to focus on Eq. 40 which describes the concentration of product ions. If the reactions of various molecules (in the sample mixture) with the reagent ions result in different product ions and if the reaction rate constants for said reactions are known, all individual molecules within the mixture may be quantified. [136] The first assumption applied in the calculation of neutral molecule number densities in the flow tube is that the concentration of reagent ions is not highly affected by the analyte. In other words, the sample flow rate and therefore the concentration of analyte species in the flow tube is small. Therefore, the reagent ion number density, $[H_3O^+]$ in Eq. 40, may be

considered independent from the analyte number density, [M]. An analytical solution for the differential Eq. 40 leads to the time variation of the number density of the product ion [MH^+]:

$$[MH^+]_t = [H_3O^+]_t \, k[M]t \frac{exp\left(k[M]t + \frac{D_{H_3O^+} - D_{MH^+}}{\Lambda^2} t\right) - 1}{k[M]t + \frac{D_{H_3O^+} - D_{MH^+}}{\Lambda^2} t}. \tag{42}$$

For a trace amount of [M] in the system we can modify the solution as (as applied in trace gas analysis):

$$\lim_{[M]\to 0} [MH^+]_t = [H_3O^+] k[M] t D_e \, , \tag{43}$$

where

$$D_e = \lim_{[M]\to 0} \frac{exp\left(k[M]t + \frac{D_{H_3O^+} - D_{MH^+}}{\Lambda^2} t\right) - 1}{k[M]t + \frac{D_{H_3O^+} - D_{MH^+}}{\Lambda^2} t} = \frac{exp\left(\frac{D_{H_3O^+} - D_{MH^+}}{\Lambda^2} t\right) - 1}{\frac{D_{H_3O^+} - D_{MH^+}}{\Lambda^2} t} \tag{44}$$

is the differential diffusion enhancement coefficient. [136] If both MH^+ and H_3O^+ ion diffusion coefficients, D_{MH^+} and $D_{H_3O^+}$, are similar, D_e converges close to 1. In this case, the product ion number density, as well as the detected ion count rate, are proportional to the neutral analyte gas number density.

It is important to state that if the *m*/*z* value of the product ion differs from the value of the reagent ion, the effect of the differential diffusion coefficient must be considered for the analysis. Fortunately, quadrupole mass spectrometry used in the analysis also provides a mass discrimination correction which is applied to larger ions. As the treated analyte product ions are usually heavier comped to reagent ions, the mass discrimination factor tends to cancel out the effect of the diffusion coefficient. [137] However, for precise analysis, both phenomena must be considered within the SIFT-MS operational software.

Finally, we have to consider the presence of various parallel and secondary reactions. In our previous assumption (Eq. 39, 40), we considered only one primary proton transfer reaction, producing only one product ion MH^+. The primary process may

however be accompanied by additional reactions including the potential dissociation of product ions into ion fragments. These fragments contribute to the total reaction yield and must be considered in the calculation. Additionally, the presence of water vapour in the system causes the formation of various water clusters, following the association reaction described in the previous chapter. Clusters may be formed not only from reagent ions (making ions like $H_3O^+(H_2O)_{1,2,3}$ or $NO^+(H_2O)$) but also from product ions (like $MH^+(H_2O)$), increasing the overall complexity of the reaction system. Formed reagent ion clusters are also able to react with our analyte molecule, M. We may still treat this problem with the assumption that all reaction products originate from M and thus the overall number density of a neutral analyte is proportional to the sum of product ions intensities produced by individual reaction channels. The neutral number density of the analyte [M] may then be calculated from the corresponding ion count rate [37], following reaction 14 as:

$$[\mathrm{M}] = \frac{1}{t_r} \frac{f_{p1} {I_{p1}}/{D_{ep1}} + f_{p2} {I_{p2}}/{D_{ep2}} + \cdots}{f_{i1} I_{i1} k_1 + f_{i2} {I_{i2} \frac{k_1 + k_2}{2}}/{D_{ei2}} + \cdots}, \tag{45}$$

where I_{p1}, I_{p2}, etc. correspond to the count rates of individual product ions corrected for mass discrimination, I_{i1}, I_{i2}, etc. represent the count rates of individual reagent ions reacting with M. k_1 and k_2 are the reaction rate coefficients for the main and secondary reagent ions, respectively. D_{ep} and D_{ei} are the respective differential diffusion enhancement coefficients, and t_r is the reaction time. Finally, the auxiliary factors f_p and f_i correct for the calculation of non-linear reaction kinetics. For example, f_i coefficients adjust the conversion of hydronium reagent ions into its hydrates, whereas f_p may be used to correct for the calculation of parasitic ions or isotopes (found at the same mass as the analyte ion). [136] This refined determination of the analyte concentration is important, especially for humid air and breath analysis. [138] Even the calculation contains several coefficients and looks difficult to execute, although these calculations have already been integrated into the SIFT-MS software. Differential diffusion enhancement coefficients may be calculated from their ion diffusion coefficients, which may be calculated [139], or just estimated using the ion mass [136]. Mass discrimination may also be interpreted as a simple function of ion mass. The important conclusion is that all parameters may be obtained before analysis and may be universally used in SIFT-MS. Therefore, to achieve quantitative analysis,

a calibration for each trace gas species analysed by SIFT-MS is not necessary. [140] However, this only applies if the ion chemistry in the flow tube is fully understood.

The concentration of the trace gas in the sampled air may be determined from the previously calculated number density [M] if both the sample gas flow (Φ_s) and carrier gas flow (Φ_c) are carefully measured. The concentration, C, may then be calculated as:

$$C = [\mathrm{M}] \frac{k_b T_g}{p_g} \frac{(\Phi_c + \Phi_s)}{\Phi_s}, \tag{46}$$

where k_b is the Boltzman constant, p_g represents the total pressure of the carrier gas and T_g is the gas temperature. One may directly calculate the relative concentration of the trace gas as p_M/p_0, using Loschmidt`s number ($n_0 = 2.687 \times 10^{19}$ cm^{-3}) which represents the reference concentration at standard atmospheric pressure (p_0 = 1,013.25 mbar) and temperature (T_0 = 273.15 K):

$$\frac{p_M}{p_0} = [\mathrm{M}] \frac{p_0}{n_0 p_g} \frac{T_g}{T_0} \frac{(\Phi_c + \Phi_s)}{\Phi_s}. \tag{47}$$

The calculated concentration may be converted into the commonly used parts-per-million (ppm) or parts-per-billion (ppb) units, by multiplying by 10^6 or 10^9, respectively.

At this stage, it should be understood that SIFT-MS can quantitatively determine the traces of molecules in sampled air if the ion chemistry of targeted trace molecules is understood. The error of determined concentration depends on all involved instrumental parameters, as gas flow measurements and estimations of diffusion and mass discrimination functions. Therefore, it is difficult to estimate the error directly. However, as most of the parameters for concentration calculation are associated with the instrument, the errors are mostly systematic. Therefore, the relative changes in analyte concentration will always be true. Additionally, the quality of parameters may be tested by providing an analysis of a single volatile molecular standard (i.e. acetone) and therefore clarifies whether the determined concentration agrees with the concentration of the standard.

The sensitivity depends predominantly on the reaction rate of the selected reagent ion with the target molecules. Under standard experimental conditions (using a reaction rate of 3×10^{-9} cm^{3}s^{-1} [64]) and detecting a signal down to 0.1 cps (using longer integration times), this technique is able to detect molecules at the 0.1 ppb level. For

the upper limit, we need to guarantee that each ion-molecular reaction does not significantly affect the reagent ion concentration. Therefore, the product ion concentration should be at a maximum of 2 orders of magnitude below the concentration of the reagent ions. Using a count rate of 10^9 cps for the reagent ions and thus 10^7 cps for the product ions (total product ion count rate), one may reach the top molecular concentration at 10,000 ppm. As we see, the instrument may analyse molecular ions in a range of over 7 orders of magnitude.

The concentration of the sample injected into the flow tube may be adjusted by a regulation of the sample flow rate. For highly concentrated samples, the flow rate may always be reduced to achieve the required ion product intensity criteria. For low concentrated samples, the sample flow rate may be increased, however, this possibility is limited. Helium carrier gas needs to be the dominant gas in the system. Therefore, the flow rate of the sample into the flow tube should not exceed 5-10% of the helium flow rate. For the Profile 3 instrument used in this work, the carrier gas flow rate is around 500 sccm. Therefore, we commonly used a sample flow rate of 30 sccm. It is important to note that the present sample flow limitation directly impacts the detection limit. New SIFT-MS instruments use nitrogen gas instead of helium and as a result of this, the flow rate of sampled air may be increased. [141] This however brings other complications which will not be addressed here, as they are outside the scope of the presented work.

Finally, the analysis may be carried out using two methods. Firstly, SIFT-MS may obtain a classical mass spectrum, where we can identify all reagent and product ions. Secondly, the apparatus can monitor the selected *m/z* values and provide real-time analyses of selected molecules. The acquisition time depends only on the integration time and therefore the instrument is able to detect rapid changes in sample concentrations, such as in breath analysis.

Proton transfer reaction mass spectrometry (PTR-MS)

The PTR-MS (see Figure 5) is a technique developed by Lindinger et al. [59], based on discoveries obtained by the FA and SIFT. The initial intention of the authors, however, was to make a purely analytical instrument rather than an instrument capable of investigating ion chemistry and its reaction kinetics. The instrument is tuned to provide a highly sensitive analysis of various organic compounds in real-time with a high level of resolution. Three major upgrades were conducted to achieve such properties which were: an absence of an injection mass filter allowing for a high ion flux of reagent ions; secondly, the absence of a carrier gas but with the full volume of the reaction chamber being filled with the sample gas; and finally, the introduction of an axial homogenous electric field (drift tube) accelerating ions through the reaction region into the detecting mass spectrometer (while increasing the reaction energy of each ion-molecular reaction). As a result, the detection limit of the PTR-MS may be up to three orders of magnitude better than for other SCIMS techniques. Some studies even showed detection limits up to 1 pptv. [142, 143] Now let's focus on a careful description of the PTR-MS instrument.

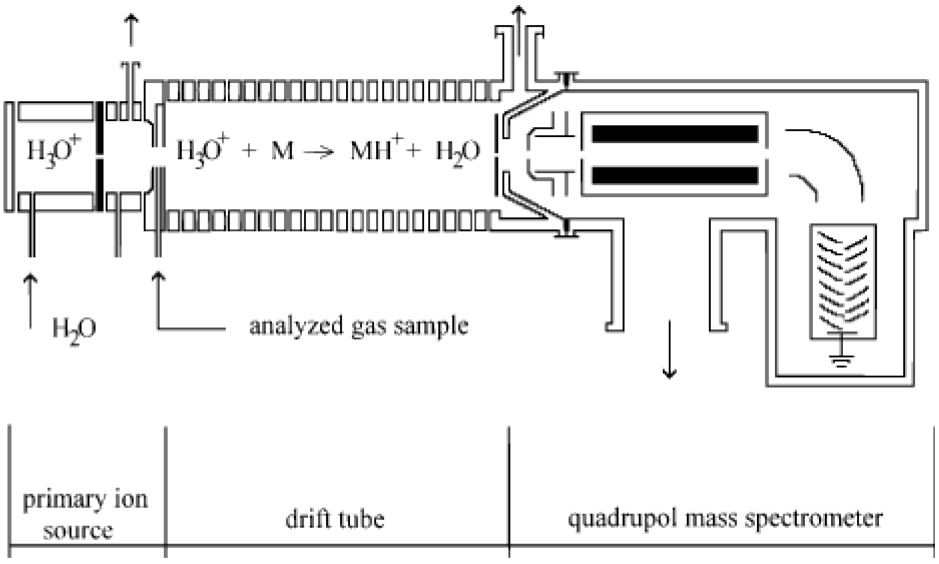

Figure 5 A scheme showing the PTR-MS instrument. [144]

For the ion source, PTR-MS often uses a DC hollow cathode discharge which can achieve higher current densities (several mA) compared to a classical cathode discharge. The plasma in the discharge is generated in pure water vapour at pressures

of around 1 mbar, producing a flow of hydronium ions. The ions formed in the discharge pass through a pin hole which introduces them to the next separation chamber. The separation chamber lies between the discharge and the drift tube and is continuously evacuated by a vacuum pump. This region is crucial, as it provides a constant gas flow from both the discharge and the drift tube, preventing gas from the drift tube from entering the discharge (and vice versa). Any gas contamination coming from the drift tube may negatively affect the discharge ion chemistry; and thus, the generation of reagent ions. The chamber also prevents other radicals, generated by the discharge, from entering the drift tube. After entering the separation chamber, reagent ions are injected into the drift tube via a set of electrostatic lenses.

As a final note on the ion source, the PTR-MS is optimised for hydronium as the reagent ion. This is because the water-based discharge produces minimal other undesirable ions which may interfere with the ion chemistry occurring in the drift tube. It is however possible to modify the ion source to produce other reagent ions as well. For this to be possible, the discharge gas and its pressure must change accordingly. It has been demonstrated, that NO^+, O_2^+ and Kr^+ ions may be used for analyses, enhancing the flexibility of the instrument and its capabilities. [145-147] These reagent ions are however rarely used in typical procedures using this instrument as proton transfer from H_3O^+ ions is already highly effective. Additionally, changing over the reagent ion requires time (as the change of gas and its pressure cannot be done rapidly) and thus it is not possible for the conventional PTR-MS instrument to switch between reagent ions in the same way as SIFT-MS. For the first-generation instruments (equipped with quadrupole mass spectrometers) this was considered a limitation as it was difficult to distinguish between isobaric and isomeric molecules. Later generations of the PTR-MS were equipped with powerful time-of-flight mass spectrometers (ToF-MS), providing much better mass resolution of product ions and making isobaric molecules distinguishable. The latest generation of PTR-MS instruments is equipped with a modified ion source containing three separated ion sources placed perpendicular to the axis of the drift tube. All three ion sources can generate different reagent ions, which may be rapidly switched between (using electrostatic optics). [148]

Ions introduced into the drift tube are immediately accelerated along the central axis of the drift tube. The homogeneous electric field is generated by a series of stainless-steel rings, usually isolated by Teflon. The details of the dimensions and a total number

of electrodes used differ between producers, but typically a drift tube length is 10 cm. A characteristic parameter used in PTR-MS is the reduced strength of the electric field, *E/N*, accelerating ions along the drift tube. This value is calculated from the drift tube length; applied electric potential; and the pressure of the analysed sample gas in the drift tube. The PTR-MS operates at a pressure of around 2 mbar. The sample inlet is placed at the beginning of the drift tube, where the inlet gas may effectively mix with the reagent ions. The pressure in the drift tube is regulated by the inlet flow controller (with a sample flow of around 20-30 sccm), while the drift tube is continuously evacuated. Using this approach, the pressure in the drift tube remains stable and therefore we can obtain the number density of the sample gas, *N*, as:

$$N = \frac{N_A}{V_M}\frac{273.15}{T_d}\frac{p_d}{101.325}, \tag{48}$$

where N_A is Avogadro`s number (6.022 x 10^{23} mol^{-1}); V_M is the molar volume of an ideal gas at a temperature of 273.15 K and a pressure of 1 atm (101.325 kPa); T_d is the drift tube temperature; p_d is the drift tube pressure. Knowing the gas number density, *N*, the drift tube length, *d*, and the electric potential across the drift tube, ΔV, we can determine the value of the reduced electric field

$$\frac{E}{N} = \frac{\Delta V}{Nd}, \text{where } \left[\frac{E}{N}\right] = \text{V.m}^2 \text{ and } 1\ \text{Td} = 10^{-21}\ \text{V.m}^2. \tag{49}$$

The *E/N* used in PTR-MS ranges from 80 Td to 300 Td, depending on the instrument. The most widely used value (and often used as the reference) of *E/N* is 130 Td.

As mentioned previously, the primary function of the drift field is to carry the reagent and product ions along the drift tube. Additionally, the presence of an electric field also positively affects the ion chemistry in the drift tube, as we will now explain. The presence of the water vapour in the sample gas affects the composition of reagent ions through association reactions, producing water clusters which affect the regent ions' reactivity. In SIFT, the presence of water clusters is limited as the sample gas is diluted in a flow of helium which avoids the water vapour from overwhelming the overall ion chemistry. In other words, hydronium ions are usually dominant over other hydronium water clusters. In PTR-MS, the concentration of water vapours in the drift tube is around two orders of magnitude higher compared to SIFT-MS and hydronium clusters are thus formed more rapidly. This would decrease the reagent ions' reactivity with neutral molecules. Increases in the kinetic energy of ions as a result of the presence of

an electric field decreases the reaction rate for association reactions, keeping the main ionization channels unaltered. At *E/N* 130 Td (standard), the kinetic energy of hydronium water clusters is also sufficient to initiate collisional induced dissociation (CID) with buffer gas, thus hydronium ions remain the dominant species. After this initial note, let's carefully describe the interaction of the ion with the electric field.

The drift velocity of ions, v_d, in the drift tube with an electric field (E) is characterized by ion mobility, μ (Eq. 10). The ion mobility depends on the collisional cross-section between the ions and neutral gas particles but is also highly sensitive to neutral gas pressure and temperature. Ion mobility is often expressed in a condensed form for reduced ion mobility, μ_0, scaled on normal pressure (760 Torr, 1013.25 mbar) and temperature (273 K) from where the ion mobility at selected pressure p and temperature T can be obtained as:

$$\mu = \frac{760}{p}\frac{T}{273}\mu_0. \tag{50}$$

Using the reduced ion mobility formula (Eq. 50) together with the reduced electric field (Eq. 48, 49), the ion drift velocity may be expressed as:

$$v_d = \mu_0 N_0 \frac{E}{N}, \tag{51}$$

where N_0 = 2.6867 x 10^{19} cm^{-3} represents the gas number density at standard temperature (273.16 K) and pressure (760 Torr). The ion transit time through the drift tube (of length, L) is given by the formula:

$$t_d = \frac{L}{v_d}. \tag{52}$$

In a typical situation for a drift tube with length L = 10 cm and E/N = 130 Td (operating with hydronium ions in nitrogen), the hydronium reduced ion mobility is ~2.85 cm^2 V^{-1} s^{-1}. The mean ion drift velocity is 995 m s^{-1} and the transit time is 100 µs. Compared to SIFT-MS, the ion drift velocity in PTR-MS is around 10 times larger compared to the ion flow velocity in SIFT-MS. Therefore, it is preferable to increase the length of the drift to compensate for the reduction of ion transit time; and subsequently the reaction time.

Calculation of the absolute concentration of a specific species in PTR-MS follows a similar principle to the one already described for SIFT-MS in the previous chapter. We assume that the concentration of the neutral molecule of interest resides at trace levels

and therefore the concentration of reagent ions is not affected by the reactions with it. The higher ion velocity reduces the effect of ion diffusion, increasing ion intensities. The kinetic equation, however, differs from one used for flow tubes (Eq. 39, 40). The transient velocity of ions is defined by ion mobility (different for individual particles) and therefore the transient time of multiple ions is not the same. As a consequence, it is not possible to form a differential equation as a function of time, but rather as a function of the axial position of molecules, x, by applying the substitution $dt = dx / v_d$. Thus, considering Eq. 51, the differential equation for the simple example of a proton transfer reaction, $H_3O^+ + M \rightarrow MH^+ + H_2O$ takes the form:

$$\frac{d[\mathrm{H_3O^+}]}{dx} = \frac{-k[\mathrm{M}][\mathrm{H_3O^+}] - [\mathrm{H_3O^+}]\frac{D_{\mathrm{H_3O^+}}}{\Lambda^2}}{v_g + \mu_{0,\mathrm{H_3O^+}}(E/N)N_0\frac{E}{N}}, \tag{53}$$

$$\frac{d[\mathrm{MH^+}]}{dx} = \frac{k[\mathrm{M}][\mathrm{H_3O^+}] - [\mathrm{MH^+}]\frac{D_{\mathrm{MH^+}}}{\Lambda^2}}{v_g + \mu_{0,\mathrm{MH^+}}(E/N)N_0\frac{E}{N}}, \tag{54}$$

where v_g is the buffer gas velocity; $\mu_{0,\mathrm{H3O+}}$ and $\mu_{0,\mathrm{MH+}}$ are the reduced field-dependent ion mobilities of H_3O^+ and MH^+ ions; and the remaining parameters have been previously mentioned. If the detected ion signal is corrected by the ion mass discrimination, we may use Eq. 41 and determine the concentration of analyte [M] from the detected ions signals, $i(MH^+)$ and $i(H_3O^+)$, as follows:

$$\frac{[\mathrm{MH^+}]\mu_{0,\mathrm{MH^+}}}{[\mathrm{H_3O^+}]\mu_{0,\mathrm{H_3O^+}}} = \frac{i(\mathrm{MH^+})\mu_{0,\mathrm{MH^+}}}{i(\mathrm{H_3O^+})\mu_{0,\mathrm{H_3O^+}}} = k[\mathrm{M}]t_d, \tag{55}$$

where k represents the reaction rate constant. To determine the concentration of the analyte, we need to know the transition properties of individual ions. For product ions with ion mobilities close to that of the reagent ions, Eq. 55 simplifies and leads to Eq. 42. In most situations, however, the instrument must be calibrated to obtain transition ratio coefficients for individual substances. [149] Once obtained, the absolute concentration of analyte ion in the sampled gas may be calculated (Eq. 46, 47).

Even though the presence of an electric field complicates the determination of the absolute analyte concentration, it is a necessary part of the instrument due to the high concentrations of H_2O vapour present in the discharge and the drift tube. The H_3O^+ ion formed in the discharge reacts with neutral H_2O molecules, forming hydrated

hydronium ions $H_3O^+(H_2O)_n$, where n >1. Ions entering the drift tube thus mainly consist of hydronium hydrates. Additionally, the concentration of water vapour in the drift tube induces the continuous formation of hydronium hydrates. Water vapour in the drift tube originates from humidity from within the sample, but also from the ion source due to diffusion. Additionally, as most gas samples consist of mostly diatomic molecules (N_2, O_2), three body association reactions in the drift tube proceed at rates which are faster compared to association reactions in monoatomic noble gasses (He in SIFT-MS). As a result, the distribution of reagent ions would consist mostly of larger clusters of the hydronium hydrates, complicating the analysis (see Chapter 1.4). The introduction of an electric field results in decreased formation of hydronium hydrates in the drift tube (association reaction rates decrease rapidly with collisional energy and *E/N*) and also causes CID of already existing hydrates:

$$H_3O^+.(H_2O)_n + H_2O + N \underset{k_{diss}(E/N)}{\overset{k_{ass}(E/N)}{\longleftrightarrow}} H_3O^+.(H_2O)_{n+1} + N, \qquad (56)$$

where N represents a neutral molecule presented in the system (in PTR-MS this is often N_2 or O_2). The final reaction equilibrium and therefore the distribution of hydronium hydrates depends on the total water concentration in the drift tube; concentration of the analyte sample; as well as the type of buffer gas used; and *E/N*. As water clusters are usually weakly bounded (see Table 2), for increasing *E/N* the equilibrium quickly shifts towards higher concentrations of H_3O^+. An example of hydronium hydrates distribution at various *E/N* is presented in Figure 6. At *E/N* = 80 Td, the H_3O^+ ion already dominates over its cluster hydrates. An additional increase in *E/N* reduces the number of hydrates even more. Increasing *E/N* to higher values is beneficial for a greater distribution of hydronium hydrates, however, this also causes negative secondary effects. These include a reduction in the reaction time leading to a decreased abundance of product ions and therefore a decrease in the sensitivity as well as an increased probability of dissociation reactions with the analyte affecting the selectivity of the technique. Therefore, in most applications, *E/N* ~ 130 Td is chosen as a compromise between having a sufficient reduction in hydronium hydrates concentration (abundance of $H_3O^+H_2O$ around 10% of H_3O^+ intensity); and fragmentation induced by electric field, of an insignificant level.

Table 2 Selected thermodynamic properties of hydronium hydrates formation $H_3O^+(H_2O)_n + H_2O \leftrightarrow H_3O^+(H_2O)_{n+1}$

n, n + 1	$PA(H_2O(H_2O)_n)$[a]	$-\Delta H$[b]	$-\Delta S$[b]	$-\Delta G$[b]	BDE[c]
0,1	7.16	1.37	24.3	1.05	1.25
1,2	8.56	0.85	21.7	0.56	0.91
2,3	9.07	0.78	28.4	0.41	0.67
3,4	9.37	0.55	23.4	0.24	0.43

PA, $-\Delta H$, $-\Delta G$, BDE in eV, $-\Delta S$ in cal K^{-1} mol^{-1}, [a] Michalczuk et al. [150], [b] Lau et al. [70], [c] Wróblewski et al. [151]

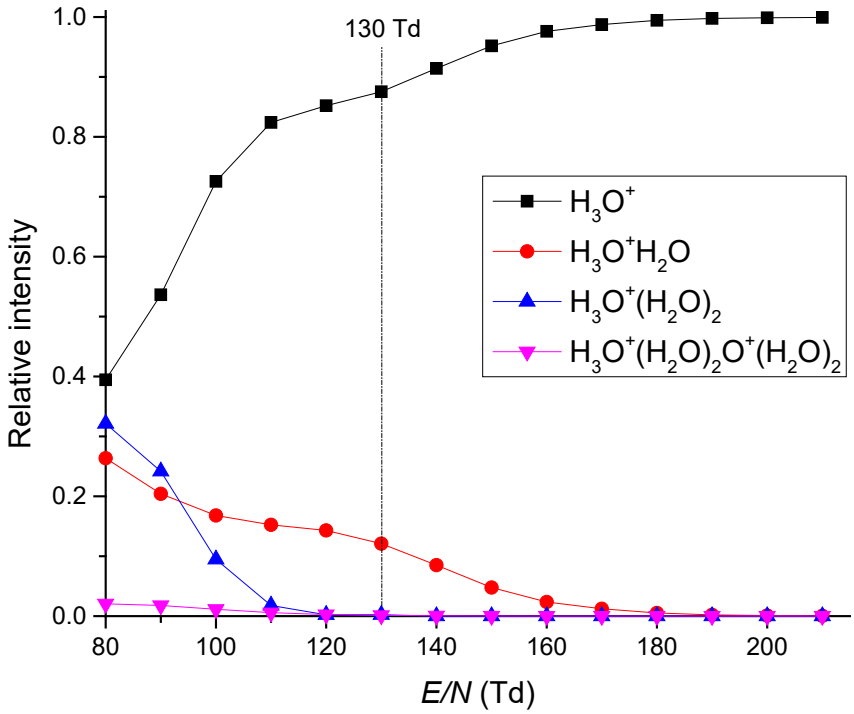

Figure 6 Relative intensity of hydrated hydronium clusters $H_3O^+(H_2O)_n$, n =0,1,2,3 in PTR-MS determined for various *E/N* values for a sample containing 0.6% humidity (absolute).

Selected ion flow-drift tube mass spectrometry (SIFDT-MS)

SIFDT-MS is a compilation of both PTR-MS and SIFT-MS, exploiting the strengths of both instruments. SIFDT-MS is equipped with an injection mass filter, allowing for a specific reagent ion to be selected. Selected ions are then injected into a flow-drift tube reactor. Flow-drift tubes use helium carrier gas in combination with an axial electric field, reducing diffusion losses to the walls as well as pumping speed requirements. The abundance of primary ion hydrates in the carrier gas in SIFDT-MS is lower compared to PTR-MS. Therefore, the *E/N* used in the SIFDT-MS reactor is lower than in the PTR-MS reactor. In the present work, we used a SIFDT-MS instrument developed by Spesyvyi et al. [39] This instrument additionally contains the possibility to directly determine the ion retention time via the application of a modulated signal on the injection ion optics. This therefore allows for the acquisition of ion mobilities and reaction energies data.

For SIFDT-MS used in this work (see Figure 7), the reagent ions are generated in a glowing cathode discharge, operating in a water vapor/synthetic air mixture. After extraction from the discharge, reagent ions are introduced via ion optics into the quadrupole mass filter. Ions with selected *m/z* are injected into the transition ion optics, equipped by the shutter grid. The shutter grid can modulate the ion transmission by applying the Hadamard modulation. [152] From the transition ion optics, ions are injected into the flow-drift tube (as a continuous stream or modulated by Hadamard modulation). The drift tube reactor is 145 mm long; has an ID of 10 mm; and is made of a PHOTONIS resistive glass tube with a total resistance of 14 MΩ. In the flow-drift tube, ions are carried along the tube by a homogenous electric field in a ~150 sccm reverse flow of He (1.5 mbar and 24 °C). Application of the voltage along the resistive layer (100 to 500 V) creates a homogenous electric field (from 10 to 100 Td) inside the cylinder. At the end of the flow-drift tube, ions are introduced via an orifice into the quadrupole mass spectrometer and are detected by the electron multiplier with conversion dynode. Sample gas is introduced into the helium gas stream at the end of the flow-drift tube and is carried through in helium flow reverse to the ion movement.

During the study, the SIFDT-MS instrument was frequently modified. A notable improvement as a result of this study was in the modification of the ion source. [153] In the modification, a hollow cathode discharge operating in a water vapor/synthetic

air mixture produces primary reagent ions. Ions are then transferred through to the stacked ring ion guide (SRIG) housed in a polypropylene vacuum chamber, operating in helium buffer gas (5.3 mbar), where they thermalize. Thermalized ions carried by the electric field and helium flow enter the next chamber (with a 50 mm long octupole), with an He pressure of about 0.3 mbar. Using an octupole, ions are guided through an aperture into the quadrupole mass filter. Filtered ions are introduced via the Venturi inlet to the small flow-drift tube (VDT in Figure 8), where ions are mixed with He buffer gas and thermalized again. At the end of the VDT, a series of three meshes are present which are required for Hadamard modulation of the ion current.

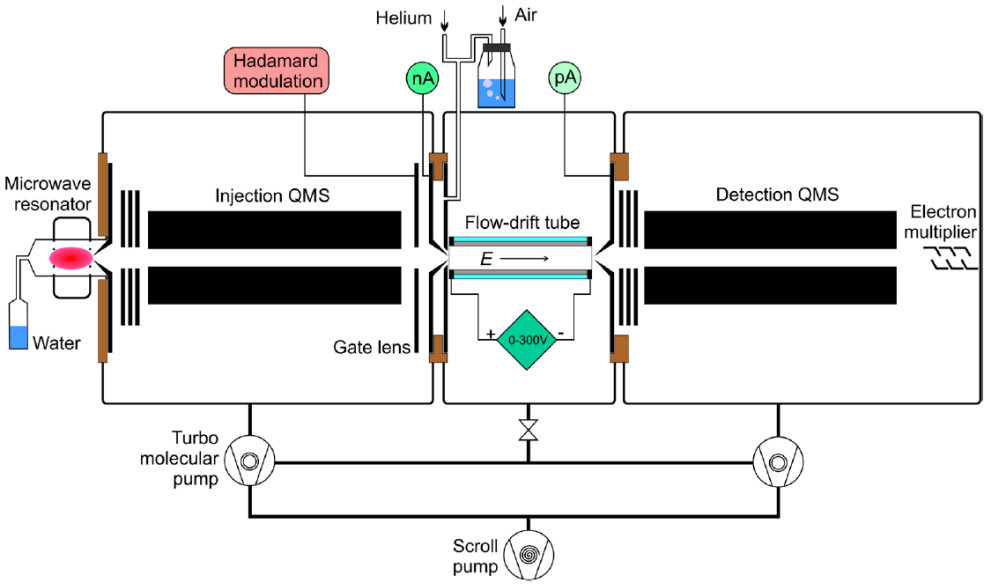

Figure 7 The SIFDT-MS instrument; the initial concept. [39]

The second design was built to generate a wider spectrum of reagent ions. The octupole chamber is equipped with a separate gas inlet. The gas molecules then react with primary reagent ions and become ionized via CI, for example via proton transfer from hydronium hydrates. The newly formed ions may be then introduced into the flow-drift tube via a quadrupole mass filter. This instrumental design allows for the generation of several various ions, allowing for a more in-depth study of particular (mainly secondary) reaction channels.

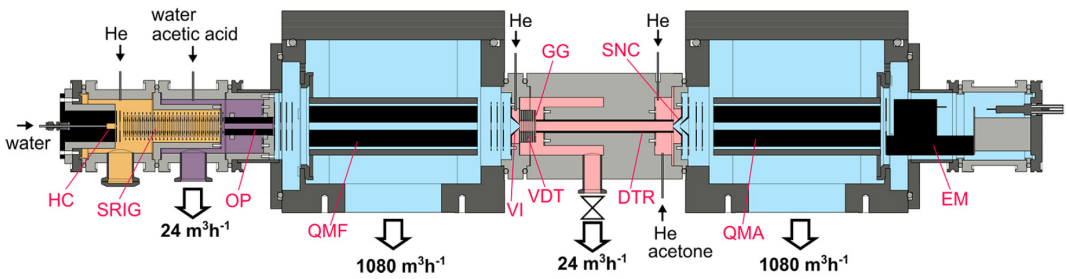

Figure 8 The SIFDT-MS instrument; the final design. [153] The coloured areas represent individual pressure regions: 5 mbar (yellow), 0.3 mbar (violet), 5×10^{-6} mbar (blue), 1.9 mbar (pink). HC - hollow cathode ion source, SRIG – stacked ring ion guide, OP - octupole, QMF - quadrupole mass filter, VI - Venturi inlet, VDT - Venturi flow-drift tube, GG - gating grid, DTR - drift tube reactor, SNC - ion sampling nose cone, QMA - quadrupole mass analyser, EM - electron multiplier with conversion

As ion velocity in the drift field changes with different ion mobilities, is necessary to measure the ion reaction/residence time (Eq. 55) for the precise calculation of trace sample concentrations. Ion residence time is determined by applying a pseudo-random Hadamard modulation on a specific electrode of the ion optics at the front of the flow-drift tube. The residence time is then reduced by the detector transfer time (time interval required for ions to travel from the end of the flow-drift tube to the detector), determined by applying the same modulation on the ion optics directly after the flow-drift tube. Knowing the length of the flow-drift tube, ion velocities may be determined. Ion velocity may then be used to calculate the ion mobility μ (Eq. 10); reduced ion mobility μ_0 (Eq. 50); and the mean reaction energy using the Wannier equation (Eq. 17, 18). It is important to note that application of the Hadamard modulation and the determination of the ion residence time requires ion intensities above 10k cps. The ion residence time therefore cannot always be determined.

The SIFDT-MS used in the present study is an instrument which bridges the SIFT-MS and PTR-MS techniques. The ability of SIFDT-MS to determine the residence time as well as the reaction energy is invaluable for ion chemistry studies under homogenous electric fields.

1.3. Areas of application

In previous sections, we have compared some aspects of SCIMS techniques and the reference technique, GC-MS. Now, we should discuss the benefits of SCIMS related to analytical applications, mainly high sensitivity, selectivity and rapid response time.

To recapitulate, the power of the GC-MS as an analytical technique comes from combining two differing analytical techniques. Firstly, pre-separation of a complex mixture occurs in the chromatographic column where individual components of the gas mixture interact with the active phase of the column and thus progress through the column at different velocities. As a result, each species travels through the column with a different retention time. Secondly, the separation by retention time is combined with EI-MS using an electron energy of 70 eV. The high electron energy induces fragmentation of molecules via dissociative electron ionization. The final fragmentation pattern represents a footprint of the molecular structure. Molecules can thus be identified based on the MS fragmentation pattern as well as on the retention time.

Chromatography is however a time-consuming process requiring tens of minutes to be completed. This clearly disables the possibility of analysing rapidly changing samples and limits sampling frequency. Additionally, if the targeted analyte compounds are at trace levels, pre-concentration of samples is required, usually using absorption or cryogenic traps. [154] This combination of multiple stages of analyses increases not only the complexity, but also requires frequent calibration procedures to be carried out for each analysed component.

Chemical ionization mass spectrometry has its advantages over GC-MS. The reaction energy for chemical ionization (usually 1-2 eV) is significantly lower compared to electron ionization (typically 70 eV), resulting in less fragmentation. Product ions generated by CI via charge transfer, proton transfer, or association reactions, form M^+, MH^+ or MR^+ respectively (where R represents the reactant ion). This carries information about the mass of the reactant neutral, M. It is therefore possible to directly identify the reaction neutrals from the mass spectrum. It is true that isobaric molecules may produce ion products with similar mass-to-charge ratios. This may however be overcome by using multiple reagent ions (commonly used in SIFT-MS) or by implementation of high-resolution mass spectrometry (commonly used in PTR-MS).

As long as the ionization mechanism is a fast reaction (which is usually the analytical aim), ionization occurs close to the collisional rate. Therefore, even for trace concentrations of analytes in the sample, we are able to achieve sufficient abundances of product ions for their MS analysis. This is true for most VOCs. The detection limit is a critical parameter that determines the applicability of individual SCIMS techniques. The first series of instruments had detection limits at levels of ppb. [37] The modern series of instruments however claim to achieve detection limits as low as ppt for SIFT-MS [155] and ppq for PTR-MS [156]. This reduces the need for sample pre-concentration. Low detection limits combined with high selectivity allows for SCIMS techniques to conduct the analyses of complex gas mixtures without pre-separation in a chromatographic column. The analytical time is therefore defined by the velocity of gases and ions in the reactor tube (usually at around tens of milliseconds). The ability to rapidly monitor the concentration of analytes is an important feature of SCIMS. Finally, SCIMS instruments are easily calibrated. The concentration of product ions in the reactor is directly dependent on the concentration of neutral reactants. Thus, knowing the mass discrimination functions of the mass spectrometer and the detector, we can directly relate the ion count rate to the concentration of the reactant molecule. The response is linear as long as the physical parameters of the instruments are constant (pressure, temperature, ion velocity, *E/N*). Therefore, after initial calibration, there is no need to recalibrate the instrument for every analyte species, as is needed for GC-MS. *N.B* This is true unless SCIMS analyses uses a pre-concentration step; is coupled with chromatography; or contains an ion funnel as a part of the ion optics.

GC-MS will always be a much better option for analysis of a completely unknown sample. Combination of precise chromatography, EI-MS and careful calibration provides much better selectivity and analytical quality. However, benefits of SCIMS are excellent for the monitoring of gas samples with known composition. Over the years, SCIMS was successfully recognised as a useful analytical technique, providing real-time quantitative analysis of organic compounds in various applications requiring fast response times. In the following paragraphs we would like to introduce the most promising areas where SCIMS techniques are positively recognised and frequently applied.

Probably the most notable area of application is analysis of human breath. As breath is exhaled through alveoli in lungs (in direct contact with the blood stream) there is potential for obtaining valuable clinical data using a non-invasive approach. For a decade, researchers have been analysing the potential of breath analysis within clinical applications, identifying several characteristic metabolites presented in human breath: ammonia, acetone, methanol, ethanol and isoprene. [157-160] However, it was also found that volatile compounds in breath are not necessarily metabolites originating from blood (endogenous source), but rather originate from exogenous sources, such as from bacteria found in the airways or mouth. Nevertheless, direct breath analysis via SCIMS techniques may be used to monitor (or eventually help diagnose) several diseases. Most typical is the analysis of acetone (as a direct metabolic product) for type 2 diabetes. [161] Targeted analysis and quantification of acetic acid may be used for monitoring patients with gastroesophageal reflux disease. [162] A promising application is the monitoring of VOCs emitted from bacterial infection [163-166] related to cystic fibrosis - autosomal recessive disorder affecting mainly children. [166, 167] This non-invasive approach was also used for the monitoring of advanced chronic kidney disease [168, 169] and chronic liver disease [170, 171]. Asthma is an additional disease which may also be diagnosed by SCIMS. [172, 173] Interestingly and promisingly, it is possible to analyse n-pentane with this method; a metabolite produced from inflammation within the body which may be a valuable in the diagnosis of chronical Crohn's disease. [174, 175] A big effort has been made to find a biomarker for lung cancer diagnosis, however, little success has been gained so far. [154] It is out of the scope of this thesis to cover all applications of SCIMS in breath research. More details can be found in the literature. [52, 158, 160]

The monitoring of breath volatiles is not restricted only for clinical diagnosis. It was demonstrated that SCIMS may be used to monitor drug levels in the human body. [176-179] This is beneficial in the surgical environment, where doctors may need to monitor the levels of drugs within a patient, (i.e. anaesthetics) from exhaled breath in real time. VOCs are not only emitted by breath but also by the skin [180-182]. In addition, the type and quantity of VOCs emitted from the human body may be directly related to one's mental state of mind (i.e. happiness, fear). This effect was observed in various studies in which human breath composition was shown to change while participants watched a film in the cinema; and the composition of breath has also been

shown to change during other collective activities, like football events. [183-185] The data showed variations in CO_2, isoprene and ethanol related to specific events. Overall, human breath composition may also be analysed in the field of forensics and security. Mobile SCIMS instruments based on IMS technology may be used to detect human presence in restricted areas, (i.e. refugees hiding in cars or lorries). [186, 187]

SCIMS techniques are also highly used in environmental applications. They are used in the identification and monitoring of biogenic VOCs (mainly monoterpenes) emitted from various ecosystems. Several studies were carried out investigating emission cycles in tropical rainforests [188-190], coniferous forests [191-193], deciduous forests [194-196], plantations [197-200], grasslands [201-203] and many more. [204, 205] The aim of such studies is to describe not only the ecosystem itself, but also its influence on atmospheric chemistry. Selective monitoring of individual biogenic VOCs, for example, does not correspond to the total [VOCs] determined from total reactivity measurements (Biogenic VOCs reacting with a controlled concentration of OH radicals, where the reduction on OH concentrations represents the concentration of VOCs in the sample). [206, 207] The study indicates that more than 30% of total reactivity (varying by season) is not described by monitored VOCs. This indicates a significant knowledge gap in environmental and atmospheric science. These environmental studies are also combined with studies of emissions from individual plants. [208, 209] Atmospheric chemistry is a topic directly related to global warming. Studies related to investigating emissions from rural and livestock activities; [210-212] the marine environment including bio-emissions of sea floor [213-215]; as well as industrial contamination; are of significant importance [216, 217].

Besides natural sources, atmospheric chemistry is heavily influenced by anthropogenic emissions which are also frequently studied and monitored by SCIMS. In the urban environment (mainly big cities) VOCs like isoprene, benzene and toluene together with NO_x are an important source of pollution via the production of ground-level ozone. The concentration of VOCs, as well as their secondary products during daytime hours have been investigated in many big cities including Houston [218], Barcelona [219], Tokyo [220], Paris [221, 222] and more. [223, 224] Related research focuses on individual sources of pollutants, such as diesel [225] and aircraft engine emissions [226, 227], as well as industrial sources [228, 229]. Besides outdoor air quality, indoor air quality studies focus on various emissions present in indoor environments. This

includes the study of volatiles released from the use of everyday domestic products [230-232], wall paintings [233] and building materials [234]. Apart from the analysis of domestic indoor air quality, SCIMS are also frequently used to monitor the air quality of clean rooms in industrial settings. This is required especially in the semiconductor industry, where even small contamination of specific halogen compounds can damage and decrease the quality of silicon component end products. [235]

Determination of odour and characteristic VOC emissions of products is also applied in food science and emissions related to food market products. The analysis of characteristic volatiles is used either to monitor the quality of products; identify product origin (through characteristic geographical labelling); to develop characteristic artificial odours; and to analyse complex food texture. The typical products with the need for quality assurance and geographical control is coffee [59, 236, 237], tea [238], wine [239] and cheese [240, 241]. These products are often characterised by their unique composition of volatiles, related to their geographic origin. Additionally, specific compounds responsible for the reduction of quality within these foods may be identified (the presence of halogenated anisoles in wine originated form corks, for example). [41, 242] Additionally, SCIMS may be used to monitor the growth of fruit and therefore help estimate the best time for harvesting [243, 244]. Almost every food product has a characteristic profile of volatile compounds, and it is therefore not possible to cover all of these in this thesis. Finally, food processing may also be monitored (i.e. fermentation of milk [245, 246], or yeast activity in beer production [247]).

The final significant application of SCIMS is homeland security and detection of warfare and threat agents. This includes the detection of drugs, explosives or others dangerous chemicals. [248-251] The detection of explosives is dominated by IMS systems, achieving very low detection limits (even though explosives are known for their low volatility). [252] By using PTR-MS, however, much better selectivity of individual explosives may be achieved. [253-255] SIFT-MS is used by customs offices in New Zealand and Canada to screen the shipping containers for the presence of toxic chemicals (fumigants) which may endanger staff during container inspection. [256]

The presented overview reflects the most common applications of SCIMS techniques. Each application has a specific requirement for sensitivity, selectivity and therefore also on the type of SCIMS technique used. For breath analysis, SIFT-MS provides the most consistent results; highly sensitive PTR-MS is often used in environmental applications. The field of applicability of SCIMS is however limited by several factors outlined in the next chapter. The aim of future development is to reduce said limitations and increase the possibility of using SCIMS in new areas of study.

1.4. Limitations of chemical ionization mass spectrometry

The applicability of SCIMS techniques for analytical applications is limited by two main factors: sensitivity and selectivity. Sensitivity describes the minimal concentration of trace gas in the analyte at which the SCIMS instrument is able to determine its presence (and quantify the analyte concentration) with respect to the background noise. Selectivity represents the ability of instruments to distinguish individual analyte components as well as determine their exact molecular composition. The aim of SCIMS instruments is to optimise both sensitivity and selectivity, without losing any of the benefits of using SCIMS. This is namely the use of pre-concentration systems and chromatography affecting the calibration requirements and rapid detection possibility, respectively.

The sensitivity of SCIMS is mainly determined by the design and type of instrument. The new generation of instruments is reaches detection limits up to ppt/ppq levels. This is mainly due to the advanced design of transfer ion optics and their implementation in the drift tube.

Selectivity on the other hand is mainly determined by ion chemistry occurring inside the SCIMS reactor, as well as by the resolution of the mass spectrometer. The characteristic feature of chemical ionization is the formation of product ions which carry information about the mass of the neutral reactant (M), by formation of M^+, MH^+, $M\text{-}H^+$, … ions. This however also occurs for isobaric and isomeric molecules which thus cannot be easily distinguished. For example, using a proton transfer reaction with H_3O^+, both acetone and 1-propanal produce MH^+ (*m/z* 59). [64, 66] The same applies for acetic acid and methyl formate when producing the MH^+ ion (*m/z* 61). [257] With increasing molecular mass, the number of isobaric compounds increase. Both main analytical SCIMS instruments (SIFT-MS and PTR-MS) use different approaches to resolve isobaric molecules. SIFT-MS uses a combination of multiple reagent ions (H_3O^+, NO^+ and O_2^+) that may be selectively introduced into the flow tube. Different types of molecules, producing similar ion products using one reagent ion, tend to react differently with other one. For example, when using NO^+, ketones mainly form $M.NO^+$ while alcohols produce $(M\text{-}H)^+ + HNO$. [64, 66] Early PTR-MS instruments, equipped with a quadrupole mass spectrometer, have limited possibilities to differentiate isobaric compounds. This was solved later by the installation of high-resolution Time-

of-Flight mass spectrometry (ToF-MS, resolution power > 10.000), able to differentiate between isobaric molecules.

Even though modern instruments now have the possibility to differentiate between isobaric compounds, secondary effects affecting the selectivity of these instruments are still present. The predominant remaining limitation is the reduced possibility to differentiate between various isomers. Isomeric molecules often produce similar product ions regardless to their reagent ion type. Thus, isomers are difficult to recognize in the obtained mass spectrum. For example, monoterpenes ($C_{10}H_{16}$) emitted by trees and plants react with all main reagent ions, H_3O^+, NO^+ and O_2^+. However, ion products are almost identical among all monoterpenes. [258] This is also true for branching ratios of individual product channels. Furthermore, H_3O^+ and NO^+ are the only reagent ions practical for monoterpene analysis in SIFT-MS as O_2^+ induces dissociative charge transfer, forming multiple ion fragments and in turn reducing selectivity significantly. If ion product branching ratios differ, it is possible to use a pseudoinverse matrix to determine the concentration of individual isomers if branching ratios of individual isomers are known. This approach was used in SIFDT, applying specific potential differences triggering CID in the flow-drift tube at witch ion products of individual monoterpenes started to differ. [259] This is, however, not always possible and can only be used with limited accuracy.

Peak interference is however not only caused by isobaric and isomeric molecules, but also by the presence of various parallel or secondary reactions. Ideally, the aim is to optimise the instrument so that each analyte produces only one product ion, as secondary ion products may interfere with the ion products from the compound. This is however not always possible and represents one of the main challenges of SCIMS. The ion chemistry is affected by the choice of the reagent ion as well as by the composition of the buffer gas. Proton transfer from H_3O^+ is often very rapid and is therefore the preferred ion for CI. Dissociative proton transfer may however also occur (as is seen in the analysis of monoterpenes, which forms $C_6H_9^+$ *m/z* 81). The alternative to H_3O^+ is used of the NO^+ reagent ion, with low IE(NO) = 9.2 eV [57], mainly reacting via association reactions producing $M.NO^+$ or $(M-H)^+ + HNO$ ions. However, NO^+ does not react with all VOCs and resonance capturing for association reactions is often slower than for proton transfer, which reduces the detection limit. O_2^+ is able to ionize most VOCs, although the IE(O_2) = 12.1 eV [57] is greatly above most VOCs,

frequently resulting in dissociative charge transfer producing multiple fragments. O_2^+ is therefore used as a reagent ion much less frequently.

Last but not least, selectivity and also sensitivity depend on the type and concentration of major components of the gas sample, in which an analyte is diluted. Reagent ions are purposely chosen so their reactivity with the main components of the gas solvent is limited. In reality, H_3O^+, NO^+ and O_2^+ commonly used for CI also react with N_2 and O_2, or CO_2. [260] Their reactions are however often neglected as water vapour is much more influential in the CI system. In the presence of water vapour, all formed ion products of N_2, O_2 and CO_2 quickly react with H_2O via proton transfer or ligand switching. Additionally, H_2O also reacts with reagent ions via an association reaction (as we already pointed out in the description of the PTR-MS instrument). The presence of water in acquired samples is inevitable. Even pure technical gases contain trace levels water impurities. Additionally, because of a dipole moment (μ_{H2O} = 1.85 D) [261], H_2O is much more influential compared to CO or CO_2 (also present in air). *N.B.* water vapour influences all reagent ions, although its presence is most notable for H_3O^+.

The concentration of water vapour in a sample gas depends on the sample sources and may vary from few ppm in an extremely dry sample gas, up to tens of thousands of ppm in gases saturated by water vapour. The pressure of a gas which is saturated with water vapour is very temperature sensitive. In breath analysis, the water concentration of a healthy patient with a body temperature of 36 °C is about 5%. Similar concentrations are seen in tropical forests. At room temperature, the absolute humidity may vary from 1% to 2.5%. The level of water vapour within a sample is important as this directly affects the selectivity and sensitivity of analysis, via a series of secondary reactions:

1, Association reaction with primary ions

All three primary reagent ions, H_3O^+, NO^+ and O_2^+ associate with H_2O forming ion hydrates. In SIFT-MS, for NO^+ and O_2^+, mostly $NO^+.(H_2O)_{1,2}$ and $O_2^+.(H_2O)_{1,2}$ hydrates are seen in the spectra. However, for H_3O^+, much larger hydronium hydrates may be observed, up to $H_3O^+.(H_2O)_4$. In PTR-MS and SIFDT-MS the formation of hydrates is reduced, however not completely removed. The presence of reagent ion hydrates not only reduces the selectivity of the instrument by interfering with product

ions with similar *m/z*, but also reduces the concentration of primary reagent ions (which in turn reduces sensitivity of analysis), for samples with higher humidity.

2, Secondary reactions of reagent ion hydrates

Reagent ion hydrates, formed via the association reaction of H_2O and the buffer gas, may often also react with the studied analytes. However, the products of these reactions may not correlate with the primary reaction channels. The possibility of protonated hydronium hydrates to initiate proton transfer is reduced, as proton affinity of water clusters increases with cluster size (see Table 2). A similar reduction in this reactivity applies for the charge transfer process initiated by NO^+ and O_2^+ as well as their respective hydrates. Moreover, reagent ion hydrates often react via ligand switching, forming hydrates of analyte ions:

$$H_3O^+.(H_2O) + M \rightarrow H_3O^+.M + H_2O. \quad (57)$$

This increases the number of analyte ion products.

3, Secondary reactions of analyte product ions

Product ions also interact with water vapour, forming ion hydrates via a three-body association reaction, in the same way as primary ions:

$$MH^+ + H_2O + N \rightarrow H_3O^+.M + N. \quad (58)$$

The level of hydration is dependent on the size and molecular structure of the primary ion, hydration level as well as on other parameters as gas temperature and gas pressure. Some molecules do not form hydrates (i.e. monoterpenes [262]) whereas others form hydrates very effectively (i.e. ketones or alcohols [37]). The ion chemistry is very specific for individual product ion hydrates. The formed product ion hydrates may either be stable; undergo additional reactions with H_2O molecules as reverse ligand switching:

$$MH^+.H_2O + H_2O \rightarrow H_3O^+.H_2O + M, \quad (59)$$

as well as undergo a chemical reaction producing unique ions.

The final reaction pattern is a combination of primary ionization reactions in conjunction with all associated secondary reactions. The influence of individual secondary processes differs for individual reagent ions as well as for different analytes. To illustrate this complexity, Figure 9 shows a full reaction diagram considering all

primary and secondary reactions for the reaction between H_3O^+ with a neutral reactant, M, in the presence of water vapour.

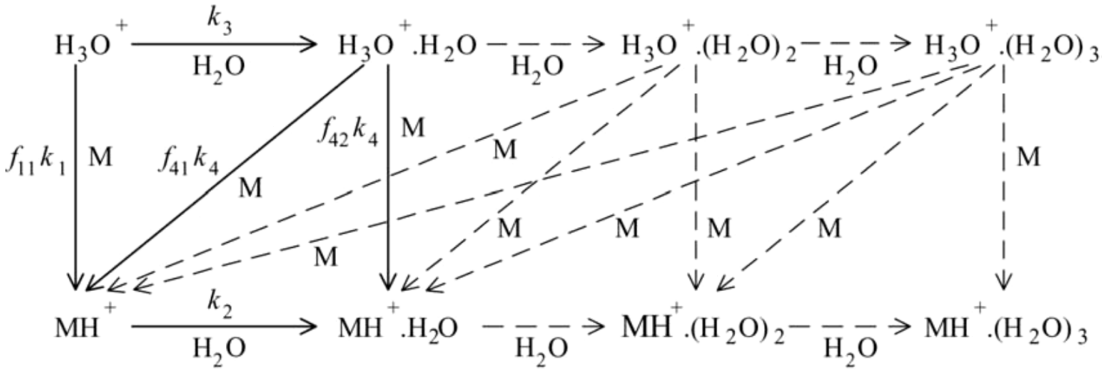

Figure 9 Illustrative reaction diagram of primary and secondary reactions of H_3O^+ with neutral a reactant, M, in the presence of water vapour. [263] Solid line reactions represent moderate humidity levels. Dashed reactions represent saturated water vapour.

It is also necessary to point out, the influence of water vapours on ion chemistry depend also on type of buffer gas and solvent gas components. Formation of water clusters via association is a three-body reaction, requiring a third particle to remove excess energy from the formed nascent complex. Increasing the concentration of two plus atomic molecules (with a high degree of levels of freedom) in the buffer or sample gas may increase the association reaction rate. For example, high concentrations of CO_2 in the sampled gas may significantly accelerate ion hydrates formation.

In conclusion SCIMS ion chemistry uses main ionization reaction channels (first order approximation) to determine the concentration of selected analytes. The presence of secondary reactions, however, induced mainly by water vapour increases the amount of ion products, affecting both sensitivity and selectivity of the analysis. Therefore, for humid samples or environments with rapidly changing humidity, it is also essential to consider the secondary reaction channels and include secondary ion products into the concentration calculation. Thus, careful understanding and analysis of secondary reaction channels is absolutely necessary.

1.5. Objectives of the thesis

The main objective of the ITN project IMPACT was to study the specific limitations of individual SCIMS techniques, to improve their selectivity and sensitivity and to introduce SCIMS to new areas of application. The project itself was divided into three main work groups: ion chemistry, applications and instrumental development. The presented thesis belongs to the ion chemistry work groups; thus, the objectives were defined as follows:

1, Mathematical description of the experimentally obtained dependencies of relative ion signals of product ions, their fragments and hydrates; on water vapour concentration, electrical fields and pressure within the SCIMS tube reactors.

2, Formulation and analytical validation of advanced algorithms resolving mass spectral overlaps of isobaric product and fragment ions, based on two-dimensional data analyses (*m/z* versus the reduced electric field, *E/N*).

3, Characterisation of a Thermal Desorption Unit (TDU) developed for PTR-MS used with SIFT-MS.

4, Formulation and analytical validation of algorithms for analyses of desorption temperature resolved TDU-SIFT-MS data, with improved selectivity.

5, Testing the developed methods in interdisciplinary studies, in clinical breath analysis and environmental science.

By solving the list of stated objectives, a list of expected results should be achieved:

1, Knowledge and data on the variation of SCIMS relative mass spectral ion intensities with humidity and electric fields.

2, New mathematical algorithms for calculations of VOC concentrations from mass spectral SCIMS data, accounting for ion overlaps.

3, Original interdisciplinary results in the areas of breath analysis and environmental science.

During the project, the list of objectives was developed and modified with respect to the scope the project. It must be noted that this list of objectives was formed as part of the official project proposal, written five to six years before thesis submission.

The development of TDU and its coupling with PTR-MS was made at KORE Technology Ltd. (One of the project beneficiaries), in the UK. The TDU was used for the analysis of drugs and other solid samples with low vapour pressures. [254, 264] The company has created and optimized hardware and software for the TDU; now available on the market. Separately, the TDU was developed in Prague by our colleagues previous to the IMPACT project, founded by another GACR national grant and thus will not be included in this thesis. [204] As a result, objectives 3 and 4 were fulfilled without contribution from the author of this thesis. Additionally, both industrial partners of the IMPACT project, KORE Technology and IONICON, have been frequently developing their operational software. One of the features included in their software package is the possibility to determine the composition of a sample by a multi-peak analysis of obtained mass spectra. The method used a pseudoinverse matrix, created from a list of ion products for each compound. The software can thus resolve mass spectral overlaps in a complex sample. Objective No. 2 was thus modified as to provide an analysis of the ion chemistry using two-dimensional data analyses techniques, including gas chromatography.

Therefore, the remaining objectives of the thesis are as follows:

- Investigation of the main limitations of SCIMS techniques with respect to improving sensitivity and selectivity of instruments, by studying the complex ion chemistry within specific SCIMS techniques, mainly focusing on secondary reactions with water.
- Mathematical descriptions of primary and secondary reactions capable of predicting the behaviour of relative ion signals of product ions, their fragments and hydrates, on water vapour concentration, electrical fields and pressure.
- Experimental study of complex ion-molecular reactions relevant for clinical breath analysis, environmental science and other applications related to SCIMS.
- To expand the capabilities of SCIMS analysis to more applications.

In the following chapters we present a summary of the main results, reflecting the individual objectives. Firstly, we introduce the construction of a fast GC pre-separation unit coupled with SIFT-MS, representing an elegant solution for separation of molecular isomers. Secondly, we present the development of a universal numerical

simulator of ion-molecular reactions which was used as a tool to supplement our experimental studies. Finally, we present a study of complex ion chemistry on molecules relevant for SCIMS applications, as well as studies further expanding applicability of SCIMS.

2. Construction of fast GC pre-separation for SIFT-MS

Identification of specific isomers in SCIMS is difficult. Isomers (especially structural isomers) react in a similar way with all reagent ions and thus it is difficult to identify them using multiple reagent ion approaches or using high-resolution MS. The same problem occurs even in the presence of an electric field. Product branching ratios for isomers may differ even if products have the same *m/z*. In a complex sample with an unknown mixture of different isomers, quantitative analysis is very difficult and sometimes impossible.

A classic method used to analyse the concentration of different isomers is gas chromatography. The different structure of individual isomers affects their interaction with the active phase of the column. Isomers may be then analysed based on different retention times. [265, 266] A difference in retention time is not guaranteed, but a difference in the molecular structure often leads to differences in the retention time. Classical GC analysis is however time consuming. Based on the type of the column and temperature profile of the analysis, one measurement may take up to an hour to run. This is in contrast to SCIMS techniques, which have built their reputation on real-time fast analysis.

To solve the problem of isomer analysis, we need to make a compromise between the speed of chromatography analysis and its quality. Comparing to classical chromatographic techniques, SCIMS does not require the separation of all molecules presented in the sample. Instead, SCIMS aims for a specific isomer presented in breath or environmental samples, as other molecules can be determined by ion chemistry. Thus, the chromatography coupled to SCIMS may be less specific. The modern solution to this problem used in SCIMS analysis is called fast gas chromatography (fast GC).

Fast GC uses a short column of 5-10 m (compared to 40 m in standard GC) as well as fast temperature ramps (>20°C/min) in order to provide chromatographic analysis in under 5 min. [267] The chromatogram cannot be used to fully determine the composition of the sample, however may be used to help analyse a specific set of isomers. The technique was successfully applied in the analysis of monoterpenes using PTR-MS with a great success. [268, 269] Following previous studies, we developed a fast GC unit to test if the same approach could be applied to SIFT-MS.

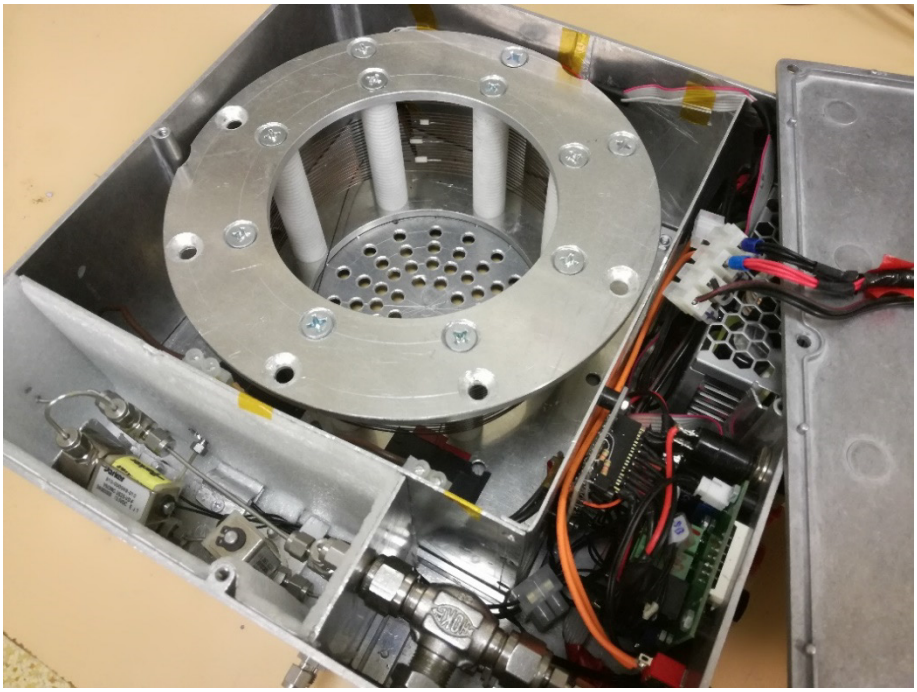

Figure 10 Photograph of the fast GC unit built for the study of individual monoterpenes in gaseous mixtures.

In our solution (see Figure 10), we used two 5 m long metallic GC columns, MXT-1 and MXT-Volatiles, having different active phases of 0.15 µm and 1.15 µm, respectively. Using their own conductivity, both columns were heated from an external power source using joule heating. The study was initiated by ion chemistry and elution times study of individual, most abundant monoterpene isomers: α-pinene, β-pinene, Camphene, Myrcene, 3-carene, R-limonene, α-terpinene and γ-terpinene. These data were later used for analysis of artificially prepared monoterpene mixtures. The selectivity of the obtained chromatogram was further improved by the combined use of H_3O^+ and NO^+ reagent ions; and by analysing the relative ratio of the two main ion products, *m/z* 81 ($C_6H_9^+$) and *m/z* 137 ($C_{10}H_{17}^+$) for H_3O^+; and *m/z* 93 ($C_7H_9^+$) and *m/z* 136 ($C_{10}H_{16}^+$) for NO^+. The obtained knowledge was then applied to the analysis of monoterpene emissions from a series of coniferous biological samples, namely *Picea Pungens Engelm*., *Abies Concolor and Pinus Nigra*.

In this work, we have demonstrated the analytical value the novel combination of fast GC coupled to SIFT-MS. As an enhancement to fast GC systems combined with PTR-MS, we went on to achieve a relatively high LOD (~ 16 ppbv). This is mainly due to

the limited sample flow eluting from the column (2-3 sccm) which seems insufficient for SIFT-MS (usually using an order of magnitude more). This could be resolved by using a wider column or by using multiple capillaries in parallel. The use of multiple reagent ions was however a clear advantage as it improved the identification of individual monoterpenes within the chromatogram which was not fully resolved. Finally, the overall benefit of fast GC (not yet stated) is the successful separation of water vapour from the sample. As we observed, the retention time of water is much faster compared to the retention time of the studied monoterpenes. Water vapour is thus evacuated from the flow tube before the analyte of interest is ionized. Consequently, ion chemistry is not significantly affected by system humidity which allows for a systematic use of product branching ratios in future analyses, regardless of sample humidity. This is a very strong benefit of this technique, improving both selectivity and sensitivity of VOC determination in environmental settings.

The full study describing the coupling of fast gas chromatography to selected ion flow tube mass spectrometry for the analysis of individual monoterpenes within mixtures is presented in **Attachment A.1**.

3. Complex model of ion chemistry in SCI-MS

The ion chemistry within the reactor tubes can be very complex. This is because the main ionization channels produce multiple ion products and all main ion reactants and products may react with water vapour in a series of secondary reactions. The presence of secondary reactions increases the complexity of mass spectra, reducing selectivity and sensitivity of the technique. In order to determine the concentration of the analyte, the calculation must consider the ion intensities of all product ions, as well as those produced by secondary reactions. Changes in samples humidity (as well as other components as CO_2) thus affects the presence of secondary ion products. For the successful application of SCIMS in ambient environments where sample humidity may change over time, the secondary reactions must be well understood. For this reason, we have built a numerical simulator capable of simulating the ion chemistry within the reactor flow-tube.

The Kinetics of Ion Molecular Interactions Simulator (KIMI Sim) is a numerical simulator of ion-chemistry found in SCIMS instruments. KIMI was produced to help users understand complex ion-neutral molecule interactions and to simulate the ion and neutral molecule number densities in a flow tube or a drift tube. KIMI may however also be used to simulate various other problems involving ion-molecule interactions. The software was built as a Windows desktop application in the .NET 4.6.1 framework in C#. KIMI uses an interactive graphical interface where the proposed set of ion-molecular reactions may be created. The KIMI then transforms the graphical reaction into a set of kinetic equations that are solved along the central axis of the reactor tube using the classical Runge-Kutta algorithm. [270] Results of the simulation may then be interactively inspected, downloaded or compared with experimental results. The details of how to access the KIMI software are presented at the end of the thesis. (See **Attachment A.7** in the list of attachments.)

The software is composed of two core programs (classes) (see Figure 11). The Main program is responsible for management of software settings; main simulation properties; management of individual reaction species as well as for the interactive graphical interface where the proposed reaction sequence is formed. After definition of all physical properties and the formation of a valid reaction scheme, the main program constructs the calculation, calculating all essential information. Calculation

control also allows the user to modify some reaction properties, for example reaction rate constants. Additionally, user may enable a homogenous electric field into the simulation. Furthermore, the calculation control also enables a multidimensional simulation by presenting a range of *E/N* values (or a range of number densities) of one of the reactants. If this option is selected then the simulation will be executed for every value of *E/N* or reactant concentration within the pre-defined range. After initialization of the calculation, the calculation control transforms the reaction objects into a set of differential kinetic equations and solves them along the central axis of the reactor. The calculation is executed by the construction of a "calculation" program, executing a one-step solution (via a differential equation). The process is repeated across selected reaction coordinates. The final data set is stored within a Data management class entity, from where it is accessed through the data plot function. Data plot is also capable of comparing simulation results with experimental data.

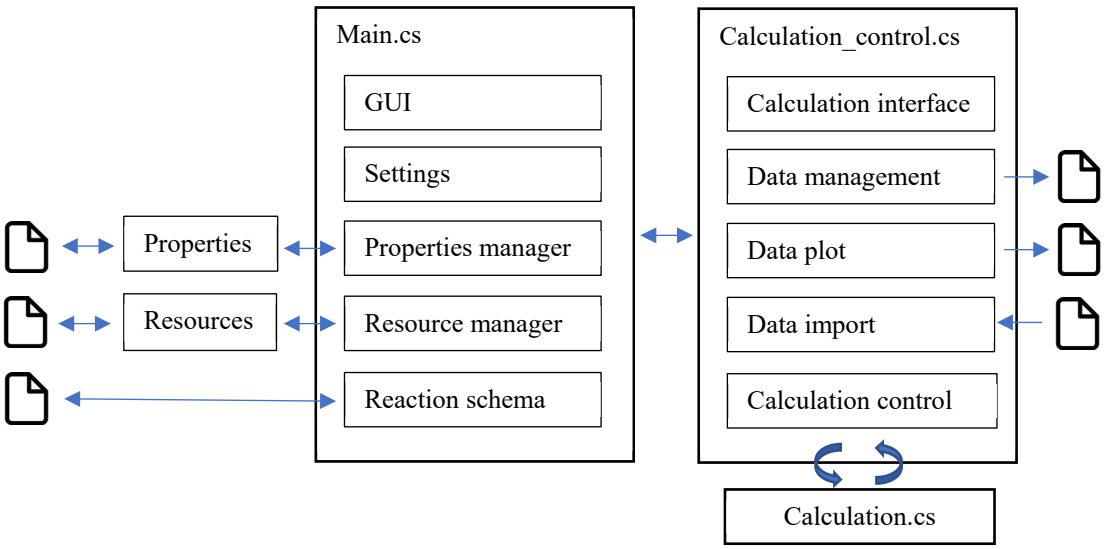

Figure 11 A schematic view of the KIMI main programs and their functionalities.

Before the creation of a reaction scheme, it is necessary to define the reactant and product entities. This may be done via accessing **Resource manager** (Properties → Resource manager, Figure 12) and by collecting a list of particles (ions and neutrals) used in the simulation. Every entity has a defined charge state; name (unique string identifier); chemical formula and a short name. The short name is a short non-unique string, used for the visual representation of the particle. The remaining parameters are

required based on the simulation settings. The ion mobility is only required for ions; and only if the simulation incorporates a drift field. The ion mobility may also be set as a function of *E/N*, if necessary. The number density represents the initial number density of particles at the beginning of the simulation. The molar mass is automatically determined from the reaction formula. Diffusion coefficients are necessary if the diffusion effect is enabled in the Diffusion setting; and must signify a diffusion coefficient value representing standard experimental conditions (reactor pressure 1 Torr = 1.33 mbar and temperature 300 K). The diffusion coefficient may be automatically estimated based on the masses of the reaction species, by using a semi-empirical function [136]

$$D_{\mathrm{He}} = 140\ \mathrm{cm^2 s^{-1}} \ln\frac{383}{m/z}. \tag{60}$$

Note that this estimation may only be used when helium is the carrier gas. The error of such an estimation should be less than 50%, although should also be better than 20% for VOCs (and their hydrates). The list of species is stored in the applications setting for later use and may be exported or imported from an external file.

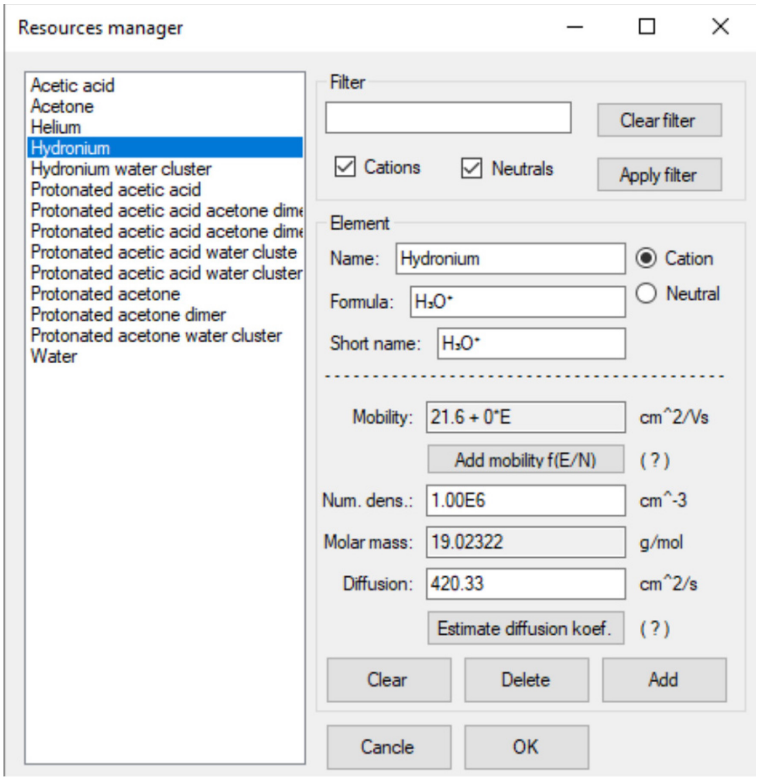

Figure 12 Resource manager responsible for the management of individual species within the simulation.

The next step is defining the **Calculation properties** (Properties → Calculation properties, Figure 13). The calculation properties include the general physical properties of the simulation, as well as the main calculation options. The definition of general properties is mandatory for a successful simulation. The carrier gas type allows for the selection of representative neutral species (previously defined in the Resource manager). This is necessary only for the advanced definition of reaction rates, where $k = f(KE_{CM})$. The carrier gas pressure and temperature are given as the mean value over the gas pressures and temperatures recorded within a reactor. The carrier gas bulk velocity (v_g) and the ion flow velocity (v_i) are parameters which are also crucial for flow-tube simulations.

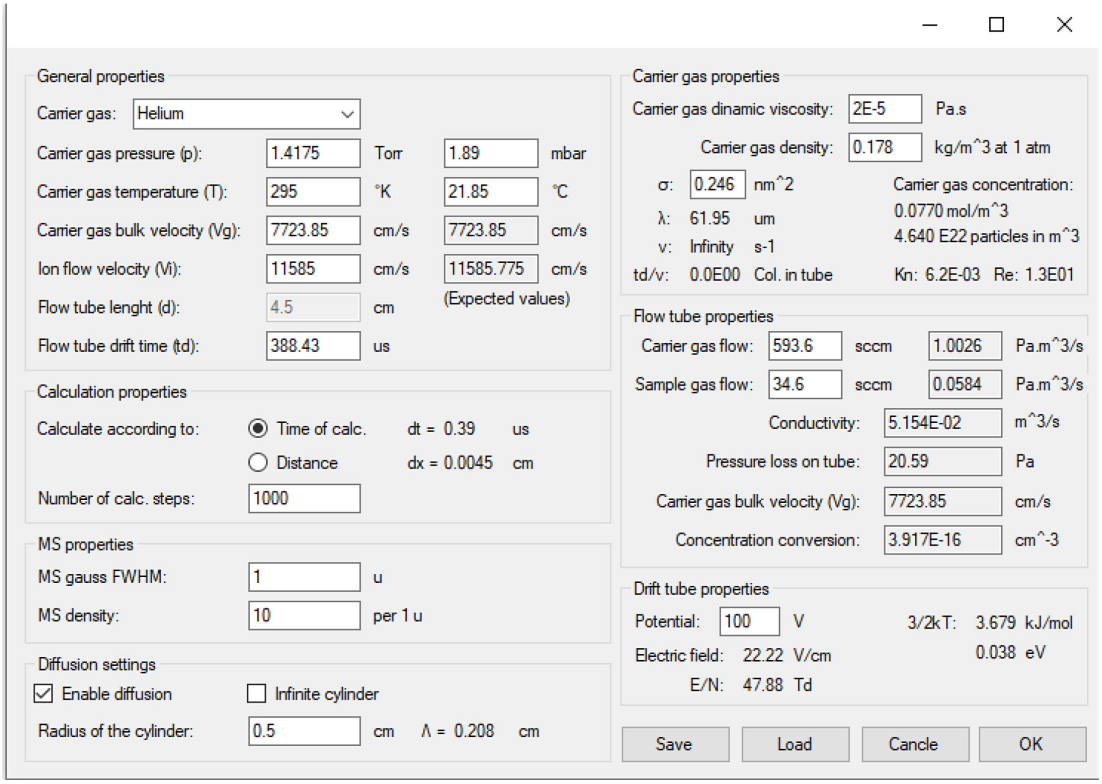

Figure 13 The calculation properties window responsible for the management of physical properties and geometries within the simulation.

The carrier gas bulk velocity represents the mean velocity of the carrier gas flowing in laminar mode through a reactor tube. The ion flow velocity represents the mean velocity of ions carried by carrier gas through the flow tube. For a flow-tube

simulation, this value is used to determine the actual reaction time. For drift-tube experiments, this component represents the parasitic ion flow causing an error in the ion drift velocity value calculated. The ion flow velocity (under normal experimental conditions) is expected to be ~ 1.5 × v_g. [23] This is an empirical value based on the ion injection geometry. Ions are injected into a reactor via an orifice situated close to the central axis. Thus, the maximum of the radial ion density distributed is also located on the reactor axis. This density is then reduced via radial ion diffusion. However, the presence of a laminar flow causes the majority of ions (which are centralized on the central reactor axis) to move faster than the ions which already diffused (and are lost) to the reactor wall. The final radial profile of ion velocities is therefore composed of the carrier gas radial velocity $v_g(r)$ and the ion radial density distribution $\rho_0(r)$, $v_g(r) \times \rho_0(r)$. The mean value of ion velocities is thus larger compared to the neutral gas velocity.[1] However, as the gas flow near the injection orifice is not laminar (but somewhat turbulent), it is difficult to properly evaluate this relationship and therefore only the empirical coefficient is applied. The next two parameters, the tube length (d) and the tube drift time (t_d), define the length of the system and are bounded through ion drift velocity. It is therefore necessary to define only one of these parameters. The drift time represents the time a reagent ion takes to pass through the reactor, $t_d = d/v_i$.

In the remaining sections, the user may define whether the reaction differential equation is solved in accordance with the reaction time or the reaction coordinate differential. The number of calculation steps subsequently define the size of the calculation differential. The size of the reaction differential requires specific attention. Too many calculation steps (causing very small reaction differentials) results in long calculation times. Too few calculation steps may cause the numerical method to oscillate, consequently producing false results, especially when large changes in the particle number density is expected. The MS properties define the visual quality of artificially generated MS spectra. The diffusion settings allow the user to define the radius of a reactor and also enable a radial diffusion term to be incorporated into the numerical calculation. The ion diffusion is consequently evaluated using the characteristic diffusion length, Λ, defined as:

[1] $v_i(r) = \int v_g(r) \times \rho_i(r,x)\mathrm{d}x$ and than $\overline{v_i(r)} > \overline{v_g(r)}$

$$\Lambda = \sqrt{\frac{1}{\left(\frac{2.405}{R}\right)^2 + \left(\frac{\pi}{L}\right)^2}}, \tag{61}$$

where R and L represent the radius and length of the cylindrical reactor, respectively. Selecting the option for infinite ciliated systems takes the solution for $L \rightarrow \infty$.

Finally, the calculation properties contain a series of assisting calculations, including those accounting for carrier gas properties; flow and drift tube properties. In the carrier gas properties section, the user may find information on the mean free path of particles in the buffer gas; the Reynold and Knudsen number; and of necessity, the value of the carrier gas number density at defined temperatures and pressures (for specific three body reactions). The flow tube properties also assist in SIFT-MS simulations. Using the reactor geometry and defining the carrier gas and sample gas flow rates (combined with carrier gas properties), the system will calculate the conductivity of the reactor tube and will estimate the reactor pressure loss. This information is useful if a pressure gauge is located on the side of a reactor, as for the simulation a mean reactor tube pressure is used. Finally, the system is able to predict the gas bulk velocity used for the calculation of ion velocities and reaction times (settings dependant):

$$\mathrm{v}_g = \frac{\theta}{pS}\frac{T}{273\ \mathrm{K}}, \tag{62}$$

where θ represents the total gas flow though the reactor tube and S is the flow tube surface area. In the drift tube properties section of the program, the user may test the value of E/N when a specific electric potential is applied along the reactor axis. In addition, the value of the thermal ion energy is presented. The set of calculation properties may also be exported to an external file.

After definition of the reaction properties as well as the individual reactant and product species, the reaction scheme may be formed by adding individual ions into the reaction grid (see Figure 14). Selecting an empty element of the grid allows the user to associate the grid element with one ion species. To simplify the reaction system, only the short names of ions are presented in the reaction scheme. Two ion species may then be connected together to create a reaction. After establishing this connection, additional parameters of ion-molecule reactions may be defined, including reactions specifications, as well as product neutrals of reaction rates. The reaction rate may be a constant, or as a function of E/N or KE_{CM}. The user is free to add and modify any

reaction species as well as alter which properties are included in the simulation. Every reaction applied in the scheme is saved and man be reused later. The only limitation is that every used species must be a product of at least one reaction. The reaction scheme may be saved for later use, or loaded from the file. When all ions on the reaction grid are properly connected, the Proceed button is enabled and the Calculation control window can be open.

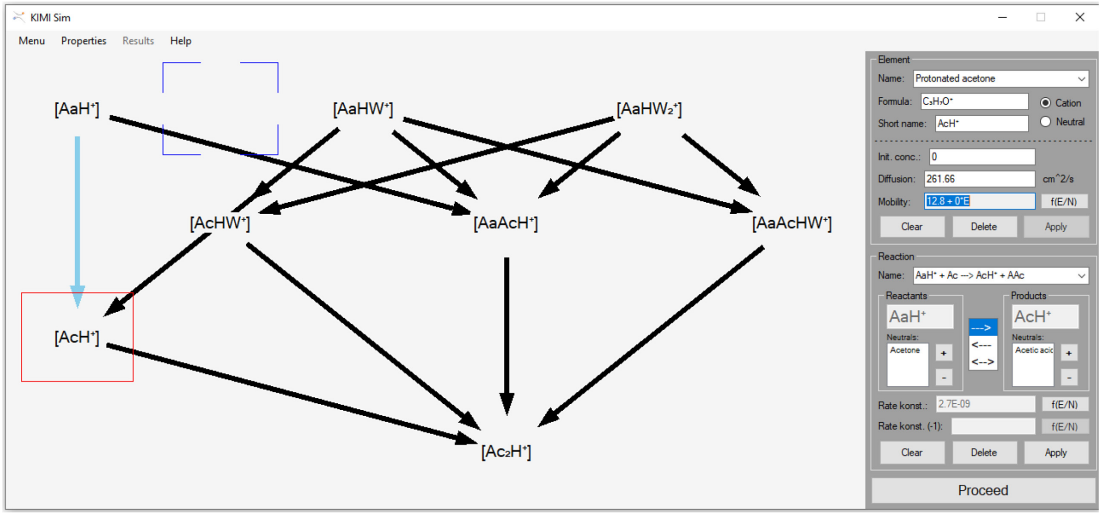

Figure 14 The Calculation properties window is responsible for the management of physical properties and geometry of simulation.

The **Calculation control** gives access to the simulation properties as well as the reactions and species defined in the reaction grid. Each reaction included together with all ions and neutrals are listed in the overview (see Figure 15). The overview allows for the modification of reaction rate constants or initial number densities before each simulation. If the reaction rate is introduced as a function of *E/N* then the individual parameters of a function may also be modified, although the format of the reaction rate must remain unchanged. One of the implemented features is the possibility of grouping individual species into sub-groups. This allows for the calculation of the relative concentrations of species within the respective sub-groups. This may be used, for example, when studying the relative distribution of reagent and product ions, individually.

Calculation control also enables dynamic changes in the number density of one selected species. If enabled, the simulation will be executed for every defined value.

This option may be used for the study of secondary reactions, simulating the effect of an increase in the water vapour, on the ion chemistry. Similarly, this may be pre-defined for a range of *E/N* values.

Initialization of the simulation triggers a series of processes leading to the transformation of reaction objects into calculation objects. Due to the object-oriented architecture of KIMI, Calculation control has access to objects defined in the Resource manager (if they were introduced into the reaction grid previously). Within the reaction grid, reactions represent the main objects defining relations between ions. During transformation, individual ions and neutrals become the main objects, carrying information about other particle objects and their relation to them. After transformation, a new constructed series of objects follows the format of a kinetic equation (see Figure 16).

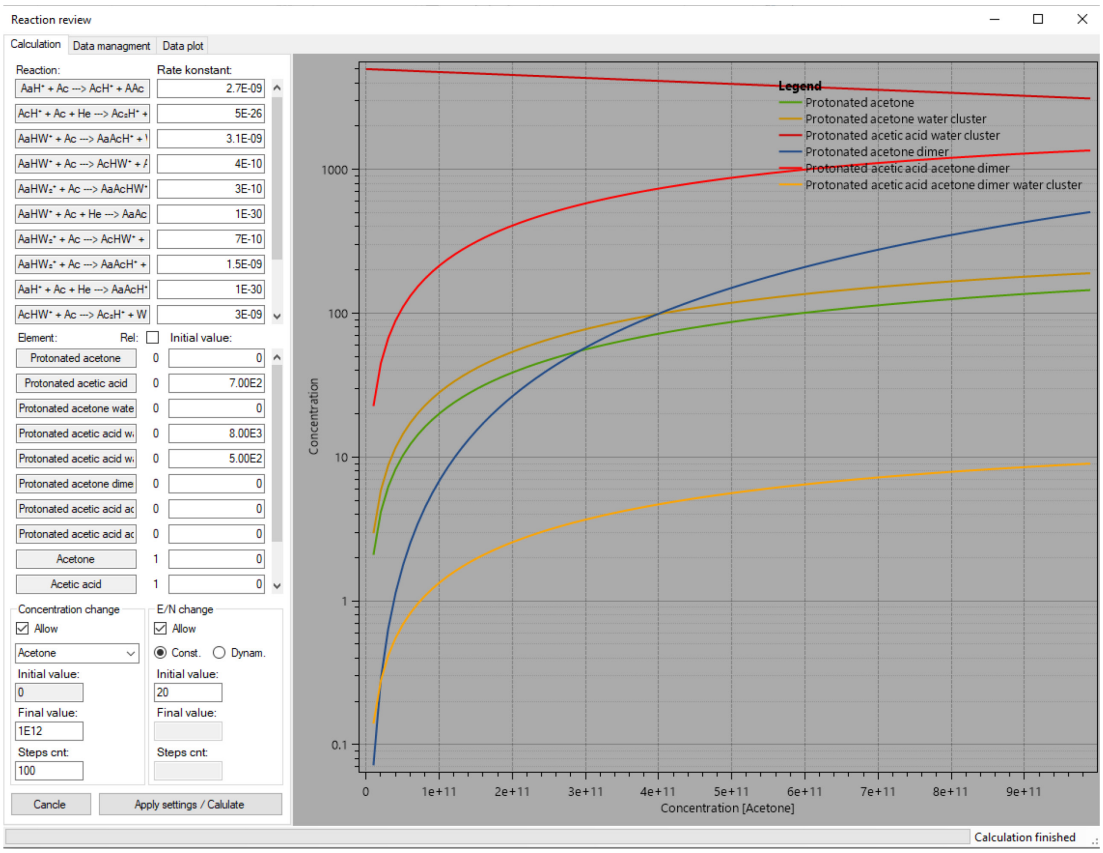

Figure 15 Calculation control window.

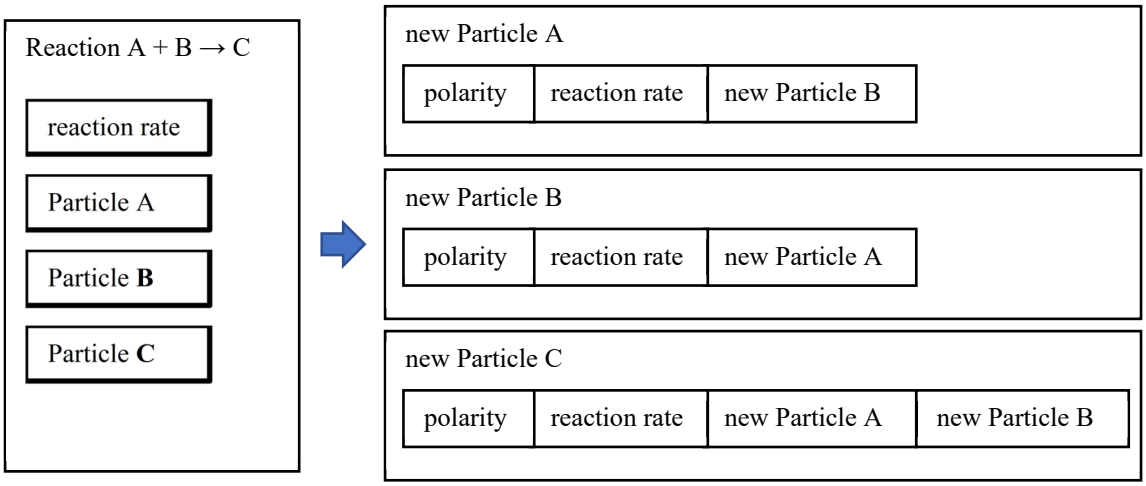

Figure 16 A visualisation of the transformation process. The main reaction object (left) is transformed into a series of calculation objects (left). The new objects are later used by Calculation class to calculate a single step numerical solution of differential kinetic equations.

After data transformation, Calculation control initiates its internal loop. During each iteration**, Calculation control** creates a calculation class, providing a single step solution for a kinetic differential equation, for every particle object. After every iteration, the one step solution of particle number density is stored in memory and is used in the next iteration as a new starting value. The actual differential form of the kinetic equations is also generated within the calculation class, based on the input variables prepared by the Calculation control. This includes the size and type of differential, as well as values of reaction rate or ion mobility for actual *E/N*. At the end of the calculation, differential equations follow the time dependent format for the flow tube (Eq. 39, 40), or the axial coordinate format for the drift-tube (Eq. 53, 54), for constant *E/N*.

Following this, the calculation class program solves the system of differential equations using the classical Runge-Kutta method. This method solves a differential equation as:

$$\frac{\mathrm{d}y}{\mathrm{d}t} = f(t, y), \quad y(t_0) = y_0 \tag{63}$$

where y is an unknown function of t and y_0 is the initial value. Using the discrete parameter $h > 0$, the method estimates the following for $n \geq 0$:

$$y_{n+1} = y_n + \frac{1}{6}h(k_1 + k_2 + k_3 + k_4),$$
$$t_{n+1} = t_n + h, \tag{64}$$

where:

$$k_1 = f(t_n, y_n),$$
$$k_2 = f\left(t_n + \frac{h}{2}, y_n + h\frac{k_1}{2}\right),$$
$$k_3 = f\left(t_n + \frac{h}{2}, y_n + h\frac{k_2}{2}\right), \tag{65}$$
$$k_4 = f(t_n + h, y_n + hk_3).$$

Thus, the value y_{n+1} is an approximation for $y(t_{n+1})$. In the present solution, y represents the particle number density and h is the time or axial differential. It is important to note that the stability of the numerical solution is related to both dy/dt and h. For large changes of y, h needs to be sufficiently small or the solution will be unstable.

All determined values of particle concentration are stored in the **Data storage**, which may be freely accessed by the user. Under the **Data management** list option, the user may browse through previously executed calculations; export them or recover any settings from previous calculations. The user may also import any external experimental data (for comparison with the simulation results). Finally, under the data plot list option, the user may inspect their calculation results and download individual data plots.

The functionality of KIMI was tested on a series of experimental data, produced by SIFT-MS and SIFDT-MS methods. For the initial test, we studied the influence of water vapour concentration on the formation of hydronium hydrates in SIFT-MS. In later work, we conducted similar experiments involving acetone vapours. Both the hydronium reactions with water

vapour as well as with acetone are well described in literature. [64, 136, 139, 271] As a result, we used the set of known reaction rate constants as a foundation the for simulation of ion chemistry in the program. Reaction rate constants were subsequently

optimised to interpolate experimental data. For the experiment, we used a nalophan bag filled with dry air and acetone for the second study. The humidity of our sample was changed by injecting warm liquid water into the sample bag while the sample gas was introduced into inlet of the SIFT-MS. SIFT-MS is capable of directly calculating the water vapour concentration of sampled gas based on the hydronium hydrates intensity (of c/s) distribution. However, in order to reduce the systematic difference between the experiment and simulation, we decided to use a dimensionless parameter H,

$$H = ln\left(\frac{[H_3O^+] + [H_3O^+.H_2O] + [H_3O^+(H_2O)_2] + \cdots}{[H_3O^+]}\right) = ln\left(\frac{i(H_3O^+) + i(H_3O^+.H_2O) + i(H_3O^+(H_2O)_2) + \cdots}{i(H_3O^+)}\right), \quad (66)$$

representing the logarithm of the ratio between all water related reagent and product ions (hydronium and its respective clusters). These values were linearly dependent on the water vapour concentration in the flow-tube.

Table 3 The list of reactions and reaction rate constants used for the simulation of humid ion chemistry; and its dependence on water vapour concentration in the flow tube. The reaction rates for the three body association reactions are presented as effective two-body reaction rate coefficients. k_{lit} represents data taken from [137].

Reaction	k_{lit} (cm^3s^{-1})	k_{KIMI} (cm^3s^{-1})
$H_3O^+ + H_2O \rightarrow H_3O^+H_2O$	2.1×10^{-11}	1.36×10^{-11}
$H_3O^+H_2O + H_2O \rightarrow H_3O^+(H_2O)_2$	5.7×10^{-11}	3.23×10^{-11}
$H_3O^+(H_2O)_2 + H_2O \rightarrow H_3O^+(H_2O)_3$	6.2×10^{-11}	3.1×10^{-11}
$H_3O^+(H_2O)_3 \rightarrow H_3O^+(H_2O)_2 + H_2O$		$1000\ s^{-1}$

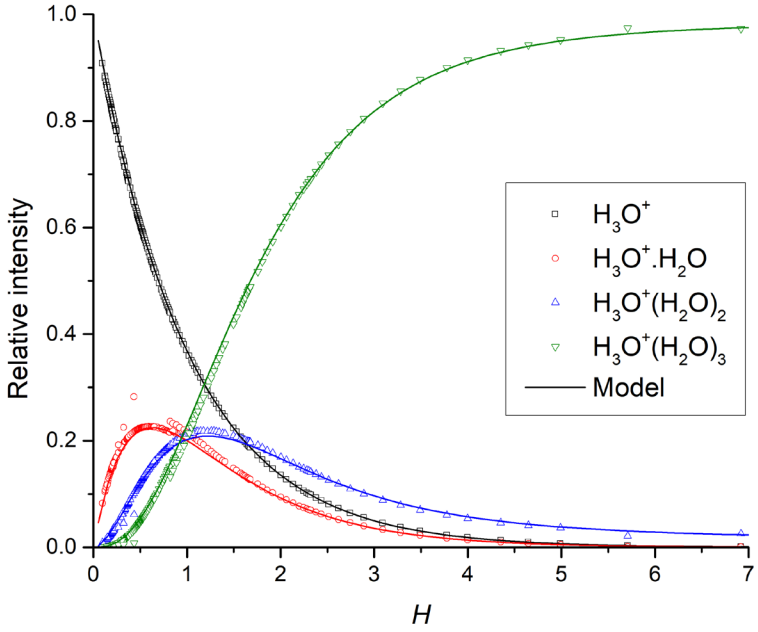

Figure 17 Initial simulation of the formation of hydronium hydrates. Experimental data (in symbols) were interpolated by the set of reactions listed in Table 3.

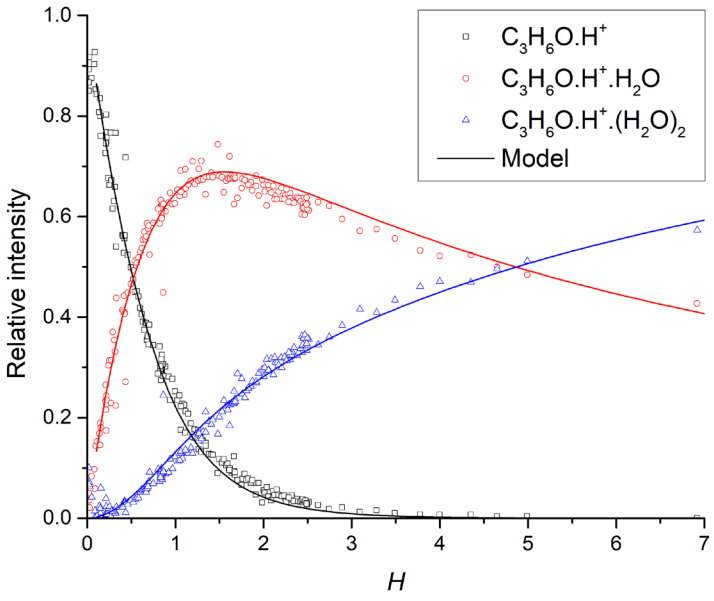

Figure 18 An initial simulation of acetone's ion chemistry under the experimental conditions described in the text. Experimental data (in symbols) were interpolated by the set of reactions shown in Figure 19.

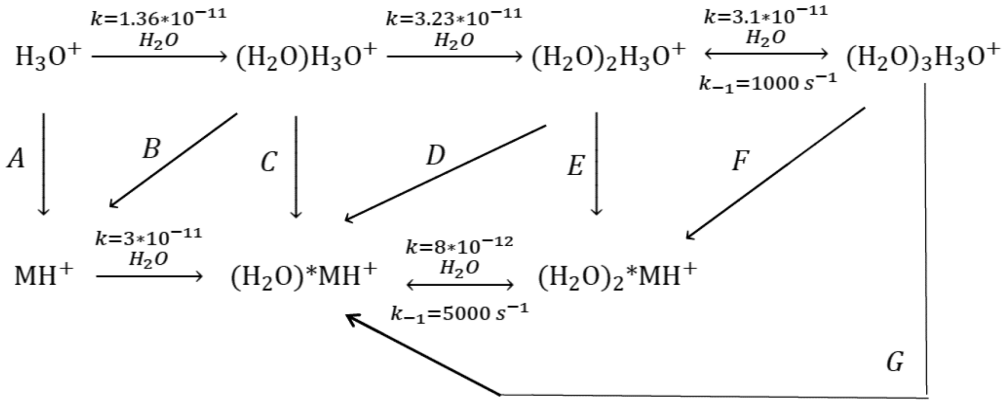

A: $k = 2.7 * 10^{-9}$; $H_3O^+ + M \rightarrow MH^+ + H_2O$
B: $k = 3 * 10^{-9}$; $(H_2O) * H_3O^+ + M \rightarrow MH^+ + 2H_2O$
C: $k = 2 * 10^{-9}$; $(H_2O) * H_3O^+ + M \rightarrow (H_2O) * MH^+ + H_2O$
D: $k = 1 * 10^{-9}$; $(H_2O)_2 * H_3O^+ + M \rightarrow (H_2O) * MH^+ + 2H_2O$
E: $k = 1 * 10^{-10}$; $(H_2O)_2 * H_3O^+ + M \rightarrow (H_2O)_2 * MH^+ + H_2O$
F: $k = 3 * 10^{-9}$; $(H_2O)_3 * H_3O^+ + M \rightarrow (H_2O)_2 * MH^+ + 2H_2O$
G: $k = 1 * 10^{-8}$; $(H_2O)_3 * H_3O^+ + M \rightarrow (H_2O) * MH^+ + 3H_2O$

Figure 19 Schematic visualization of acetone ion chemistry simulated by KIMI. Three body association reactions behave as effective two-body reactions (at a helium number density of [He] = 3.6×10^{16} cm^{-3}). All rate coefficients are in cm^3s^{-1}.

The results of initial tests are presented in Figures 17, 18 and 19. The experiment was carried out under a carrier gas pressure of 1.5 mbar and at a temperature of 295 K. Three body association reactions are presented as effective two-body reaction rate coefficients in cm^3s^{-1} (at a helium number density [He] = 3.6 x 10^{16} cm^{-3}). The simulation of the acetone ion chemistry presented in this work was directly based on known hydronium ion chemistry. As a starting point we used the reaction rate coefficients from the SIFT-MS library [271], 3.9×10^{-9} cm^3s^{-1} and 3.3×10^{-9} cm^3s^{-1} for channels A and B, respectively (see Figure 19).

Note that all the optimised values of the reaction rates calculated by the simulation were smaller compared to the reference values. This is because at the initial stage of the SIFT-MS system, the radial diffusion of ions was not properly implemented into the KIMI. However, initial tests showed that we are able to simulate complex ion chemical interactions.

Final tests were performed on the ion chemistry of methanol and ethanol with H_3O^+ and NO^+ reagent ions in the presence of an electric field. The references for this system

were limited and therefore we optimised the reaction rates only to interpolate experimental data. The primary alcohol molecular reactions were studied by using the SIFDT (2 mbar He; 0.08 mbar air sample; 300 K; reduced field strength *E/N* up to 28 Td; and over a range of sample gas humidity up to 5.5%). The NO^+ reactions resulted in the formation of $(M\text{-}H)^+$ product ions together with NOH neutral molecules, followed by the formation of ion hydrates $(M\text{-}H)^+(H_2O)_{1,2}$. [66] The variation of the percentages of the hydrated product ions depend on both *E/N* and the humidity of the sample. To change the sample humidity, we used an approach identical to the acetone study. From the full set of simulations, we selected one example to demonstrate the ability of KIMI to solve the ion chemistry within a drift tube (Figure 20) simulation. Presented data were obtained for variable *E/N* using high sample humidity. H_2O concentration in the drift tube was ~5×10^{13} cm^{-3}.

The benefit of KIMI is that one is able to simulate a proposed ion chemistry model and subsequently compare it with real-life experimental results. This allows the user to test several ion chemistry theories; to determine effect of individual reaction channels; or to estimate unknown reaction rates. Therefore, we used KIMI Sim to supplement our experimental results of the ion chemistry in several of our publications.

Table 4 The list of reaction and rate constants used for the simulation of humid ion chemistry and its dependence on water vapour concentration in the flow tube. As previously mentioned, the reaction rates for the association reactions are presented as effective two-body reaction rate coefficients.

Reaction	k_{KIMI} (cm^3s^{-1})
$NO^+ + H_2O \rightarrow NO^+.H_2O$	$2 \times 10^{-17} \times KE_{CM,r}^{-3.6}$
$NO^+.H_2O + H_2O \rightarrow NO^+(H_2O)_2$	$8 \times 10^{-17} \times KE_{CM,r}^{-3.6}$
$NO^+ + M \rightarrow (M\text{-}H)^+ + NOH$	3×10^{-9}
$NO^+H_2O + M \rightarrow (M\text{-}H)^+.H_2O + NOH$	3×10^{-9}
$NO^+(H_2O)_2 + M \rightarrow (M\text{-}H)^+(H_2O)_2 + NOH$	3×10^{-9}
$NO^+H_2O + M \rightarrow (M\text{-}H)^+ + H_2O + NOH$	1×10^{-11}
$(M\text{-}H)^+ + H_2O \rightarrow (M\text{-}H)^+.H_2O$	$7 \times 10^{-14} \times KE_{CM,r}^{-2.2}$
$(M\text{-}H)^+.H_2O + H_2O \rightarrow (M\text{-}H)^+(H_2O)_2$	$2.2 \times 10^{-14} \times KE_{CM,r}^{-2.2}$

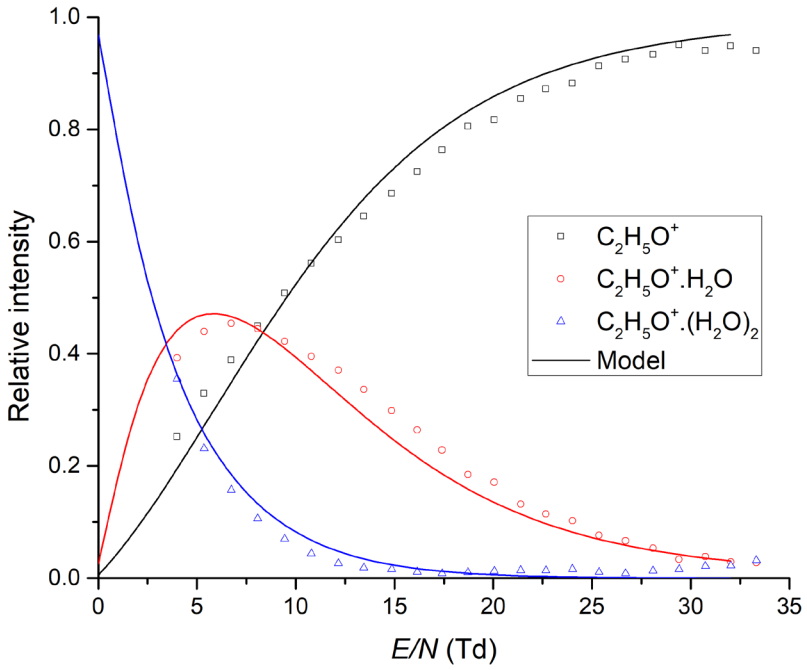

Figure 20 Initial simulation of NO^+ ion chemistry with ethanol. Experimental data (presented as symbols) were interpolated by the set of reactions shown in Table 4.

4. Results

4.1. Complex study of glyoxal ion chemistry

Glyoxal ($C_2H_2O_2$) is the simplest highly reactive dialdehyde. In biological systems, glyoxal is associated with oxidation stress. [272] In the gas phase however, glyoxal may be found as a reaction intermediate in the photo-catalytical reduction of carbon dioxide to methane [273, 274] and also in the earth's atmosphere as a product of the oxidation and photo-oxidation of VOCs (such as toluene, xylene or isoprene) [275-280].

From the stance of chemical ionization, glyoxal represents an analytical challenge as the PA of glyoxal (690 kJ mol^{-1}) estimated by theroretical calculations [281], is simillar to the PA of water (691 kJ mol^{-1}) [57]. Additionaly, neutral glyoxal reacts rapidly with humidity forming a series of oligomers that contribute to the formation of atmospheric aerosol. [272, 282] The ion chemistry of glyoxal with H_3O^+ had been previously studied using SIFT-MS [263, 283], confirming the presence of the proton transfer reaction forming protonated glyoxal. In addition, under increased sample humidity, protonated formaldehyde was also observed. A recent PTR-MS study showed interesting behavior [284] (in contrast to flow tube studies) where the concentration of protonated formaldehyde was very intensive at low humidity, decreasing for higher water vapor concentrations. As none of these studies explained this opposite trend in formation of protonated fornaldehyde, we decided to study this behaviour.

Our study is separated into two parts. Firstly, we investigated glyoxal ion chemistry in the SIFT-MS under variable humidity. This work has already been published and details are in **Attachment A.2**. Secondly, we studied glyoxal's ion chemistry in the presence of an electric field using a PTR-MS as well as a SIFDT-MS instrument. This study has not yet been published, although all details on this work are also available in the manuscript, in **Attachment A.3**.

To summarize, the ion chemistry (for reagent ions in the Profile 3 SIFT-MS: H_3O^+, NO^+ and O_2^+) was investigated, although only H_3O^+ showed a significant change when the water vapour concentration was varied. The high reactivity of neutral glyoxal molecules with water did not allow us to change the humidity of the sample directly.

Instead, we needed to humidify helium carrier gas. Finally, to support study of glyoxal ion chemistry, we also studied the ion chemistry of formaldehyde.

The results confirmed the formation of the protonated glyoxal as the main product ion, as a result of proton transfer from H_3O^+ to glyoxal. An increase in the water concentration leads to the formation of the protonated glyoxal primary hydrate via an association reaction. The protonated glyoxal (primary) hydrate is stable until presented with additional water molecules, resulting in several reaction channels:

$$C_2H_3O_2^+.H_2O + H_2O \leftrightarrow H_3O^+.H_2O + C_2H_2O_2, \quad (67)$$

$$\rightarrow CH_2OH^+ + HCOOH + H_2O, \quad (68)$$

$$C_2H_3O_2^+.H_2O + H_2O + He \rightarrow C_2H_3O_2^+(H_2O)_2 + He. \quad (69)$$

Protonated formaldehyde is formed via the secondary reaction of protonated glyoxal with water (Eq. 68). This assumption was also confirmed by the KIMI simulation, complementing our experimental study.

Additionally, the protonated formaldehyde reacts via a three-body association reaction with water molecules at high system humidity, forming the protonated formaldehyde hydrate. This reaction is of high significance, as the protonated formaldehyde hydrate has the ability to further react with water molecules via a ligand switching reaction into hydronium hydrate:

$$CH_2OH^+ + H_2O + He \rightarrow CH_2OH^+.H_2O + He, \quad (70)$$

$$CH_2OH^+.H_2O + H_2O \rightarrow H_3O^+.H_2O + CH_2O. \quad (71)$$

Reaction 71 is endothermic and relatively slow (5.3×10^{-10} cm^3s^{-1} [285]), however the high number density of water molecules in a humid (up to 3×10^{13} cm^{-3}) reaction equilibrium shifts the system to the production of hydronium hydrate ($H_3O^+.H_2O$). The consequence of this process is a reduction of product ions, characteristic for the detection of glyoxal (when the sample humidity increases).

In conclusion, we clarified that the formation of protonated formaldehyde is caused by the secondary reaction of protonated glyoxal with water vapour. The relative fraction of protonated formaldehyde thus increases with sample humidity. The situation however changes in the presence of an electric field.

Note that the glyoxal ion chemistry was studied using two instruments: the PTR-MS and SIFDT-MS. Important differences in these two methods are found in the type of

buffer gas used in these experiments. While the PTR-MS experiments were carried out in N_2, He was used in SIFDT-MS study. This is significant, as the ion mobility differs between the two buffer gases. The ion mobility determined by the SIFDT instrument is also used in the KIMI simulation and therefore the simulation is unsuitable to be compared to empirical PTR-MS results.

The ion chemistry in both experiments at low *E/N* (where the kinetic energy of ions is close to the thermal energy) follows the reaction pathway found in the SIFT-MS (where protonated formaldehyde is formed via the secondary reaction of protonated glyoxal with water vapour). At high *E/N*, protonated formaldehyde is also formed, although via CID reactions:

$$H_3O^+ + C_2H_2O_2 \rightarrow CH_2OH^+ + HCOOH, \quad (72)$$

$$C_2H_3O_2^+ + BG \rightarrow CH_2OH^+ + CO + BG, \quad (73)$$

where BG represents the respective N_2 and He buffer gases. The calculation of reaction energies in He shows reaction 72 to be more energetic (KE_{CM} = 0.6 eV at *E/N* 50 Td for Eq. 72; KE_{CM} = 0.08 eV at *E/N* 50 Td for Eq. 73). Nevertheless, reaction 73 also contributes to the formation of protonated formaldehyde. Further theoretical calculations are needed to evaluate the energetics and reaction mechanisms for these two processes.

Using the SIFDT-MS experimental results, supplemented by the numerical simulations of the ion chemistry, we were also able to identify the reactions responsible for the decreasing abundance of protonated formaldehyde at increasing sample humidity. Firstly, the humidity decreases the mobility of the primary H_3O^+ reagent ions, resulting in a decrease in reaction energy (in Eq. 72). This leads to a reduction in the formation of protonated formaldehyde. By increasing the water vapour concentration in the drift tube (from dry up to 6.4×10^{13} cm^{-3} water molecules), we observed a 10% reduction in the reaction energy. However, the numerical simulation of the ion chemistry showed that this reduction of reaction energy is not highly significant. What is more significant is the reverse proton transfer reaction of the primary and secondary product ions with water molecules back to the hydronium ion:

$$C_2H_3O_2^+ + H_2O \rightarrow H_3O^+ + C_2H_2O_2, \quad (74)$$

$$CH_2OH^+ + H_2O \rightarrow H_3O^+ + CH_2O. \quad (75)$$

Individual injection of product ions into the humidified drift tube showed that both protonated glyoxal and protonated formaldehyde produce hydronium according to the Arrhenius function. The PA difference between glyoxal and water is almost 0 (based on a theoretical estimation) while the PA differrence between water and formaldehyde is 0.23 eV. [281] [57] This may suggest that reaction 74 proceeds faster compared to reaction 75. The determined ion mobility of protonated formaldehyde is however larger compared to the ion mobility of the protonated glyoxal product ion and consiquenly the relative KE_{CM}. For increasing *E/N*, the KE_{CM} for Eq. 75 increaseses faster compared to Eq. 74 and tehrefore the reaction rate for Eq. 75 will eventually overtake the reaction rate of Eq. 74. This equlilibrium change is also seenin the ion chemistry of glyoxal at high *E/N*. An increase of humidity causes protonated formaldehyde to convert into hydronium faster compared to protonated glyoxal. This in turn reduces the concentraion of protonated formaldehyde, relative to protonated glyoxal. Numerical simulations of the proposed reaction mechanisms confirm this behaviour.

It is important to note that the aim of KIMI simulation was not to fully interpolate experimental data, but to explain the chemical mechanisms leading to the experimentally observed data. The simulation uses several approximations covering various reaction parameters. Further theoretical and experimental work is however required (especially for the purposes of fully simulating PTR-MS data).

4.2. Ion chemistry of phthalates studied by SIFT-MS

Phthalates (esters of phthalic acid) are used as plasticizers in the production of plastics. Their negative health effects on human genitalia have however been reported [286, 287]. To date, phthalates have been characterized as endocrine disruptors making this species of chemicals hazardous for pregnant women and children under the age of 3 years. Several of the most dangerous phthalate compounds are under EU regulations [288] or are tracked by the European Chemical Agency (*EHCA*) [289]. For the exception of children's toys, the regulations surrounding phthalates imposed by the EHCA do not cover any other daily plastic products (i.e. plastic containers [290], cosmetics [291], toothbrushes [292] and more). Such plastic products which can be bought in Europe are predominantly manufactured in countries such as China and India where the EHCA (or any other regulatory body) does not prohibit the regulation of phthalate contamination within these plastics. Plastic products imported into the EU should therefore be more controlled.

Several analytical techniques are used for the detection of phthalates; mainly liquid or gas chromatography coupled to mass spectrometry (GC-MS / LC-MS) [120] primarily using electron ionization at 70 eV. The primary product of dissociative ionization which is shown in the mass spectrum is the protonated phthalate anhydride (*m/z* 149), which characteristic for most phthalates [57]. The presence of a phthalate species may be confirmed by the detection of the phthalate anhydride ion; however, mass spectrometry measurements possess poor selectivity (phthalate species dependant). Using chemical ionization, individual phthalate species may be identified. [293] Ion mobility spectrometry (IMS) is a suitable SCI technique for the detection of phthalates. SCIMS techniques may potentially be used for real time analysis and for the accurate detection of phthalate contamination in plastics. The ability to achieve this has already been demonstrated by Michalczuk et al. [150]. As IMS operates near atmospheric pressure, analyte molecules react mainly with hydronium clusters $H_3O^+(H_2O)_n$.

To evaluate the ability of these methods in detecting phthalate species using IMS, one first needs to understand the ion chemistry. To aid us in this understanding, we present a study of several simple phthalates: dimethyl phthalate (DMP), dimethyl isophthalate (DMIP), dimethyl terephthalate (DMTP), diethyl phthalate (DEP), dipropyl phthalate (DPrP) and dibutyl phthalate (DBP); from SIFT-MS experiments. The study focuses

on phthalate ion chemistry when these molecules interact with $H_3O^+(H_2O)_n$ primary ions. The respective isomerization effects are also discussed, which compliments the previous work by Michalczuk et al. [150].

A full description of our experiments, results and the corresponding discussion are presented in **Attachment A.4** (as this study has already been published). In this work, the phthalate ion chemistry was studied by using H_3O^+, NO^+ and O_2^+ reagent ions under variable system humidification. Depending on the reagent ion used, the type of interaction occurring between the sample molecule and the bombarding ion may either (primarily) be a proton transfer reaction (H_3O^+)**;** a charge transfer process (O_2^+); or a charge transfer or association process (NO^+).

Previously recorded IMS/MS studies show that the location of ester groups on a benzene core significantly changes the ability for clustering (hydration) of phthalate isomers to hydrate. The 1,2 position (DMP) of an ester group does not provide an accessible angle for hydrogen bonding to occur and does not allow for stable hydrate formation. The presence of phthalate esters on carbons 1 and 3 (DMIP) does however allow for the effective association of two water molecules. The [fully open] 1,4 isomer of phthalate esters (DMTP) effectively binds only one water molecule. These observations were also confirmed in our SIFT-MS studies. The effect of humidity on the ion chemistry is based on two main aspects. The first is the interaction of reagent ion with water molecules, forming water clusters of reagent ions which goes on to affect the ion chemistry. The second aspect is the presence of secondary reactions between products of primary reactions and water molecules. The effect of humidity on the ion chemistry was mainly studied for H_3O^+ reagent ions, where it has the most significant impact.

In our investigation we observed differences between the IMS and SIFT-MS ion chemistry, namely the formation of $(M\text{-}OR)^+$ (characteristic for CI and EI ionization not observed in IMS, presumably, due to the higher pressure). The effect of isomerization on the formation of phthalate hydrates for DMP, DMIP and DMTP has been explained using a computational DFT theoretical approach, showing that the energetic difference between individual states of hydration for *ortho* isomers is very small. Therefore, at a high number density of water molecules, the reaction equilibrium moves in favour of the dominant formation of protonated DMP. The remaining

isomers have their energetic minima for the hydration process lower and therefore the formation of protonated hydrates is possible. Finally, we used KIMI simulations to clarify the reaction channels leading to the formation of protonated phthalate hydrates. We confirmed that the hydrates are formed through sequential association reactions of the protonated phthalate entity with water molecule, rather than via ligand switching reaction between hydronium hydrates and neutral phthalates. The presented work helps one to understand the ion chemistry of phthalates in SCIMS and reveals the additional possibilities of differentiating phthalate isomers using their secondary reactivity in the presence of water vapour.

4.3 Study of secondary ligand switching reactions of protonated acetic acid hydrates with acetone

Ligand switching reactions are important ionization mechanisms at atmospheric or near-atmospheric pressure and covers the IMS and SESI analytical techniques. The presence of such processes is crucial for analytical applications. If an analysed sample contains several neutral reactants, the primary ionization reactions between the reagent ions and neutral reactants may also be supplemented by secondary reactions (between the product ions of primary ionization channels and the remaining reactant neutrals). For example, a polar organic molecule, A, reacting via ligand switching with hydronium hydrates

$$H_3O^+(H_2O)_n + A \rightarrow AH^+(H_2O)_n + H_2O \quad (76)$$

can additionally react with a second polar molecule, M, also via ligand switching, replacing A or forming a proton-bound mixed dimer:

$$AH^+(H_2O)_n + M \rightarrow MH^+(H_2O)_n + A \quad (77a)$$

$$\rightarrow AH^+(M)(H_2O)_{n-1} + H_2O. \quad (77b)$$

If the molecule, M, is abundant in the system, secondary ligand switching processes may lead to the replacement of A, forming a symmetrical dimer:

$$AH^+(M)(H_2O)_n + M \rightarrow MH^+M + A + nH_2O. \quad (78)$$

This processes clearly complicates analytical methods, decreasing selectivity and sensitivity of particular components in a sample.

Such an effect needs to be considered in SESI-MS studies of exhaled breath. Studies have shown that the concentration of acetic acid in exhaled breath is typically a hundred times lower than the concentration of acetone. [162, 257, 294] In the present work, we studied such effects, specifically looking at the secondary ligand switching reactions between acetic acid hydrates and acetone vapours. The study was carried out using the new generation of SIFDT-MS instrument, (developed at the J. Heyrovsky institute by Dr. Spesyvyi) equipped with an ion source capable of generating protonated hydrates of acetic acid (see Fig 8). In the experiment, hydrated and protonated acetic acid clusters, $CH_3COOH.H^+(H2O)_2$ were generated in the ion source and filtered via an injection filter. These ions were subsequently fragmented via a CID at the entrance of the drift tube, into the hydrated protonated acetic acid entity,

$CH_3COOH.H^+.H_2O$, by using a high kinetic transmission energy for $CH_3COOH.H^+(H2O)_2$ ions in the injection quadrupole. The drift tube operated at a low *E/N* = 14.2 Td was used to study the reaction of hydrated protonated acetic acid with acetone in the presence of a helium carrier gas (at a pressure of 1.9 mbar and temperature of 293 K). This complex experimental study was supplemented by the theoretical DFT calculations of individual protonated hydrates, as well as KIMI simulations of a proposed set of reactions.

This work has already been published and all details may be found in **Attachment A.5**. This case study demonstrates the possibility of instigating study ligand switching reactions in the SIFDT-MS. We also characterised specific ligand switching reactions between protonated acetic acid hydrates and acetone, relevant for breath analysis.

4.4 Real time detection of Arsene and Selene hydrides by SIFT-MS

SCIMS techniques are mainly used for real-time trace analysis of VOCs. However, SCIMS is not limited to only organic analytes, but may also be used for any compound reacting rapidly with one of the primary reagent ions (H_3O^+, NO^+ and O_2^+). In the present study, we investigated the possibility of being able to analyse the inorganic volatile species selenium hydride (SeH_2), arsenic hydride (AsH_3), monomethylarsane (CH_3AsH_2) and dimethylarsane ($(CH_3)_2AsH$). These are all relevant for the detection of Arsenic and Selenic elements in atomizers.

Atomization is a popular method for the trace element analysis of several elements (As, Se, Sb, Sn, …) and is conducted via the generation of volatile hydrides. [295] These are produced from an analyte in the liquid phase, using the reaction between tetrahydridoborate(-1) (TBH) and an acid. This achieves almost 100% conversion (in some cases). During the reaction, the analyte is released into the gaseous phase in form of a volatile hydride where it may be detected by various techniques. It is assumed that the relation between the active hydride species (for example MAs^V) and the volatile hydrides (for example CH_3AsH_2) is explicit (i.e. the specific hydride active species produce specific volatile hydrides). This argument was however questioned by Talmi and Bostick (1975), who suggested that the reaction may be pH dependent. [296]

Generated volatile hydrides are mainly detected by atomic absorption spectrometry. Consequently, volatile hydrides are often decomposed after their generation into atomic species using a quartz tube atomizer, heated up to 900 °C. [297, 298]. Besides standard atomization (decomposing volatiles by heat), plasma dielectric barrier discharge (DBD) atomizers may also be used [299]. In the present study, the SIFT-MS was used to analyse the formation and atomization of selected hydrides in a DBD atomizer. This study was conducted in cooperation with the Institute of Analytical Chemistry of the Czech Academy of Science.

Aside to the volatile hydrides generated from a liquid solution, several other molecules are present in the sample as well: hydrogen gas as a by-product of hydride generation; argon as a carrier gas; water vapour from the sample solution and traces of oxygen penetrating into the generator gas lines. To reduce sample humidity for arsene hydrides, NaOH pellets were introduced into the sample gas line. For selenium hydrides, dryers however cannot be applied, as selenium hydrides, compared to arsenic

hydrides, are affected by the presence of a drying agent. The presence of hydrogen gas in the atomizer is crucial as it reacts together with traces of oxygen within the plasma, to produce water. Water consequently influences the property of the DBD discharge, affecting the atomization.

In our study, we first confirmed the formation of the protonated hydrides of all the studied species, in our SIFT-MS. Secondly, we analysed the concentration of the protonated hydrides in the DBD atomizer, together with the formation of secondary products (predominantly H_2O). Finally, we introduced an excess of oxygen gas into the sample to characterize the effect of H_2O on the atomization process in the DBD. As the study has also already been published, all details surrounding this work may be found in **Attachment A.6**.

The present study shows a new application of SCIMS, which goes beyond the detection and analysis of VOCs. We have shown that SIFT-MS, as well as all other SCIMS techniques, may be implemented in the analytical applications of inorganic chemistry. This may either be conducted by direct (or indirect) analysis of inorganic volatile compounds (helping us to understand established analytical procedures, such as atomization).

Conclusion

In conclusion, this thesis discusses the ion chemistry processes used for trace gas analysis carried out by CI-MS techniques, operating in the mbar pressure range. The focus was to understand the limitations of SCIMS techniques; mainly on the aspects of reduced selectivity and sensitivity. Besides many positives (such as high sensitivity, a large dynamic range and a real-time response for most of the VOCs detected), the SCIMS techniques demonstrate limited ability to conduct selective analysis of isomeric molecules. Additionally, water vapour present in the reaction chamber of the instruments (introduced by sample humidity) may reduce sensitivity and selectivity of the analytes, via the secondary reactions of water molecules with ions.

The main objectives of the thesis were to analyse the limitations of these techniques which reduced the sensitivity and selectivity of the SCIMS methods, via the study of complex ion chemistry. This work predominantly focused on secondary reactions with water. Additionally, we aimed to provide a mathematical description of the associated primary and secondary reactions which made it capable to predict the behaviour of the relative ion signals. The mathematical description will be supplemented by an experimental study of complex ion-molecular reactions relevant to typical SCIMS applications (such as breath analysis, environmental science etc.). Finally, we aimed to investigate the new possible applications for SCIMS analysis.

We first presented a unique combination of a fast GC pre-separation unit, coupled to a SIFT-MS experiment. This set-up was developed to try and improve the analytical selectivity of monoterpenes; common isomers in investigated in atmospheric chemistry when studying the formation of secondary organic aerosol; and air quality. In this work, we combined a fast-chromatographic separation technique with the SIFT-MS. As a result, we identified individual isomers of the monoterpene family in under 45 s, using an MXT-1 metallic column in association with the calculation for the ion ratio of the two product ion pairs, generated by H_3O^+ (*m/z* 137 / *m/z* 81) and NO^+ (*m/z* 136 / *m/z* 93). The relative intensities of the fragment ions were shown to be characteristic for the individual monoterpenes. However, we also found that the sample flow rate from the GC column (< 4 sccm) is not sufficient to achieve a sub-ppbv detection limit, which is commonly achieved by fast GC PTR-MS. Interestingly, we also noticed that water vapour has a retention time which is much lower compared

to the VOCs detected the samples that we ran. Therefore, fast GC may potentially be used to separate VOCs from sample humidity. This may therefore be a welcomed benefit to the field as water vapour often influences the ion chemistry within these CIMS techniques. In addition, a high humidity within the instrument reduces the selectivity and sensitivity of the methods.

The experimental and mathematical studies conducted of the influence of water vapour on the ion chemistry of the discussed techniques makes-up the main body of this work. We first developed a numerical simulation for the computational investigation of ion-molecule reactions (KIMI) and carried out two sets of experiments. In these experiments we focused on understanding the secondary reactions of product ions with water (the study of the ion chemistry of glyoxal and phthalates).

KIMI is a simple numerical simulator capable of mathematically describing complex reaction systems. The simulator solves a set of differential equations based on a proposed reaction system along the axis of the reactor using the classical Runge-Kutta algorithm. Therefore, KIMI is capable of simulating the ion chemistry which occurs within the SIFT-MS, PTR-MS as well as the SIFDT-MS instruments. To demonstrate its functionality, KIMI was first tested on several simple and well understood reaction systems(i.e. acetone and alcohols), where we observed changes in the product ion distribution. On successfully simulating this chemistry, we later used our KIMI program to investigate more complex reaction systems.

The glyoxal study was divided into two sections. The first part describes the ion chemistry and the associated secondary reactions with water vapour in a flow tube (where we identified the water induced generation of protonated formaldehyde). The second section describes a similar situation for the drift tube, where protonated formaldehyde is also generated; via CID. The aim of the of the drift tube study was to explain the changes in the relative ratios of the main product ions to the protonated formaldehyde and protonated glyoxal ions. Using several experimental techniques together with KIMI, we identified the secondary reactions responsible for the observed changes (primarily induced via secondary reverse proton transfer reactions).

In the study of phthalates, our objective was to describe the ion chemistry of selected phthalates with H_3O^+, NO^+ and O_2^+ reagent ions (as well as the secondary reactions of selected protonated phthalates, with water vapour). The list of selected phthalates

included the DMP, DMIP and DMTP isomers. These were chosen to study the effect of varying the position and length of the substituents around the benzene ring on the ion chemistry. The length of the phthalate substituent prominently affects the ion chemistry of charge transfer reactions via the opening of a new rearrangement channel leading to the formation of $(M-(R-2H))^+$ products. The secondary reactions (with water molecules) were also studied for the protonated phthalate molecules. We have demonstrated that protonated phthalates in the *ortho* position do not form hydrides. For the isomers with *meta* and *para* geometries, however, phthalates form hydrides very effectively. For the DMTP isomer, we detected the association of one H_2O molecule to the analyte ion. For DMIP, we detected the clustering of a second H_2O molecule. The hydration does not continue to form any larger clusters, as a strong potential minimum exist only for the specific DMTP and DMIP structures. Finally, we used KIMI to confirm that the protonated phthalate hydrates in the flow tube were formed via the association of water molecules on the protonated phthalate, rather than via ligand switching of the H_2O molecules with hydrated hydronium.

The initial product ions may however (additional to analyte) also react with other abundant neutral molecules in secondary reactions. Subsequently, we studied such reactions between protonated acetic acid hydrates and acetone. This reaction system is interesting as both acetic acid and acetone are abundant and analytically important components in breath analysis. In breath analysis carried out by SESI-MS or IMS techniques in the near-to-atmospheric pressure region of conditions, ion hydrates are formed frequently. As we have shown, hydrates of protonated acetic acid (reflecting the concentration of acetic acid in the sample) undergo secondary ligand switching reactions with acetone. This process leads to the fast formation of the asymmetric proton-bounded dimer $(CH_3COCH_3)H^+(CH_3COOH)$ and ultimately the production of the strongly bound protonated-acetone dimer. This reaction sequence was also simulated using KIMI. This study clearly demonstrates that the presence of highly abundant polar compounds in SESI-MS and IMS may negatively affect the accuracy of quantification of other analytes at low concentrations.

In summary, the presence of secondary reactions complicates the identification and quantification of absolute concentrations of species in SCIMS techniques. The most abundant cause of secondary reactions are water molecules, resulting from sample humidity. Water molecules react with product ions via several secondary reaction

channels. In the present work, we identified three secondary reaction channels which were seen to be the most detrimental to accurate analysis of species when using SCIMS techniques:

1. Three-body association reactions forming ion hydrates of both reagent and product ions (Eq. 56).

2. Reverse proton transfer reactions between product ions (or their hydrates) and water molecules (Eq. 59).

3. Reaction channels between product ions and water molecules, producing new and unexpected ions.

The last point reflects the most interesting part of the ion chemistry. An example of point 3 is the formation of protonated formaldehyde from protonated glyoxal via a series of water assisted reactions; or secondary formation of protonated phthalate while using NO^+ reagent ions, via the reaction:

$$M.NO^+ + H_2O \rightarrow MH^+ + HONO. \quad (79)$$

Additionally, secondary reactions are not only induced by water vapour, but also by other molecules present at sufficiently high concentrations in the reaction chamber. (see study of secondary ligand switching reactions of protonated acetic acid hydrates with acetone, section 4.3).

The effect of the secondary reactions may be minor, but also significant, depending on the analytical situation. So far, we are able to identify three different approaches to reduce the impact of secondary reactions on analysis. The first approach is to carefully increase the effective temperature of the gases in the flow tube (as for example in PTR-MS or SIFDT-MS), as to reduce the formation of ion hydrates. This may however induce both a reverse proton transfer reaction as well as a new reaction channel (as we observed in the glyoxal study). The second approach is to remove the humidity from the sample (either via filters or via pre-separation using the fast GC technique we developed). This however reduces the speed of SCIMS as well as limits its sensitivity. The last approach is an understanding the water-based ion chemistry. This however requires a careful and systematic; theoretical and experimental study of complex reaction systems.

In the final study we pioneered the possibility of using SCIMS for the analysis of inorganic volatile hydrides, produced during atomization. The process of atomization is used to quantify the absolute concentrations of inorganic species of germanium, arsenic, tin etc., primarily in solid samples. The inorganic species are in controlled environments; chemically converted into hydrides. Volatile hydrides are then atomized using a quartz tube or discharge-based atomizers; and are detected via atomic absorption spectrometry. In this study, we investigated the possibility of detecting selected hydrides of selenium and arsenic using SIFT-MS which has in-turn helped us to understand the process of atomisation in dielectric barrier discharge (DBD) under various conditions, much better. The focus of this study was to analyse non-atomised hydrides and subsequently evaluate the effectivity of the atomization process. We have shown that the hydrides are not always atomised; but are often decomposed in the DBD. Additionally, atomization is affected by humidity which is delivered to the atomizer from the sample or is formed in the atomizer via the by-reaction of residual hydrogen and oxygen. The possibility of SCIMS to detect non-atomised hydrides as well as humidity levels is of high interest.

The presented work fulfils the defined objectives of the thesis, as well as the aims of the IMPACT project. The obtained results reported in this thesis have been frequently presented at conferences on the national and international stage. So far, our results have led to the production of 5 high-impact publications; and more publications based on these works are expected to be published soon. The KIMI simulator is still under development but may already be used to assist with ion-molecule interaction research. We believe that the knowledge gained from this work will help to improve the application of current as well as future SCIMS technologies.

List of Tables and Figures

Table 1 List of ion-molecular reactions used for CI.

Table 2 Selected thermodynamic properties of hydronium hydrates formation $H_3O^+(H_2O)_n + H_2O \leftrightarrow H_3O^+(H_2O)_{n+1}$

Table 3 The list of reactions and reaction rate constants used for the simulation of humid ion chemistry; and its dependence on water vapour concentration in the flow tube. The reaction rates for the three body association reactions are presented as effective two-body reaction rate coefficients. k_{lit} represents data taken from [137].

Table 4 The list of reaction and rate constants used for the simulation of humid ion chemistry and its dependence on water vapour concentration in the flow tube. As previously mentioned, the reaction rates for the association reactions are presented as effective two-body reaction rate coefficients.

Figure 1 The mass coefficient for conversion of the laboratory ion kinetic energy into the centre-of-mass collisional energy (see Eq. 15). The profile represents the energy conversion for the hydronium ion colliding with neutrals from 4 up to 200 amu.

Figure 2 The schema of SIFT-MS experiment. *QMS* - quadrupole mass filter

Figure 3 List of relevant ion-molecular reactions occurring in the RF plasma ion source in the mixture of air and water vapours. [134] Reactions in blue represent those active in pure water vapour discharges. The remaining reactions are active in water vapour/air mixtures. The ions in bold (H_3O^+, NO^+ and O_2^+) are the main reagent ions produced in the discharge at high concentrations.

Figure 4 The schematic interpretation of physical and chemical processes in the flow tube. The reagent ions (orange) are injected into the flow tube and mixed with the helium carrier gas. Sample gas (red) is introduced into the mixture as well. The laminar flow of the helium carrier gas transports the reagent ions and sample gas along the defined reaction

length l_r, from the injection point up until the end of the flow tube, where neutrals are separated from the ions. Ion-neutral reactions take place along the reaction length (in the flow tube).

Figure 5 A scheme showing the PTR-MS instrument. [144]

Figure 6 Relative intensity of hydrated hydronium clusters $H_3O^+(H_2O)_n$, n = 0,1,2,3 in PTR-MS determined for various *E/N* values for a sample containing 0.6% humidity (absolute).

Figure 7 The SIFDT-MS instrument; the initial concept. [39]

Figure 8 The SIFDT-MS instrument; the final design. [153] The coloured areas represent individual pressure regions: 5 mbar (yellow), 0.3 mbar (violet), 5×10^{-6} mbar (blue), 1.9 mbar (pink). HC - hollow cathode ion source, SRIG – stacked ring ion guide, OP - octupole, QMF - quadrupole mass filter, VI - Venturi inlet, VDT - Venturi flow-drift tube, GG - gating grid, DTR - drift tube reactor, SNC - ion sampling nose cone, QMA - quadrupole mass analyser, EM - electron multiplier with conversion

Figure 9 Illustrative reaction diagram of primary and secondary reactions of H_3O^+ with neutral a reactant, M, in the presence of water vapour. [263] Solid line reactions represent moderate humidity levels. Dashed reactions represent saturated water vapour.

Figure 10 Photograph of a fast GC unit built for the study of individual monoterpenes in gaseous mixtures.

Figure 11 A schematic view of the KIMI main programs and their functionalities.

Figure 12 Resource manager responsible for management of individual species within the simulation.

Figure 13 The calculation properties window responsible for the management of physical properties and geometries within the simulation.

Figure 14 The Calculation properties window is responsible for the management of physical properties and geometry of simulation.

Figure 15 Calculation control window.

Figure 16 A visualisation of the transformation process. The main reaction object (left) is transformed into a series of calculation objects (left). The new objects are later used by Calculation class to calculate a single step numerical solution of differential kinetic equations.

Figure 17 Initial simulation of the formation of hydronium hydrates. Experimental data (in symbols) were interpolated by the set of reactions listed in Table 3.

Figure 18 An initial simulation of acetone's ion chemistry under the experimental conditions described in the text. Experimental data (in symbols) were interpolated by the set of reactions shown in Figure 19.

Figure 19 Schematic visualization of acetone ion chemistry simulated by KIMI. Three body association reactions behave as effective two-body reactions (at a helium number density of [He] = 3.6×10^{16} cm^{-3}). All rate coefficients are in cm^3s^{-1}.

Figure 20 Initial simulation of NO^+ ion chemistry with ethanol. Experimental data (presented as symbols) were interpolated by the set of reactions shown in Table 4.

List of Abbreviations

APCI	Atmospheric Pressure Chemical Ionization
BDE	Bound Dissociation Energy
CI	Chemical Ionization
CID	Collision Induced Dissociation
CI-MS	Chemical Ionization Mass Spectrometry
DBD	Dielectric Barrier Discharge
DFT	Density Functional Theory
EI-MS	Electron Ionization Mass Spectrometry
FA	Flowing Afterglow
FAIMS	Field Asymmetric Ion Mobility Spectrometry
FDT	Flow-Drift Tube
GC-MS	Gas Chromatography Mass Spectrometry
HIKE-IMS	High Kinetic Energy Ion Mobility Spectrometry
IMS	Ion Mobility Spectrometry
NOAA	National Oceanic and Atmospheric Administration
ppb	parts-per-billion
ppm	parts-per-million
ppq	parts-per-quadrillion
ppt	parts-per-trillion
PTR-MS	Proton Transfer Reaction Mass Spectrometry
SCIMS	Soft Chemical Ionization Mass Spectrometry
SESI	Secondary Electrospray Ionization
SIFDT-MS	Selected Ion Flow-Drift Tube Mass Spectrometry

SIFT	Selected Ion Flow Tube
SIFT-MS	Selected Ion Flow Tube Mass Spectrometry
SRIG	Stacked Ring Ion Guide
ToF-MS	Time-of-Flight Mass Spectrometry
VOCs	Volatile Organic Compounds

List of publications

Lacko M, Wang N, Sovová K, Pásztor P, Španěl P.
Addition of fast gas chromatography to selected ion flow tube mass spectrometry for analysis of individual monoterpenes in mixtures.
Atmospheric Measurement Techniques. 2019. 12(9): 4965-82.

Lacko M, Piel F, Mauracher A, Španěl P.
Chemical ionization of glyoxal and formaldehyde with H_3O^+ ions using SIFT-MS under variable system humidity.
Physical Chemistry Chemical Physics. 2020. 22(18): 10170-10178

Lacko M, Michalczuk B, Matejčík Š, Španěl P.
Ion chemistry of phthalates in selected ion flow tube mass spectrometry: isomeric effects and secondary reactions with water vapour.
Physical Chemistry Chemical Physics. 2020. 22(28): 16345-52.

Spesyvyi A, **Lacko M**, Dryahina K, Smith D, Španěl P.
Ligand Switching Ion Chemistry: An SIFDT Case Study of the Primary and Secondary Reactions of Protonated Acetic Acid Hydrates with Acetone.
Journal of the American Society for Mass Spectrometry. 2021. 32(8): 2251-60.

Kratzer J, **Lacko M**, Dryahina K, Matoušek T, Španěl P, Dědina J.
Atomization of As and Se volatile species in a dielectric barrier discharge atomizer after hydride generation: Fate of analyte studied by selected ion flow tube mass spectrometry.
Analytica chimica acta. 2022. 1190: 339256.

Bibliography

1. Swings, P. and L. Rosenfeld, *Considerations Regarding Interstellar Molecules.* The Astrophysical Journal, 1937. **86**: p. 483-486.
2. McKellar, A., *Evidence for the Molecular Origin of Some Hitherto Unidentified Interstellar Lines.* Publications of the Astronomical Society of the Pacific, 1940. **52**: p. 187.
3. Dalgarno, A. and J. Black, *Molecule formation in the interstellar gas.* Reports on Progress in Physics, 1976. **39**(6): p. 573.
4. Herbst, E. *Molecular ions in interstellar reaction networks*. in *Journal of Physics: Conference Series*. 2005. IOP Publishing.
5. Glosık, J., et al., *The recombination of H_3^+ ions with electrons: dependence on partial pressure of H_2.* Chemical Physics Letters, 2000. **331**(2-4): p. 209-214.
6. Adams, N.G. and L.M. Babcock, *Advances in gas phase ion chemistry*. Vol. 3. 1998, Greenwich, London: JAI PRESS.
7. Johnson, C.Y., E.B. Meadows, and J.C. Holmes, *Ion composition of the arctic ionosphere.* Journal of Geophysical Research, 1958. **63**(2): p. 443-444.
8. Dickinson, P.H.G. and J. Sayers, *Ion Charge Exchange Reactions in Oxygen Afterglows.* Proceedings of the Physical Society, 1960. **76**(1): p. 137-148.
9. Sayers, J. and D. Smith. *Ion-atom interchange processes*. in *Proc. IIIrd int. conf. on the physics of electronic and atomic collisions*. 1964. Amsterdam.
10. McDaniel, E.W., et al., *Ion-Molecule reactions*. 1970, New York: Wiley.
11. Schmeltekopf, A., et al., *Reaction of atomic oxygen ions with vibrationally excited nitrogen molecules.* Planetary and Space Science, 1967. **15**(3): p. 401-406.
12. Ferguson, E., F. Fehsenfeld, and A. Schmeltekopf, *Flowing afterglow measurements of ion-neutral reactions*, in *Advances in atomic and molecular physics*. 1969, Elsevier. p. 1-56.
13. Bohme, D., in *Interactions between ions and molecules*, P. Ausloos, Editor. 1975, Plenum Press: New York. p. 489-504.
14. Howard, C.J., H.W. Rundle, and F. Kaufman, *Water cluster formation rates of NO+ in He, Ar, N2, and O2 at 296 K.* The Journal of Chemical Physics, 1971. **55**(10): p. 4772-4776.

15. Bolden, R. and N. Twiddy, *A flowing afterglow study of water vapour.* Faraday Discussions of the Chemical Society, 1972. **53**: p. 192-200.
16. Bierbaum, V., M. Golde, and F. Kaufman, *Flowing afterglow studies of hydronium ion clustering including diffusion effects.* The Journal of Chemical Physics, 1976. **65**(7): p. 2715-2724.
17. Liddy, J., C. Freeman, and M. McEwan, *Reactions of H_3^+ with XCN where X= H, CH_3, Cl, Br, I and CN.* International Journal of Mass Spectrometry and Ion Physics, 1977. **23**(2): p. 153-161.
18. McFarland, M., et al., *Flow‐drift technique for ion mobility and ion‐molecule reaction rate constant measurements. I. Apparatus and mobility measurements.* The Journal of Chemical Physics, 1973. **59**(12): p. 6610-6619.
19. McFarland, M., et al., *Flow‐drift technique for ion mobility and ion‐molecule reaction rate constant measurements. II. Positive ion reactions of N^+, O^+, and H_2^+ with O_2 and O^+ with N_2 from thermal to 2 eV.* The Journal of chemical physics, 1973. **59**(12): p. 6620-6628.
20. McFarland, M., et al., *Flow‐drift technique for ion mobility and ion‐molecule reaction rate constant measurements. III. Negative ion reactions of O^- with CO, NO, H_2, and D_2.* The Journal of Chemical Physics, 1973. **59**(12): p. 6629-6635.
21. Albritton, D., et al., *Effects of ion speed distributions in flow‐drift tube studies of ion‐neutral reactions.* The Journal of Chemical Physics, 1977. **66**(2): p. 410-421.
22. Adams, N. and D. Smith, *The selected ion flow tube (SIFT); a technique for studying ion-neutral reactions.* International Journal of Mass Spectrometry and Ion Physics, 1976. **21**(3-4): p. 349-359.
23. Smith, D. and N. Adams, *The selected ion flow tube (SIFT): studies of ion-neutral reactions.* Advances in atomic and molecular physics, 1988. **24**: p. 1-49.
24. Albritton, D., *Ion-neutral reaction-rate constants measured in flow reactors through 1977.* Atomic data and nuclear data tables, 1978. **22**(1): p. 1-89.
25. Ikezoe, Y., S. Matsuoka, and M. Takebe, *Gas phase ion-molecule reaction rate constants through 1986*. 1987: Ion reaction research group of the Mass spectroscopy society of Japan.

26. Fehsenfeld, F.C., in *Interactions between Ions and Molecules*, P. Ausloos, Editor. 1975, Plenum Press: New York. p. 387-412.
27. Smith, D. and N.G. Adams, *Elementary plasma reactions of environmental interest*, in *Plasma Chemistry I*. 1980, Springer. p. 1-43.
28. Smith, D. and P. Spanel, *Studies of interstellar ion reactions using the SIFT technique: isotope fractionation.* Accounts of chemical research, 1992. **25**(9): p. 414-420.
29. Smith, D. and P. Spanel, *Ions in the terrestrial atmosphere and in interstellar clouds.* Mass Spectrometry Reviews, 1995. **14**(4‐5): p. 255-278.
30. Smith, D. and N. Adams, *Elementary interactions between charged and neutral species in plasmas.* Pure and Applied Chemistry, 1984. **56**(2): p. 175-188.
31. Eiceman, G.A., *Advances in ion mobility spectrometry: 1980–1990.* Critical Reviews in Analytical Chemistry, 1991. **22**(1-2): p. 471-490.
32. Lindinger, W., J. Hirber, and H. Paretzke, *An ion/molecule-reaction mass spectrometer used for on-line trace gas analysis.* International journal of mass spectrometry and ion processes, 1993. **129**: p. 79-88.
33. Phillips, M., *Breath tests in medicine.* Scientific American, 1992. **267**(1): p. 74-79.
34. Smith, D. and P. Španěl, *Application of ion chemistry and the SIFT technique to the quantitative analysis of trace gases in air and on breath.* International Reviews in Physical Chemistry, 1996. **15**(1): p. 231-271.
35. Španěl, P. and D. Smith, *Selected ion flow tube: a technique for quantitative trace gas analysis of air and breath.* Medical and Biological Engineering and Computing, 1996. **34**(6): p. 409-419.
36. Španěl, P. and D. Smith, *A selected ion flow tube study of the reactions of NO^+ and O_2^+ ions with some organic molecules: The potential for trace gas analysis of air.* The Journal of chemical physics, 1996. **104**(5): p. 1893-1899.
37. Smith, D. and P. Španěl, *Selected ion flow tube mass spectrometry (SIFT‐MS) for on‐line trace gas analysis.* Mass spectrometry reviews, 2005. **24**(5): p. 661-700.

38. Lagg, A., et al., *Applications of proton transfer reactions to gas analysis.* International Journal of Mass Spectrometry and Ion Processes, 1994. **134**(1): p. 55-66.
39. Spesyvyi, A., D. Smith, and P. Španěl, *Selected ion flow-drift tube mass spectrometry: quantification of volatile compounds in air and breath.* Analytical chemistry, 2015. **87**(24): p. 12151-12160.
40. Niessen, W., *Atmospheric pressure ionization in mass spectrometry*, in *Encyclopaedia of spectroscopy and spectrometry*, T.G. Lindon JC, Holmes JL, Editor. 1999, Academic Press: London.
41. Lichvanova, Z., et al., *Using corona discharge-ion mobility spectrometry for detection of 2,4,6-Trichloroanisole.* Talanta, 2014. **127**: p. 239-43.
42. Sabo, M., et al., *Atmospheric pressure corona discharge ionisation and ion mobility spectrometry/mass spectrometry study of the negative corona discharge in high purity oxygen and oxygen/nitrogen mixtures.* International Journal of Mass Spectrometry, 2010. **293**(1-3): p. 23-27.
43. Wu, C., W.F. Siems, and H.H. Hill, *Secondary electrospray ionization ion mobility spectrometry/mass spectrometry of illicit drugs.* Analytical chemistry, 2000. **72**(2): p. 396-403.
44. Field, F.H., *Chemical ionization mass spectrometry.* Accounts of Chemical Research, 1968. **1**(2): p. 42-49.
45. Langevin, M. *Une formule fondamentale de théorie cinétique*. in *Annales de chimie et de physique, Series*. 1905.
46. Jones, J.E., *On the determination of molecular fields.—II. From the equation of state of a gas.* Proceedings of the Royal Society of London. Series A, Containing Papers of a Mathematical and Physical Character, 1924. **106**(738): p. 463-477.
47. Gioumousis, G. and D.P. Stevenson, *Reactions of gaseous molecule ions with gaseous molecules. V. Theory.* The Journal of Chemical Physics, 1958. **29**: p. 294-299.
48. Moran, T.F. and W.H. Hamill, *Cross Sections of Ion–Permanent‐Dipole Reactions by Mass Spectrometry.* The Journal of Chemical Physics, 1963. **39**(6): p. 1413-1422.
49. Su, T. and M.T. Bowers, *Ion-polar molecule collisions: the effect of ion size on ion-polar molecule rate constants; the parameterization of the average-*

dipole-orientation theory. International Journal of Mass Spectrometry and Ion Physics, 1973. **12**(4): p. 347-356.

50. Bass, L., et al., *Ion-polar molecule collisions. A modification of the average dipole orientation theory: The cos θ model.* Chemical Physics Letters, 1975. **34**(1): p. 119-122.
51. Su, T. and M.T. Bowers, *Parameterization of the average dipole orientation theory: temperature dependence.* International Journal of Mass Spectrometry and ion processes, 1975. **17**: p. 211-212.
52. Ellis, A.M. and C.A. Mayhew, *Proton transfer reaction mass spectrometry: principles and applications*. 2013: John Wiley & Sons.
53. Chesnavich, W.J., T. Su, and M.T. Bowers, *Collisions in a noncentral field: a variational and trajectory investigation of ion–dipole capture.* The Journal of Chemical Physics, 1980. **72**(4): p. 2641-2655.
54. Su, T. and W.J. Chesnavich, *Parametrization of the ion–polar molecule collision rate constant by trajectory calculations.* The Journal of Chemical Physics, 1982. **76**(10): p. 5183-5185.
55. Zhao, J. and R. Zhang, *Proton transfer reaction rate constants between hydronium ion (H_3O^+) and volatile organic compounds.* Atmospheric Environment, 2004. **38**: p. 2177-2185.
56. Bowers, M.T. and D.D. Elleman, *Thermal energy charge transfer reactions of rare-gas ions to methane, ethane, propane, and silane. The importance of franck-condon factors.* Chemical Physics Letters, 1972. **16**(3): p. 486-491.
57. NIST. *NIST WebBook Chemie, NIST Standard Reference Database Number 69*. Available from: http://webbook.nist.gov/chemistry/.
58. Bohme, D.K., G.-I. Mackay, and H. Schiff, *Determination of proton affinities from the kinetics of proton transfer reactions. VII. The proton affinities of O_2, H_2, Kr, O, N_2, Xe, CO_2, CH_4, N_2O, and CO.* The Journal of Chemical Physics, 1980. **73**(10): p. 4976-4986.
59. Lindinger, W., A. Hansel, and A. Jordan, *On-line monitoring of volatile organic compounds at pptv levels by means of proton-transfer-reaction mass spectrometry (PTR-MS) medical applications, food control and environmental research.* International Journal of Mass Spectrometry and Ion Processes, 1998. **173**(3): p. 191-241.

60. Adams, N.G., et al., *Selected ion flow tube study of NH_4^+ association and of product switching reactions with a series of organic molecules.* International Journal of Mass Spectrometry, 2003. **223**: p. 459-471.
61. Blake, R.S., et al., *Chemical ionization reaction time-of-flight mass spectrometry: Multi-reagent analysis for determination of trace gas composition.* International Journal of Mass Spectrometry, 2006. **254**(1-2): p. 85-93.
62. Field, F. and F. Lampe, *Reactions of gaseous ions. VI. Hydride ion transfer reactions.* Journal of the American Chemical Society, 1958. **80**(21): p. 5587-5592.
63. Španěl, P. and D. Smith, *SIFT studies of the reactions of H_3O^+, NO_+ and O_2^+ with several ethers.* International journal of mass spectrometry and ion processes, 1998. **172**(3): p. 239-247.
64. Španěl, P., Y. Ji, and D. Smith, *SIFT studies of the reactions of H_3O^+, NO_+ and O_2^+ with a series of aldehydes and ketones.* International journal of mass spectrometry and ion processes, 1997. **165**: p. 25-37.
65. Španěl, P. and D. Smith, *Selected ion flow tube studies of the reactions of H_3O^+, NO_+ and O_2^+ with several amines and some other nitrogen-containing molecules.* International Journal of Mass Spectrometry, 1998. **176**(3): p. 203-211.
66. Spanel, P. and D. Smith, *SIFT studies of the reactions of H_3O^+, NO_+ and O_2^+ with a series of alcohols.* International journal of mass spectrometry and ion processes, 1997. **167**: p. 375-388.
67. Španěl, P., T. Wang, and D. Smith, *A selected ion flow tube, SIFT, study of the reactions of H_3O^+, NO_+ and O_2^+ ions with a series of diols.* International Journal of Mass Spectrometry, 2002. **218**(3): p. 227-236.
68. Ŝpaněl, P. and D. Smith, *SIFT studies of the reactions of H_3O^+, NO_+ and O_2^+ with a series of volatile carboxylic acids and esters.* International journal of mass spectrometry and ion processes, 1998. **172**(1-2): p. 137-147.
69. Harrison, A.G., *Chemical ionization mass spectrometry*. 1992: Routledge.
70. Lau, Y., S. Ikuta, and P. Kebarle, *Thermodynamics and kinetics of the gas-phase reactions $H_3O^+ (H_2O)_{n-1}$ + water= $H_3O^+(H_2O)_n$.* Journal of the American Chemical Society, 1982. **104**: p. 1462-1469.

71. Španěl, P., et al., *Analysis of formaldehyde in the headspace of urine from bladder and prostate cancer patients using selected ion flow tube mass spectrometry.* Rapid communications in mass spectrometry, 1999. **13**(14): p. 1354-1359.

72. Lacko, M., et al., *Chemical ionization of glyoxal and formaldehyde with H_3O^+ ions using SIFT-MS under variable system humidity.* Phys. Chem. Chem. Phys., 2020. 22(18): 10170-10178

73. Bowers, M.T., *Gas phase ion chemistry, Volume 1*. Vol. 1. 1979: Academic Press.

74. Linden, F., et al., *Is the Reaction of $C3N^-$ with C_2H_2 a Possible Process for Chain Elongation in Titan's Ionosphere?* The Journal of Physical Chemistry A, 2016. **120**(27): p. 5337-5347.

75. Zymak, I., et al., *Experimental study of the reaction of O^- ions with CO_2 molecules with different ternary gases at temperatures relevant to the Martian ionosphere.* Icarus, 2020. **354**: p. 114057.

76. Zymak, I., et al., *Experimental study of the reaction of $NO2^-$ ions with CO_2 molecules at temperatures and energies relevant to the Martian atmosphere.* Icarus, 2020. **335**: p. 113416.

77. Kebarle, P. and S. Chowdhury, *Electron affinities and electron-transfer reactions.* Chemical Reviews, 1987. **87**(3): p. 513-534.

78. Laramee, J., B. Arbogast, and M. Deinzer, *Electron capture negative ion chemical ionization mass spectrometry of 1, 2, 3, 4-tetrachlorodibenzo-p-dioxin.* Analytical chemistry, 1986. **58**(14): p. 2907-2912.

79. Mackay, G., et al., *Rate constants at 297. degree. K for proton-transfer reactions with hydrocyanic acid and acetonitrile. Comparisons with classical theories and exothermicity.* The Journal of Physical Chemistry, 1976. **80**(26): p. 2919-2922.

80. Ellis, H., et al., *Transport properties of gaseous ions over a wide energy range.* Atomic data and nuclear data tables, 1976. **17**(3): p. 177-210.

81. Ellis, H., et al., *Transport properties of gaseous ions over a wide energy range. Part II.* Atomic data and nuclear data tables, 1978. **22**(3): p. 179-217.

82. Ellis, H.W., et al., *Transport properties of gaseous ions over a wide energy range. Part III.* Atomic Data and Nuclear Data Tables, 1984. **31**(1): p. 113-151.

83. Wannier, G.H., *Motion of gaseous ions in strong electric fields.* The Bell System Technical Journal, 1953. **32**(1): p. 170-254.
84. Viehland, L.A. and E. Mason, *Statistical–mechanical theory of gaseous ion–molecule reactions in an electrostatic field.* The Journal of Chemical Physics, 1977. **66**(2): p. 422-434.
85. Su, T., *Parametrization of kinetic energy dependences of ion–polar molecule collision rate constants by trajectory calculations.* The Journal of chemical physics, 1994. **100**(6): p. 4703-4703.
86. Su, T., A. Viggiano, and J.F. Paulson, *The effect of the dipole‐induced dipole potential on ion‐polar molecule collision rate constants.* The Journal of chemical physics, 1992. **96**(7): p. 5550-5551.
87. Bei, H.C., P.K. Bhowmik, and T. Su, *Trajectory calculations of high temperature and kinetic energy dependent ion–polar molecule collision rate constants.* The Journal of chemical physics, 1989. **90**(12): p. 7046-7049.
88. Schmeltekopf, A., E. Ferguson, and F. Fehsenfeld, *Afterglow studies of the reactions He^+, He (23S), and O^+ with vibrationally excited N2.* The Journal of Chemical Physics, 1968. **48**(7): p. 2966-2973.
89. Bowers, M., et al., *Temperature dependence of ion-molecule collision phenomena: An application of ion cyclotron resonance spectroscopy to the determination of reactive and momentum transfer rate constants.* International Journal of Mass Spectrometry and Ion Physics, 1977. **25**(1): p. 103-116.
90. Dunkin, D., et al., *Ion–Molecule Reaction Studies from 300° to 600° K in a Temperature‐Controlled Flowing Afterglow System.* The Journal of Chemical Physics, 1968. **49**(3): p. 1365-1371.
91. Meot-Ner, M. and F. Field, *Temperature dependences of some fast ion-polar molecule proton transfer and of slow hydride (1-) ion transfer reactions.* Journal of the American Chemical Society, 1975. **97**(8): p. 2014-2017.
92. Lindinger, W., et al., *Translational and internal energy dependences of some ion–neutral reactions.* The Journal of Chemical Physics, 1975. **63**(5): p. 2175-2181.
93. Smith, D. and R. Fouracre, *The temperature dependence of the reaction rate coefficients of O^+ ions with molecular oxygen and nitrogen.* Planetary and Space Science, 1968. **16**(2): p. 243-252.

94. Ferguson, E., et al., *Temperature dependence of slow ion–atom interchange reactions.* The Journal of Chemical Physics, 1969. **50**(11): p. 5039-5040.
95. Kebarle, P., *Ion thermochemistry and solvation from gas phase ion equilibria.* Annual Review of Physical Chemistry, 1977. **28**(1): p. 445-476.
96. Pierce, R.C. and R.F. Porter, *Low-temperature chemical ionization mass spectrometry of methane-hydrogen mixtures.* The Journal of Physical Chemistry, 1974. **78**(2): p. 93-97.
97. Abramson, F.P. and J.H. Futrell, *Ion—Molecule Reactions of Methane.* The Journal of Chemical Physics, 1966. **45**(6): p. 1925-1931.
98. Good, A., D.A. Durden, and P. Kebarle, *Ion–molecule reactions in pure nitrogen and nitrogen containing traces of water at total pressures 0.5–4 Torr. Kinetics of clustering reactions forming H+ (H2O) n.* The Journal of Chemical Physics, 1970. **52**(1): p. 212-221.
99. Meot‐Ner, M. and F. Field, *Thermal transitions between collisionally and tight‐complex limited kinetics in the gas phase. Reactions involving carbonium ions.* The Journal of Chemical Physics, 1976. **64**(1): p. 277-281.
100. Perez-Benito, J.F., *Some considerations on the fundamentals of chemical kinetics: steady state, quasi-equilibrium, and transition state theory.* Journal of Chemical Education, 2017. **94**(9): p. 1238-1246.
101. Kassel, L.S., *Studies in homogeneous gas reactions. I.* The Journal of Physical Chemistry, 2002. **32**(2): p. 225-242.
102. Marcus, R.A., *Unimolecular dissociations and free radical recombination reactions.* The Journal of Chemical Physics, 1952. **20**(3): p. 359-364.
103. Callear, A., *Basic RRKM Theory.* Comprehensive Chemical Kinetics, 1983. **24**: p. 333-356.
104. Skinner, G.B. and B. Rabinovitch, *Comparisons of the RRK [Rice-Ramsperger-Kassel] and RRKM [Markus-Rice] theories of thermal unimolecular reaction. Energy distributions and the s parameter.* The Journal of Physical Chemistry, 1972. **76**(17): p. 2418-2424.
105. Durup‐Ferguson, M., et al., *Enhancement of charge‐transfer reaction rate constants by vibrational excitation at kinetic energies below 1 eV.* The Journal of Chemical Physics, 1983. **79**(1): p. 265-272.

106. Viggiano, A. and R.A. Morris, *Rotational and Vibrational Energy Effects on Ion− Molecule Reactivity as Studied by the VT-SIFDT Technique.* The Journal of Physical Chemistry, 1996. **100**(50): p. 19227-19240.

107. Lindinger, W., et al., *Rate constants for the reactions of O_2^+ (a 4Π u) ions with N_2, Ar, CO, CO_2, H_2, and O_2 at relative kinetic energies 0.04–2 eV.* The Journal of Chemical Physics, 1975. **62**(10): p. 4101-4110.

108. Hansel, A., et al., *Energy dependencies of the proton transfer reactions $H_3O^+ + CH_2O \leftrightharpoons CH_2OH^+ + H_2O$.* International journal of mass spectrometry and ion processes, 1997. **167**: p. 697-703.

109. Smith, S.C., et al., *Unimolecular decomposition of a polyatomic ion in a variable-temperature selected-ion-flow-drift tube: experiment and theoretical interpretation.* International journal of mass spectrometry and ion processes, 1990. **96**(1): p. 77-96.

110. Malásková, M., et al., *Compendium of the reactions of H_3O^+ with selected ketones of relevance to breath analysis using proton transfer reaction mass spectrometry.* Frontiers in chemistry, 2019. **7**: p. 401.

111. Glosik, J., et al., *Energy dependencies of fast reactions of positive ions X^+ with HCl from near thermal to ≈ 2 eV center - of - mass collision energy ($X^+ = H^+$, H_2^+, H_3^+, N^+, N_2^+, Ar^+, C^+, CH^+, CH_2^+, CH_3^+, CH_4^+, CH_5^+).* The Journal of chemical physics, 1993. **98**(9): p. 6995-7003.

112. Glosik, J., P. Zakouřil, and W. Lindinger, *Selected ion flow drift tube studies of the reactions of Si^+ (2P) with HCl, H_2O, H2S, and NH_3: Reactions which produce atomic hydrogen.* The Journal of chemical physics, 1995. **103**(15): p. 6490-6497.

113. Zakouril, P., et al., *Selected ion flow drift tube studies of the reactions of S^+ (4S) with CH_4, C_2H_2, C_2H_4, and C_3H_8.* The Journal of Physical Chemistry, 1995. **99**(43): p. 15890-15898.

114. Adams, N. and D. Smith, *SIFDT studies of some CH_3^+ ternary association reactions.* International journal of mass spectrometry and ion processes, 1987. **81**: p. 273-287.

115. Glosik, J., et al., *SIFDT studies of the reactions of C^+, CH^+ and CH_2^+ with HCl and CO_2, and CH_3^+ with HCl.* International journal of mass spectrometry and ion processes, 1993. **129**: p. 131-143.

116. Chiu, Y.h., et al., *Reaction mechanisms and energy disposal in the [C_2H_2: OCS]$^+$ system: A mode - selective differential cross section study.* The Journal of chemical physics, 1996. **105**(8): p. 3089-3107.
117. Honma, K., L. Sunderlin, and P. Armentrout, *Reactions of protonated water clusters with deuterated ammonia: H (H_2O)^+_n (n= 1–4)+ ND_3.* International journal of mass spectrometry and ion processes, 1992. **117**: p. 237-259.
118. Fairley, D.A., et al., *Competitive association and charge transfer in the reactions of NO^+ with some ketones: a selected ion flow drift tube study.* International journal of mass spectrometry, 1999. **193**(1): p. 35-43.
119. Bartle, K.D. and P. Myers, *History of gas chromatography.* TrAC Trends in Analytical Chemistry, 2002. **21**(9–10): p. 547-557.
120. Russo, M.V., et al., *Extraction and GC-MS analysis of phthalate esters in food matrices: a review.* RSC Adv., 2015. **5**(46): p. 37023-37043.
121. Fialkov, A.B., et al., *Sensitivity and noise in GC–MS: Achieving low limits of detection for difficult analytes.* International journal of mass spectrometry, 2007. **260**(1): p. 31-48.
122. George, C. and H. Prest, *Determination of Phthalate Esters by Positive Chemical Ionization MS with Retention-Time Locked GC.* LCGC NORTH AMERICA, 2002. **20**(2): p. 142-151.
123. Borsdorf, H. and G.A. Eiceman, *Ion mobility spectrometry: principles and applications.* Applied Spectroscopy Reviews, 2006. **41**(4): p. 323-375.
124. Makinen, M.A., O.A. Anttalainen, and M.E. Sillanpää, *Ion mobility spectrometry and its applications in detection of chemical warfare agents*. Anal. Chem, 2010. **82**(83): p. 9594-9600.
125. Guevremont, R., *High-field asymmetric waveform ion mobility spectrometry: a new tool for mass spectrometry.* Journal of Chromatography A, 2004. **1058**(1-2): p. 3-19.
126. Kolakowski, B.M. and Z. Mester, *Review of applications of high-field asymmetric waveform ion mobility spectrometry (FAIMS) and differential mobility spectrometry (DMS).* Analyst, 2007. **132**(9): p. 842-864.
127. Owlstone Medical Ltd, cited 2022; Available from: https://www.owlstonemedical.com/science-technology/faims-technology/.
128. Fenn, J.B., et al., *Electrospray ionization for mass spectrometry of large biomolecules.* Science, 1989. **246**(4926): p. 64-71.

129. Rayleigh, L., *XX. On the equilibrium of liquid conducting masses charged with electricity.* The London, Edinburgh, and Dublin Philosophical Magazine and Journal of Science, 1882. **14**(87): p. 184-186.

130. Španěl, P., M. Pavlik, and D. Smith, *Reactions of H_3O^+ and OH^- ions with some organic molecules; applications to trace gas analysis in air.* International journal of mass spectrometry and ion processes, 1995. **145**(3): p. 177-186.

131. Li, H., M. Xu, and J. Zhu, *Headspace gas monitoring of gut microbiota using targeted and globally optimized targeted secondary electrospray ionization mass spectrometry.* Analytical chemistry, 2018. **91**(1): p. 854-863.

132. Griffiths, W.J., et al., *Electrospray and tandem mass spectrometry in biochemistry.* Biochemical Journal, 2001. **355**(3): p. 545-561.

133. Schlottmann, F., et al., *High Kinetic Energy Ion Mobility Spectrometry (HiKE-IMS) at 40 mbar.* Journal of the American Society for Mass Spectrometry, 2020.

134. Wakelam, V. *KIDA - Kinetic Database for Astrochemistry*. 2012 [cited 2022; Available from: http://kida.obs.u-bordeaux1.fr.

135. Zymak, I., et al., *A pilot study of ion-molecule reactions at temperatures relevant to the atmosphere of Titan.* Origins of Life and Evolution of Biospheres, 2016. **46**(4): p. 533-538.

136. Španěl, P., K. Dryahina, and D. Smith, *A general method for the calculation of absolute trace gas concentrations in air and breath from selected ion flow tube mass spectrometry data.* International Journal of Mass Spectrometry, 2006. **249-250**: p. 230-239.

137. Španěl, P. and D. Smith, *Quantitative selected ion flow tube mass spectrometry: the influence of ionic diffusion and mass discrimination.* Journal of the American Society for Mass Spectrometry, 2001. **12**(7): p. 863-872.

138. Španěl, P. and D. Smith, *Selected ion flow tube mass spectrometry analyses of stable isotopes in water: isotopic composition of H_3O^+ and $H_3O^+(H_2O)_3$ ions in exchange reactions with water vapor.* Journal of the American Society for Mass Spectrometry, 2000. **11**(10): p. 866-875.

139. Dryahina, K. and P. Španěl, *A convenient method for calculation of ionic diffusion coefficients for accurate selected ion flow tube mass spectrometry, SIFT-MS.* International Journal of Mass Spectrometry, 2005. **244**(2-3): p. 148-154.

140. Smith, D., A. Pysanenko, and P. Španěl, *Ionic diffusion and mass discrimination effects in the new generation of short flow tube SIFT-MS instruments.* International Journal of Mass Spectrometry, 2009. **281**(1-2): p. 15-23.
141. Lehnert, A.S., et al., *SIFT-MS optimization for atmospheric trace gas measurements at varying humidity.* Atmos. Meas. Tech., 2020. **13**(7): p. 3507-3520.
142. IONICON ANALYTIK GES.M.B.H. *Benefits of Proton Transfer Reaction - Mass Spectrometry*. 2022; Available from: https://www.ionicon.com/technologies/details/ptr-ms.
143. TOFWERK AG. *Advantages of the Vocus PTR-TOF*. 2022; Available from: https://www.tofwerk.com/products/vocus-ptr-tof/.
144. Amann, A., et al., *Model based determination of detection limits for proton transfer reaction mass spectrometer.* Measurement Science Review, 2010. **10**(6): p. 180-188.
145. Jordan, A., et al., *An online ultra-high sensitivity Proton-transfer-reaction mass-spectrometer combined with switchable reagent ion capability (PTR+SRI−MS).* International Journal of Mass Spectrometry, 2009. **286**(1): p. 32-38.
146. Knighton, W., et al., *Adaptation of a proton transfer reaction mass spectrometer instrument to employ NO^+ as reagent ion for the detection of 1, 3 ‐ butadiene in the ambient atmosphere.* Rapid Communications in Mass Spectrometry: An International Journal Devoted to the Rapid Dissemination of Up ‐ to ‐ the ‐ Minute Research in Mass Spectrometry, 2009. **23**(20): p. 3301-3308.
147. Sulzer, P., et al., *From conventional proton-transfer-reaction mass spectrometry (PTR-MS) to universal trace gas analysis.* International Journal of Mass Spectrometry, 2012. **321**: p. 66-70.
148. IONICON ANALYTIK GES.M.B.H. *PTR3-TOF 10K mass spectrometer - Trace VOC-ELVOC Analyzer*. 2022; Available from: https://www.ionicon.com/products/details/ptr3.

149. Keck, L., U. Oeh, and C. Hoeschen, *Corrected equation for the concentrations in the drift tube of a proton transfer reaction-mass spectrometer (PTR-MS).* International Journal of Mass Spectrometry, 2007. **264**(1): p. 92-95.
150. Michalczuk, B., et al., *Isomer and Conformer Selective Atmospheric Pressure Chemical Ionisation of dimethyl phthalate.* Physical Chemistry Chemical Physics, 2019.
151. Wróblewski, T., et al., *Dissociation energies of protonated water clusters.* Radiation Physics and Chemistry, 2003. **68**(1-2): p. 313-318.
152. Spesyvyi, A. and P. Španěl, *Determination of residence times of ions in a resistive glass selected ion flow‐drift tube using the Hadamard transformation.* Rapid Communications in Mass Spectrometry, 2015. **29**(17): p. 1563-1570.
153. Spesyvyi, A., et al., *Ligand Switching Ion Chemistry: An SIFDT Case Study of the Primary and Secondary Reactions of Protonated Acetic Acid Hydrates with Acetone.* Journal of the American Society for Mass Spectrometry, 2021. **32**(8): p. 2251-2260.
154. Phillips, M., et al., *Volatile organic compounds in breath as markers of lung cancer: a cross-sectional study.* The Lancet, 1999. **353**(9168): p. 1930-1933.
155. Syft Technologies. *Voice200 ultra*. 2022; Available from: https://www.syft.com/products.
156. IONICON ANALYTIK GES.M.B.H. *FUSION PTR-TOF 10k - Ultimate*. 2022; Available from: https://www.ionicon.com/products/details/fusion-ptr-tof-10k.
157. Miekisch, W., J.K. Schubert, and G.F. Noeldge-Schomburg, *Diagnostic potential of breath analysis—focus on volatile organic compounds.* Clinica chimica acta, 2004. **347**(1-2): p. 25-39.
158. Španěl, P. and D. Smith, *Progress in SIFT‐MS: Breath analysis and other applications.* Mass spectrometry reviews, 2011. **30**(2): p. 236-267.
159. Bruderer, T., et al., *On-line analysis of exhaled breath: focus review.* Chemical reviews, 2019. **119**(19): p. 10803-10828.
160. Španěl, P. and D. Smith, *Quantification of volatile metabolites in exhaled breath by selected ion flow tube mass spectrometry, SIFT-MS.* Clinical Mass Spectrometry, 2020. **16**: p. 18-24.

161. Storer, M., et al., *Measurement of breath acetone concentrations by selected ion flow tube mass spectrometry in type 2 diabetes.* Journal of Breath Research, 2011. **5**(4): p. 046011.
162. Dryahina, K., et al., *Exhaled breath concentrations of acetic acid vapour in gastro-esophageal reflux disease.* Journal of breath research, 2014. **8**(3): p. 037109.
163. Ratiu, I.-A., et al., *Mass spectrometric techniques for the analysis of volatile organic compounds emitted from bacteria.* Bioanalysis, 2017. **9**(14): p. 1069-1092.
164. Shestivska, V., et al., *Quantification of methyl thiocyanate in the headspace of Pseudomonas aeruginosa cultures and in the breath of cystic fibrosis patients by selected ion flow tube mass spectrometry.* Rapid Communications in Mass Spectrometry, 2011. **25**(17): p. 2459-2467.
165. Shestivska, V., et al., *Variability in the concentrations of volatile metabolites emitted by genotypically different strains of Pseudomonas aeruginosa.* Journal of Applied Microbiology, 2012. **113**(3): p. 701-713.
166. Gilchrist, F.J., et al., *Hydrogen cyanide concentrations in the breath of adult cystic fibrosis patients with and without Pseudomonas aeruginosa infection.* Journal of breath research, 2013. **7**(2): p. 026010.
167. Smith, D., et al., *Breath concentration of acetic acid vapour is elevated in patients with cystic fibrosis.* Journal of breath research, 2016. **10**(2): p. 021002.
168. Davies, S.J., P. Španěl, and D. Smith, *Breath analysis of ammonia, volatile organic compounds and deuterated water vapor in chronic kidney disease and during dialysis.* Bioanalysis, 2014. **6**(6): p. 843-857.
169. Kohl, I., et al., *First observation of a potential non-invasive breath gas biomarker for kidney function.* Journal of breath research, 2013. **7**(1): p. 017110.
170. Eng, K., et al., *Analysis of breath volatile organic compounds in children with chronic liver disease compared to healthy controls.* Journal of breath research, 2015. **9**(2): p. 026002.
171. Lembo, V., et al., *Rapid" breath-print" of liver cirrhosis by Proton Transfer Reaction Time of Flight Mass Spectrometry.* 2013.

172. Smolinska, A., et al., *Profiling of volatile organic compounds in exhaled breath as a strategy to find early predictive signatures of asthma in children.* PloS one, 2014. **9**(4): p. e95668.
173. Kharitonov, S.A. and P.J. Barnes, *Exhaled markers of pulmonary disease.* American journal of respiratory and critical care medicine, 2001. **163**(7): p. 1693-1722.
174. Dryahina, K., et al., *Quantification of pentane in exhaled breath, a potential biomarker of bowel disease, using selected ion flow tube mass spectrometry.* Rapid Communications in Mass Spectrometry, 2013. **27**(17): p. 1983-1992.
175. Lechner, M., et al., *Headspace screening of fluid obtained from the gut during colonoscopy and breath analysis by proton transfer reaction-mass spectrometry: A novel approach in the diagnosis of gastro-intestinal diseases.* International Journal of Mass Spectrometry, 2005. **243**(2): p. 151-154.
176. Harrison, G., et al., *Real‐time breath monitoring of propofol and its volatile metabolites during surgery using a novel mass spectrometric technique: a feasibility study.* British journal of anaesthesia, 2003. **91**(6): p. 797-799.
177. Erhart, S., et al., *3-Heptanone as a potential new marker for valproic acid therapy.* Journal of breath research, 2009. **3**(1): p. 016004.
178. Beauchamp, J., F. Kirsch, and A. Buettner, *Real-time breath gas analysis for pharmacokinetics: monitoring exhaled breath by on-line proton-transfer-reaction mass spectrometry after ingestion of eucalyptol-containing capsules.* Journal of breath research, 2010. **4**(2): p. 026006.
179. Trefz, P., et al., *Drug detection in breath: non-invasive assessment of illicit or pharmaceutical drugs.* Journal of breath research, 2017. **11**(2): p. 024001.
180. Schmidt, F.M., et al., *Background levels and diurnal variations of hydrogen cyanide in breath and emitted from skin.* Journal of breath research, 2011. **5**(4): p. 046004.
181. Moeskops, B., et al., *Real-time trace gas sensing of ethylene, propanal and acetaldehyde from human skin in vivo.* Physiological measurement, 2006. **27**(11): p. 1187.
182. Wisthaler, A. and C.J. Weschler, *Reactions of ozone with human skin lipids: sources of carbonyls, dicarbonyls, and hydroxycarbonyls in indoor air.* Proceedings of the National Academy of Sciences, 2010. **107**(15): p. 6568-6575.

183. Williams, J. and J. Pleil, *Crowd-based breath analysis: assessing behavior, activity, exposures, and emotional response of people in groups.* Journal of breath research, 2016. **10**(3): p. 032001.
184. Wicker, J., et al. *Cinema data mining: The smell of fear*. in *Proceedings of the 21th ACM SIGKDD International Conference on Knowledge Discovery and Data Mining*. 2015.
185. Williams, J., et al., *Cinema audiences reproducibly vary the chemical composition of air during films, by broadcasting scene specific emissions on breath.* Scientific reports, 2016. **6**(1): p. 1-10.
186. Mochalski, P., et al., *Instrumental sensing of trace volatiles—A new promising tool for detecting the presence of entrapped or hidden people.* Journal of breath research, 2018. **12**(2): p. 027107.
187. Giannoukos, S., A. Agapiou, and S. Taylor, *Advances in chemical sensing technologies for VOCs in breath for security/threat assessment, illicit drug detection, and human trafficking activity.* Journal of breath research, 2018. **12**(2): p. 027106.
188. Williams, J., et al., *An atmospheric chemistry interpretation of mass scans obtained from a proton transfer mass spectrometer flown over the tropical rainforest of Surinam.* Journal of Atmospheric Chemistry, 2001. **38**(2): p. 133-166.
189. Crutzen, P., et al., *High spatial and temporal resolution measurements of primary organics and their oxidation products over the tropical forests of Surinam.* Atmospheric Environment, 2000. **34**(8): p. 1161-1165.
190. Warneke, C., et al., *Isoprene and its oxidation products methyl vinyl ketone, methacrolein, and isoprene related peroxides measured online over the tropical rain forest of Surinam in March 1998.* Journal of Atmospheric Chemistry, 2001. **38**(2): p. 167-185.
191. Müller, K., et al., *Biogenic carbonyl compounds within and above a coniferous forest in Germany.* Atmospheric Environment, 2006. **40**: p. 81-91.
192. Rinne, J., et al., *On-line PTR-MS measurements of atmospheric concentrations of volatile organic compounds in a European boreal forest ecosystem.* Boreal environment research, 2005. **10**(5): p. 425-436.
193. Williams, J., et al., *The summertime Boreal forest field measurement intensive (HUMPPA-COPEC-2010): an overview of meteorological and chemical*

influences. Atmospheric Chemistry and Physics, 2011. **11**(20): p. 10599-10618.

194. Ammann, C., et al., *Application of PTR-MS for measurements of biogenic VOC in a deciduous forest.* International Journal of Mass Spectrometry, 2004. **239**(2-3): p. 87-101.
195. Fall, R., et al., *Biogenic C5 VOCs: release from leaves after freeze–thaw wounding and occurrence in air at a high mountain observatory.* Atmospheric Environment, 2001. **35**(22): p. 3905-3916.
196. Karl, T., et al., *High concentrations of reactive biogenic VOCs at a high altitude site in late autumn.* Geophysical Research Letters, 2001. **28**(3): p. 507-510.
197. Fares, S., et al., *Biogenic emissions from Citrus species in California.* Atmospheric Environment, 2011. **45**(27): p. 4557-4568.
198. Misztal, P.K., et al., *Large estragole fluxes from oil palms in Borneo.* Atmospheric Chemistry and Physics, 2010. **10**(9): p. 4343-4358.
199. Misztal, P.K., et al., *Direct ecosystem fluxes of volatile organic compounds from oil palms in South-East Asia.* Atmospheric Chemistry and Physics, 2011. **11**(17): p. 8995-9017.
200. Kammer, J., et al. *Effect of agricultural practices on volatile organic compound (VOC) emissions from winter wheat*. in *8 th International PTR-MS Conference 2019*. 2019.
201. Holzinger, R., et al., *Diurnal cycles and seasonal variation of isoprene and its oxidation products in the tropical savanna atmosphere.* Global Biogeochemical Cycles, 2002. **16**(4): p. 22-1-22-13.
202. Bamberger, I., et al., *BVOC fluxes above mountain grassland.* Biogeosciences, 2010. **7**(5): p. 1413-1424.
203. Davison, B., et al., *Cut-induced VOC emissions from agricultural grasslands.* Plant Biology, 2007. **9**(S 01): p. e60-e68.
204. Sovová, K., et al., *Time-integrated thermal desorption for quantitative SIFT-MS analyses of atmospheric monoterpenes.* Analytical and bioanalytical chemistry, 2019. **411**(14): p. 2997-3007.
205. Bsaibes, S., et al., *Monoterpene Chemical Speciation with High Time Resolution Using a FastGC/PTR-MS: Results from the COV3ER Experiment on Quercus ilex.* Atmosphere, 2020. **11**(7): p. 690.

206. Bsaibes, S., et al., *Variability of hydroxyl radical (OH) reactivity in the Landes maritime pine forest: results from the LANDEX campaign 2017.* Atmospheric Chemistry and Physics, 2020. **20**(3): p. 1277-1300.
207. Yang, Y., et al., *Towards a quantitative understanding of total OH reactivity: A review.* Atmospheric Environment, 2016. **134**: p. 147-161.
208. Ghirardo, A., et al., *Determination of de novo and pool emissions of terpenes from four common boreal/alpine trees by $^{13}CO_2$ labelling and PTR‐MS analysis.* Plant, cell & environment, 2010. **33**(5): p. 781-792.
209. Maleknia, S.D., T.L. Bell, and M.A. Adams, *PTR-MS analysis of reference and plant-emitted volatile organic compounds.* International Journal of Mass Spectrometry, 2007. **262**(3): p. 203-210.
210. Shaw, S.L., et al., *Volatile organic compound emissions from dairy cows and their waste as measured by proton-transfer-reaction mass spectrometry.* Environmental science & technology, 2007. **41**(4): p. 1310-1316.
211. Feilberg, A., et al., *Odorant emissions from intensive pig production measured by online proton-transfer-reaction mass spectrometry.* Environmental Science & Technology, 2010. **44**(15): p. 5894-5900.
212. Hansen, M.J., et al., *Application of proton-transfer-reaction mass spectrometry to the assessment of odorant removal in a biological air cleaner for pig production.* Journal of Agricultural and Food Chemistry, 2012. **60**(10): p. 2599-2606.
213. Sprung, D., et al., *Acetone and acetonitrile in the tropical Indian Ocean boundary layer and free troposphere: Aircraft‐based intercomparison of AP‐CIMS and PTR‐MS measurements.* Journal of Geophysical Research: Atmospheres, 2001. **106**(D22): p. 28511-28527.
214. Sinha, V., et al., *Air-sea fluxes of methanol, acetone, acetaldehyde, isoprene and DMS from a Norwegian fjord following a phytoplankton bloom in a mesocosm experiment.* Atmospheric Chemistry and Physics, 2007. **7**(3): p. 739-755.
215. Williams, J., et al., *Measurements of organic species in air and seawater from the tropical Atlantic.* Geophysical research letters, 2004. **31**(23).

216. Wang, N., et al., *Measurements of carbonyl compounds around the Arabian Peninsula: overview and model comparison.* Atmospheric Chemistry and Physics, 2020. **20**(18): p. 10807-10829.
217. Colomb, A., et al., *Variation of atmospheric volatile organic compounds over the Southern Indian Ocean (30–49 S).* Environmental Chemistry, 2009. **6**(1): p. 70-82.
218. Karl, T., et al., *Use of proton‐transfer‐reaction mass spectrometry to characterize volatile organic compound sources at the La Porte super site during the Texas Air Quality Study 2000.* Journal of Geophysical Research: Atmospheres, 2003. **108**(D16).
219. Filella, I. and J. Penuelas, *Daily, weekly, and seasonal time courses of VOC concentrations in a semi-urban area near Barcelona.* Atmospheric Environment, 2006. **40**(40): p. 7752-7769.
220. MIYAKAWA, Y., S. KATO, and Y. KAJII, *Calibration of the Proton Transfer Reaction Mass Spectrometry (PTR-MS) Instrument for Oxygenated Volatile Organic Compounds (OVOCs) and the Measurement of Ambient Air in Tokyo.* Journal of Japan Society for Atmospheric Environment/Taiki Kankyo Gakkaishi, 2005. **40**(5): p. 209-219.
221. Gros, V., et al., *Volatile organic compounds sources in Paris in spring 2007. Part I: qualitative analysis.* Environmental chemistry, 2011. **8**(1): p. 74-90.
222. Gaimoz, C., et al., *Volatile organic compounds sources in Paris in spring 2007. Part II: source apportionment using positive matrix factorisation.* Environmental chemistry, 2011. **8**(1): p. 91-103.
223. Velasco, E., Pressley, S., Grivicke, R., Allwine, E., Coons, T., Foster, W, *Eddy covariance flux measurements of pollutant gases in urban Mexico City.* Atmospheric Chemistry and Physics, 2009. **9**(19): p. 7325-7342.
224. Herndon, S.C., et al., *Characterization of urban pollutant emission fluxes and ambient concentration distributions using a mobile laboratory with rapid response instrumentation.* Faraday Discussions, 2005. **130**(0): p. 327-339.
225. Jobson, B.T., et al., *On-line analysis of organic compounds in diesel exhaust using a proton transfer reaction mass spectrometer (PTR-MS).* International Journal of Mass Spectrometry, 2005. **245**(1): p. 78-89.

226. Knighton, W.B., et al., *Quantification of aircraft engine hydrocarbon emissions using proton transfer reaction mass spectrometry.* Journal of Propulsion and Power, 2007. **23**(5): p. 949.
227. Herndon, S.C., et al., *Hydrocarbon Emissions from In-Use Commercial Aircraft during Airport Operations.* Environmental Science & Technology, 2006. **40**(14): p. 4406-4413.
228. Akagi, S.K., et al., *Emission factors for open and domestic biomass burning for use in atmospheric models.* Atmos. Chem. Phys., 2011. **11**(9): p. 4039-4072.
229. Wisthaler, A., et al., *Organic trace gas measurements by PTR-MS during INDOEX 1999.* Journal of Geophysical Research: Atmospheres, 2002. **107**(D19): p. INX2 23-1-INX2 23-11.
230. Kolarik, B., et al., *The effect of a photocatalytic air purifier on indoor air quality quantified using different measuring methods.* Building and Environment, 2010. **45**(6): p. 1434-1440.
231. Vesin, A., et al., *Use of the HS-PTR-MS for online measurements of pyrethroids during indoor insecticide treatments.* Analytical and Bioanalytical Chemistry, 2012. **403**(7): p. 1907-1921.
232. Uhde, E. and N. Schulz, *Impact of room fragrance products on indoor air quality.* Atmospheric Environment, 2015. **106**: p. 492-502.
233. Schripp, T., et al., *Application of proton-transfer-reaction-mass-spectrometry for Indoor Air Quality research.* Indoor Air, 2014. **24**(2): p. 178-189.
234. Han, K.H., et al., *Determination of material emission signatures by PTR-MS and their correlations with odor assessments by human subjects.* Indoor Air, 2010. **20**(4): p. 341-354.
235. Syft Technologies. *Cleanroom Monitoring*. 2022; Available from: https://www.syft.com/applications/cleanroom-monitoring.
236. Dryahina, K., D. Smith, and P. Španěl, *Quantification of volatile compounds released by roasted coffee by selected ion flow tube mass spectrometry.* Rapid Communications in Mass Spectrometry, 2018. **32**(9): p. 739-750.
237. Yeretzian, C., et al., *From the green bean to the cup of coffee: investigating coffee roasting by on-line monitoring of volatiles.* European Food Research and Technology, 2002. **214**(2): p. 92-104.

238. Beauchamp, J.D., *Pushing the Boundaries of Dynamic Flavor Analysis with PTR-MS*, in *Dynamic Flavor: Capturing Aroma Using Real-Time Mass Spectrometry*. 2021, American Chemical Society. p. 33-50.
239. Boscaini, E., et al., *Characterization of wine with PTR-MS.* International Journal of Mass Spectrometry, 2004. **239**(2): p. 215-219.
240. Boscaini, E., et al., *Gas Chromatography−Olfactometry (GC-O) and Proton Transfer Reaction−Mass Spectrometry (PTR-MS) Analysis of the Flavor Profile of Grana Padano, Parmigiano Reggiano, and Grana Trentino Cheeses.* Journal of Agricultural and Food Chemistry, 2003. **51**(7): p. 1782-1790.
241. Galle, S.A., et al., *Typicality and Geographical Origin Markers of Protected Origin Cheese from The Netherlands Revealed by PTR-MS.* Journal of Agricultural and Food Chemistry, 2011. **59**(6): p. 2554-2563.
242. Buser, H.R., C. Zanier, and H. Tanner, *Identification of 2, 4, 6-trichloroanisole as a potent compound causing cork taint in wine.* Journal of agricultural and food chemistry, 1982. **30**(2): p. 359-362.
243. Soukoulis, C., et al., *PTR-ToF-MS, A Novel, Rapid, High Sensitivity and Non-Invasive Tool to Monitor Volatile Compound Release During Fruit Post-Harvest Storage: The Case Study of Apple Ripening.* Food and Bioprocess Technology, 2013. **6**(10): p. 2831-2843.
244. Li, H., et al., *Sensory, GC-MS and PTR-ToF-MS profiling of strawberries varying in maturity at harvest with subsequent cold storage.* Postharvest Biology and Technology, 2021. **182**: p. 111719.
245. Soukoulis, C., et al., *Proton transfer reaction time-of-flight mass spectrometry monitoring of the evolution of volatile compounds during lactic acid fermentation of milk.* Rapid Communications in Mass Spectrometry, 2010. **24**(14): p. 2127-2134.
246. Tsevdou, M., et al., *Monitoring the effect of high pressure and transglutaminase treatment of milk on the evolution of flavour compounds during lactic acid fermentation using PTR-ToF-MS.* Food Chemistry, 2013. **138**(4): p. 2159-2167.
247. Capozzi, V., et al., *PTR-MS Characterization of VOCs Associated with Commercial Aromatic Bakery Yeasts of Wine and Beer Origin.* Molecules, 2016. **21**(4): p. 483.

248. Cordell, R.L., et al., *Detection of chemical weapon agents and simulants using chemical ionization reaction time-of-flight mass spectrometry.* Analytical chemistry, 2007. **79**(21): p. 8359-8366.

249. Petersson, F., et al., *Real‐time trace detection and identification of chemical warfare agent simulants using recent advances in proton transfer reaction time‐of‐flight mass spectrometry.* Rapid Communications in Mass Spectrometry: An International Journal Devoted to the Rapid Dissemination of Up‐to‐the‐Minute Research in Mass Spectrometry, 2009. **23**(23): p. 3875-3880.

250. Agarwal, B., et al., *Use of proton transfer reaction time-of-flight mass spectrometry for the analytical detection of illicit and controlled prescription drugs at room temperature via direct headspace sampling.* Analytical and bioanalytical chemistry, 2011. **400**(8): p. 2631-2639.

251. Jürschik, S., et al., *Rapid and facile detection of four date rape drugs in different beverages utilizing proton transfer reaction mass spectrometry (PTR‐MS).* Journal of mass spectrometry, 2012. **47**(9): p. 1092-1097.

252. Sabo, M., M. Malaskova, and Š. Matejčík, *Laser desorption with corona discharge ion mobility spectrometry for direct surface detection of explosives.* Analyst, 2014. **139**(20): p. 5112-5117.

253. Mayhew, C., et al., *Applications of proton transfer reaction time-of-flight mass spectrometry for the sensitive and rapid real-time detection of solid high explosives.* International Journal of Mass Spectrometry, 2010. **289**(1): p. 58-63.

254. González-Méndez, R.n., et al., *Enhancement of compound selectivity using a radio frequency ion-funnel proton transfer reaction mass spectrometer: improved specificity for explosive compounds.* Analytical chemistry, 2016. **88**(21): p. 10624-10630.

255. Sulzer, P., et al., *Applications of switching reagent ions in proton transfer reaction mass spectrometric instruments for the improved selectivity of explosive compounds.* International Journal of Mass Spectrometry, 2013. **354**: p. 123-128.

256. Baur, X., B. Poschadel, and L.T. Budnik, *High frequency of fumigants and other toxic gases in imported freight containers—an underestimated*

occupational and community health risk. Occupational and environmental medicine, 2010. **67**(3): p. 207-212.

257. Pysanenko, A., P. Španěl, and D. Smith, *Analysis of the isobaric compounds propanol, acetic acid and methyl formate in humid air and breath by selected ion flow tube mass spectrometry, SIFT-MS.* International Journal of Mass Spectrometry, 2009. **285**(1-2): p. 42-48.
258. Lacko, M., et al., *Addition of fast gas chromatography to selected ion flow tube mass spectrometry for analysis of individual monoterpenes in mixtures.* Atmospheric Measurement Techniques, 2019. **12**(9): p. 4965-4982.
259. Spesyvyi, A., K. Sovová, and P. Španěl, *In‐tube collision‐induced dissociation for selected ion flow‐drift tube mass spectrometry, SIFDT‐MS: a case study of NO^+ reactions with isomeric monoterpenes.* Rapid Communications in Mass Spectrometry, 2016. **30**(18): p. 2009-2016.
260. Smith, D. and P. Španěl, *Ternary association reactions of H_3O^+, NO^+ and $O_2^{+\bullet}$ with N_2, O_2, CO_2 and H_2O; implications for selected ion flow tube mass spectrometry analyses of air and breath.* Rapid Communications in Mass Spectrometry, 2022. **36**(6): p. e9241.
261. Clough, S.A., et al., *Dipole moment of water from Stark measurements of H_2O, HDO, and D_2O.* The Journal of Chemical Physics, 1973. **59**(5): p. 2254-2259.
262. Wang, T., P. Španěl, and D. Smith, *Selected ion flow tube, SIFT, studies of the reactions of H_3O^+, NO^+ and O_2^+ with eleven $C_{10}H_{16}$ monoterpenes.* Int. J. Mass Spec., 2003. **228**(1): p. 117-126.
263. Michel, E., et al., *A selected ion flow tube study of the reactions of H_3O^+, NO^+ and O_2^+ with methyl vinyl ketone and some atmospherically important aldehydes.* International Journal of Mass Spectrometry, 2005. **244**: p. 50-59.
264. Olivenza-León, D., C.A. Mayhew, and R. González-Méndez, *Selective Reagent Ion Mass Spectrometric Investigations of the Nitroanilines.* Journal of The American Society for Mass Spectrometry, 2019. **30**(11): p. 2259-2266.
265. Roach, J.A., et al., *Chromatographic separation and identification of conjugated linoleic acid isomers.* Analytica Chimica Acta, 2002. **465**(1-2): p. 207-226.

266. Ecker, J., et al., *A rapid GC–MS method for quantification of positional and geometric isomers of fatty acid methyl esters.* Journal of Chromatography B, 2012. **897**: p. 98-104.
267. Matisová, E. and M. Dömötörová, *Fast gas chromatography and its use in trace analysis.* Journal of Chromatography A, 2003. **1000**(1-2): p. 199-221.
268. Materić, D., et al., *Monoterpene separation by coupling proton transfer reaction time-of-flight mass spectrometry with fastGC.* Analytical and bioanalytical chemistry, 2015. **407**(25): p. 7757-7763.
269. Jones, C., et al., *A novel fast gas chromatography method for higher time resolution measurements of speciated monoterpenes in air.* Atmospheric Measurement Techniques, 2014. **7**(5): p. 1259-1275.
270. Runge, C., *Über die numerische Auflösung von Differentialgleichungen.* Mathematische Annalen, 1895. **46**(2): p. 167-178.
271. Spanel, P. and D. Smith, *Advances in on-line absolute trace gas analysis by SIFT-MS.* Current Analytical Chemistry, 2013. **9**(4): p. 525-539.
272. Hazra, M.K., J.S. Francisco, and A. Sinha, *Hydrolysis of glyoxal in water-restricted environments: formation of organic aerosol precursors through formic acid catalysis.* The Journal of Physical Chemistry A, 2014. **118**(23): p. 4095-4105.
273. Shkrob, I.A., et al., *Photoredox reactions and the catalytic cycle for carbon dioxide fixation and methanogenesis on metal oxides.* The Journal of Physical Chemistry C, 2012. **116**(17): p. 9450-9460.
274. Civiš, S., et al., *Photocatalytic transformation of CO_2 to CH_4 and CO on acidic surface of TiO_2 anatase.* Optical Materials, 2016. **56**: p. 80-83.
275. Volkamer, R., U. Platt, and K. Wirtz, *Primary and secondary glyoxal formation from aromatics: experimental evidence for the bicycloalkyl− radical pathway from benzene, toluene, and p-xylene.* The Journal of Physical Chemistry A, 2001. **105**(33): p. 7865-7874.
276. Jang, M. and R.M. Kamens, *Characterization of Secondary Aerosol from the Photooxidation of Toluene in the Presence of NO_x and 1-Propene.* Environmental Science & Technology, 2001. **35**(18): p. 3626-3639.
277. Tuazon, E.C., et al., *Yields of glyoxal and methylglyoxal from the nitrogen oxide (NO_x)-air photooxidations of toluene and m-and p-xylene.* Environmental science & technology, 1984. **18**(12): p. 981-984.

278. Smith, D., T. Kleindienst, and C. McIver, *Primary product distributions from the reaction of OH with m-, p-xylene, 1, 2, 4-and 1, 3, 5-trimethylbenzene.* Journal of Atmospheric Chemistry, 1999. **34**(3): p. 339-364.

279. Yu, J., H.E. Jeffries, and R.M. Le Lacheur, *Identifying airborne carbonyl compounds in isoprene atmospheric photooxidation products by their PFBHA oximes using gas chromatography/ion trap mass spectrometry.* Environmental science & technology, 1995. **29**(8): p. 1923-1932.

280. Yu, J., H.E. Jeffries, and K.G. Sexton, *Atmospheric photooxidation of alkylbenzenes—I. Carbonyl product analyses.* Atmospheric Environment, 1997. **31**(15): p. 2261-2280.

281. Wroblewski, T., et al., *Ab initio and density functional theory calculations of proton affinities for volatile organic compounds.* European Physical Journal-Special Topics, 2007. **144**: p. 191-195.

282. Mattioda, G. and A. Blanc, *Glyoxal*, in *Ullmann's Encyclopedia of Industrial Chemistry*. 2000.

283. Guimbaud, C., et al., *Kinetics of the reactions of acetone and glyoxal with O_2^+ and NO^+ ions and application to the detection of oxygenated volatile organic compounds in the atmosphere by chemical ionization mass spectrometry.* International Journal of Mass Spectrometry, 2007. **263**(2-3): p. 276-288.

284. Stönner, C., et al., *Glyoxal measurement with a proton transfer reaction time of flight mass spectrometer (PTR‐TOF‐MS): characterization and calibration.* Journal of Mass Spectrometry, 2017. **52**(1): p. 30-35.

285. Bohme, D., G. Mackay, and S.D. Tanner, *An experimental study of the gas-phase kinetics of reactions with hydrated hydronium (1^+) ions (n= 1-3) at 298 K.* Journal of the American Chemical Society, 1979. **101**(14): p. 3724-3730.

286. Halden, R.U., *Plastics and health risks.* Annu Rev Public Health, 2010. **31**: p. 179-94.

287. Benjamin, S., et al., *A monograph on the remediation of hazardous phthalates.* J Hazard Mater, 2015. **298**: p. 58-72.

288. *DIRECTIVE 2005/84/EC OF THE EUROPEAN PARLIAMENT AND OF THE COUNCIL of 14 December 2005*. 2005: Official Journal of the European Union. p. 40-43.

289. EHCA – European Chemicals Agency, *Candidate List of Substances of Very High Concern of Authorisation*. 2022. Available from: http://echa.europa.eu/candidate-list-table/-/substance/

290. Shen, H.Y., *Simultaneous screening and determination eight phthalates in plastic products for food use by sonication-assisted extraction/GC-MS methods.* Talanta, 2005. **66**(3): p. 734-9.

291. Juhasz, M.L. and E.S. Marmur, *A review of selected chemical additives in cosmetic products.* Dermatol Ther, 2014. **27**(6): p. 317-22.

292. Sadeghi, G., E. Ghaderian, and A. O'Connor, *Determination of Dioctyl phthalate (DEHP) concentration in polyvinylchloride (PVC) plastic parts of toothbrushes.* The Downtown Review, 2015. **1**(2).

293. Jeilani, Y.A., B.H. Cardelino, and V.M. Ibeanusi, *Positive chemical ionization triple-quadrupole mass spectrometry and ab initio computational studies of the multi-pathway fragmentation of phthalates.* J Mass Spectrom, 2010. **45**(6): p. 678-85.

294. Španěl, P., et al., *Breath acetone concentration; biological variability and the influence of diet.* Physiological measurement, 2011. **32**(8): p. N23.

295. Marschner, K., S. Musil, and J.i. Dědina, *Demethylation of Methylated Arsenic Species during Generation of Arsanes with Tetrahydridoborate (1−) in Acidic Media.* Analytical chemistry, 2016. **88**(12): p. 6366-6373.

296. Talmi, Y. and D. Bostick, *Determination of alkylarsenic acids in pesticide and environmental samples by gas chromatography with a microwave emission spectrometric detection system.* Analytical chemistry, 1975. **47**(13): p. 2145-2150.

297. Dedina, J. and D.L. Tsalev, *Hydride generation atomic absorption spectrometry*. Vol. 130. 1995: Wiley.

298. Dędina, J., *Generation of volatile compounds for analytical atomic spectroscopy.* Encyclopedia of Analytical Chemistry: Applications, Theory and Instrumentation, 2006.

299. Duben, O., et al., *Dielectric barrier discharge plasma atomizer for hydride generation atomic absorption spectrometry—Performance evaluation for selenium.* Spectrochimica Acta Part B: Atomic Spectroscopy, 2015. **111**: p. 57-63.

Attachments

Attachment A.1 – Publication and supplement

Lacko M, Wang N, Sovová K, Pásztor P, Španěl P.
Addition of fast gas chromatography to selected ion flow tube mass spectrometry for analysis of individual monoterpenes in mixtures.
Atmospheric Measurement Techniques. 2019. 12(9): 4965-82.

Authors contribution: Contribution of individual authors is stated in the paper.

Attachment A.2 – Publication

Lacko M, Piel F, Mauracher A, Španěl P.
Chemical ionization of glyoxal and formaldehyde with H_3O^+ ions using SIFT-MS under variable system humidity.
Physical Chemistry Chemical Physics. 2020. 22(18): 10170-10178

Authors contribution: Lacko and Piel carried out initial measurements on glyoxal ion chemistry. Results were later supplemented by study of formaldehyde provided by Lacko. Theoretical calculations were done by Lacko and Mauracher. Lacko later simulated experimental data using KIMI Sim. Lacko and Španěl prepared the publication.

Attachment A.3 – Manuscript and supplement

Lacko M, Španěl P, Mayhew Ch, Malásková M, Spesyvyi A.
SIFT-MS and PTR-MS studies of H_3O^+ reaction with glyoxal in presence of water molecules forming protonated formaldehyde at different interaction energies, Manuscript

Authors contribution: Lacko and Malásková carried out the experimenal study of glyoxal on PTR-MS. Lacko and Spesyvyi carried out the experimenal study of glyoxal on SIFDT-MS. Lacko simulated experimental data using KIMI Sim. Lacko, Španěl and Mayhew prepared the manuscript

Attachment A.4 – Publication and supplement

Lacko M, Michalczuk B, Matejčík Š, Španěl P.
Ion chemistry of phthalates in selected ion flow tube mass spectrometry: isomeric effects and secondary reactions with water vapour.
Physical Chemistry Chemical Physics. 2020. 22(28): 16345-52.

Authors contribution: Lacko and Michalczuk carried out the experimenal study. Lacko simulated experimental data using KIMI Sim. Lacko, Španěl and Matejčík prepared the publication.

Attachment A.5 – Publication and supplement

Spesyvyi A, **Lacko M**, Dryahina K, Smith D, Španěl P.
Ligand Switching Ion Chemistry: An SIFDT Case Study of the Primary and Secondary Reactions of Protonated Acetic Acid Hydrates with Acetone.
Journal of the American Society for Mass Spectrometry. 2021. 32(8): 2251-60.

Authors contribution: Spesyvyi carried out the experimenal study, theoretical calculations and preparation of the initial draft. Lacko supported experimental data with simulations of the ion chemistry. All authors later participated on the preparation of the publication.

Attachment A.6 – Publication and supplement

Kratzer J, **Lacko M**, Dryahina K, Matoušek T, Španěl P, Dědina J.
Atomization of As and Se volatile species in a dielectric barrier discharge atomizer after hydride generation: Fate of analyte studied by selected ion flow tube mass spectrometry.
Analytica chimica acta. 2022. 1190: 339256.

Authors contribution: Contribution of individual authors is stated in the paper

Attachment A.7 – KIMI Sim Software

Lacko M. Kinetic of Ion Molecular Interaction Simulator (KIMI Sim). 2022.

The KIMI Sim software is available at https://github.com/Progllar/KIMI-Simulator or in the physical multimedia attached to this work.

In the physical multimedia in the "KIMI Simulator source" file you can find the source code of the program. In the "v2.2.2 KIMI" you can find the build used for latest simulations presented in this work.

Authors contribution: The full code of the KIMI Sim was written by Lacko, except external modules: MassSpectrometry library, OxyPlot.Core library and MwtWinDll library.